Structural, Electrical and Ferroelectric Properties of Substituted Barium Titanate

A Thesis Submitted

for the

Award of the Degree of

Doctor of Philosophy

by

Parveen Kumar

Roll No. 90712501

School of Physics and Materials Science
Thapar University
Patiala-147004
INDIA

October – 2011

This thesis is dedicated to my Grand Father

Giridhari Lal Paliwal

Your Love and support are still with me even if you are not.

CERTIFICATE

This is to certify that the thesis entitled ***"Structural, Electrical and Ferroelectric Properties of Substituted Barium Titanate"*** which is being submitted by **Mr. Parveen Kumar** in fulfillment of the requirement for the award of the Degree of Doctor of Philosophy in the School of Physics and Materials Science, Thapar University, Patiala is a record of candidate's own work carried out by him under our supervision and guidance. The matter presented in this thesis has not been submitted in parts or full for the awards of any degree in other university or institute.

Supervisors

.....

Dr. Chandra Prakash
Directorate of ER&IPR, DRDO,
DRDO Bhawan, New Delhi-110105
(Adjunct Professor, Thapar University, Patiala-147004)

.....

Prof. K.K. Raina
School of Physics and Materials Science
Thapar University, Patiala-147004

.....

Dr. J.K. Juneja
Department of Physics,
Hindu College, Sonepat-131001

ACKNOWLEDGMENTS

It is a great pleasure and proud privilege to express my sincere, deep sense of gratitude and profound indebtedness to my supervisors, Dr. Chandra Prakash, Prof. K.K. Raina and Dr. J.K. Juneja, who are incredibly knowledgeable in many ways. I am thanking you all for your guidance and enthusiasm in research and encouraging me to keep things organized and on schedule.

I would like to thank Dr. Abhijit Mukherjee, Director, Thapar University, Patiala, for granting me the permission to register for Ph.D. programme in his meritorious institute. I am also thankful to Dr. Kulvir Singh (Head of the Department), Dr. O.P. Pandey and Dr. Puneet Sharma (S.P.M.S., Thapar University, Patiala) for giving constant encouragement throughout my Ph.D. period.

I would like to thank Dr. R.P. Pant (NPL, New Delhi), Dr. Ratanmala Chatterjee (IIT Delhi), Prof. M. Hussain (JMI, Delhi), Dr. Sangeeta Singh (Physics Department, GVM Girls College, Sonepat) and Dr. Manjula Spah (Chemistry Department, GVM Girls College, Sonepat) for their many insightful discussions and experimental assistance like XRD, piezoelectric coefficient measurements and SEM; it has been a pleasure working with you all. Dr. Jyoti Juneja, Principal, GVM Girls College, thank you for giving me opportunity to do my experimental work at Electroceramics Research Lab, GVM College.

Pratibha Singh, Renu Rani, Rekha Rani and Ravi Shukla, who were great colleagues and even greater friends, thank you for helping make the heavy things bearable.

I would especially like to thank my parents for the encouragement, love and support, which you have always given in abundance.

Kaliwal

(Parveen Kumar)

ABSTRACT

Barium titanate ferroelectric ceramic which lies in the class of functional ceramics was the first ceramic material discovered in the mid-1940s in which ferroelectric behavior was observed. It has better ferroelectric properties, chemical and mechanical stability. It belongs to perovskite group (ABO_3) and consists of a corner-linked network of oxygen octahedral, creating an octahedral cage (B site) and the interstices (A sites). Ti^{4+} ions occupy the B site while Ba^{2+} ions occupy the A site. The ability of displacement of the central Ti^{4+} ion is the cause of the reversibility of polarization which results in ferroelectric hysteresis loop under the application of external AC electric field. It undergoes a structural phase transition from a high temperature paraelectric phase into a low temperature ferroelectric phase. The temperature of the phase transition is called as the Curie temperature (T_c). The phase transition of ferroelectrics often leads to strong anomalies in dielectric, elastic, thermal and other properties of the materials, among which dielectric variation before and after a phase transition is the most significant and thus usually used as an indication of the phase transition. The properties of BT can further be modified, in order to design a composition with desired properties, by suitable substitution and better control of processing parameters. Compositional fluctuation can be done by substitution of cations (aliovalent or isovalent) at both A and B site. Substitution of ions at different sites can modify the properties upto a great extent, which makes it an important electronic material that has a wide range of industrial and commercial applications, such as high dielectric constant capacitors, piezoelectric sonars or ultrasonic transducers, pyroelectric security sensors, medical diagnostic transducers, electro optic light valves and ultrasonic motors. In the present work, following compositions were prepared and processed using conventional solid state reaction route:

Isovalent ion substitution:

$Ba_{1-x}Pb_x\ Zr_{0.10}Ti_{0.90}O_3$ ($0 \leq x \leq 0.20$, in steps of 0.05)

$Ba_{0.80}Pb_{0.20}Zr_xTi_{1-x}O_3$ ($0 \leq x \leq 0.10$, in steps of 0.02)

$Ba_{0.80-x}Ca_xPb_{0.20}\ Zr_{0.10}Ti_{0.90}O_3$ ($0 \leq x \leq 0.30$, in steps of 0.10)

Aliovalent ion substitution:

$Ba_{0.80-x}Sm_xPb_{0.20}\ Zr_{0.10}Ti_{0.90}O_3$ ($0 \leq x \leq 0.01$, in steps of 0.0025)

$Ba_{0.80-x}La_xPb_{0.20}\ Zr_{0.10}Ti_{0.90}O_3$ ($0 \leq x \leq 0.01$, in steps of 0.0025)

The research work carried out for this Ph.D. thesis has been divided in six chapters as summarized below briefly: -

The high dielectric constant of barium titanate (BT) and BZT-based electroceramics is responsible for selecting such materials for capacitor fabrication. Such materials have potential applications practical devices due to their good structural, electrical and ferroelectric properties. The properties can be tailored to suit specific requirements by molecular engineering using substitutions for both Ba site and Ti site. Due to this reason these materials have attracted the attention of many researchers. The introduction and importance of the BT based ceramics is discussed in ***Chapter 1***. Out of the different methods of preparation of ceramics solid state reaction route was adopted since it's an easy, cheap and high yielding method. ***Chapter 2*** mainly focused on the experimentation regarding the synthesis and characterization. Synthesis and characterization of $BaZr_{0.10}Ti_{0.90}O_3$ is discussed in ***Chapter 3.*** The effect of Two-stage sintering is also discussed in this chapter. Substituents like lead for Ba results in the increase in tetragonal to cubic phase transition temperature (Curie temperature) and decrease in room temperature dielectric constant. The temperature dependence of dielectric constant of lead substituted materials found to be better in comparison to pure barium titanate and undoped barium zirconate titanate. Substituents like zirconium for Ti results in the decrease in Curie temperature of the material, while increases the room temperature dielectric constant. It was interested to investigate the effect of Pb^{2+}, Ca^{2+} and Zr^{4+} on various physical properties of $BaTi_{0.90}Zr_{0.10}O_3$ ceramics. The investigated structural, electrical and ferroelectric properties are discussed in ***Chapter 4***. Owing to their special electronic configuration, aliovalent ions can act as donor as well as acceptors depending upon the amount of substitution. La^{3+} and Sm^{3+} ions act as softener for a very small amount of substitution. An investigation on the structural, electrical and ferroelectric properties of material composition $Ba_{0.80}Pb_{0.20}Zr_{0.10}Ti_{0.90}O_3$ substituted with La^{3+} and Sm^{3+} up to 1 mol% is shown in ***Chapter 5***. ***Chapter 6*** includes the conclusion and summary of the results and significance of the ceramics prepared.

List of Publications

Work included in thesis

1. *Relaxor Ferroelectric Behavior of La substituted BPZT ceramics*, J.K. Juneja, Parveen Kumar, Sangeeta Singh, Chandra Prakash and K.K. Raina, Ceramics International, **36**, 1277–1281, 2010.

2. *Synthesis and Dielectric Properties of Substituted Barium Titanate Ceramics,* Parveen Kumar, Sangeeta Singh, J.K. Juneja, Chandra Prakash and K.K. Raina, Journal of Alloys and Compound, **489**, 59-63, 2010.

3. *Dielectric Behavior of La Substituted BPZT Ceramics*, Parveen Kumar, Sangeeta Singh, J.K. Juneja, Chandra Prakash and K.K. Raina, Physica B, **404**, 2126-2129, 2009.

4. *Ferroelectric Properties of Substituted Barium Titanate Ceramics*, Parveen Kumar, Sangeeta Singh, J.K. Juneja, Chandra Prakash and K.K. Raina, Physica B, **404**, 1752-1756, 2009.

5. *Influence of Samarium Substitution on Dielectric Properties of Barium Titanate Based Ceramics*, Parveen Kumar, Sangeeta Singh, J.K. Juneja, Chandra Prakash and K.K. Raina, Modern Physics Letters B, **23**, 1-7, 2009.

6. *Dielectric Behavior of Pb Substituted BZT Ceramics*, Parveen Kumar, J.K. Juneja, Sangeeta Singh, Chandra Prakash and K.K. Raina, Bulletin of Materials Science, *in press*

7. *Effect of Zirconium Substitution on Structural and Dielectric Properties of* $Ba_{0.80}Pb_{0.20}TiO_3$ *Ceramics*, Parveen Kumar, Pratibha Singh, Sangeeta Singh, J.K. Juneja, Chandra Prakash and K.K. Raina, Integrated ferroelectrics, **122**, 16-22, 2010.

8. *Structural and Ferroelectric Properties of Lanthanum Modified BPZT Ceramics*, Parveen Kumar, J.K. Juneja, Sangeeta Singh, Chandra Prakash and K.K. Raina, Materials Chemistry and Physics, **125**, 660-663, 2011.

9. *Effect of Two-stage Sintering on Dielectric Properties of $BaTi_{0.9}Zr_{0.1}O_3$ Ceramics*, Rekha Rani, Renu Rani, Parveen Kumar, J.K. Juneja, Chandra Prakash and K.K. Raina, Phase Transitions, **84**, 843-849, 2011.

10. *Influence of Calcium Substitution on Structural and Electrical Properties of Substituted Barium Titanate*, Parveen Kumar, Sangeeta Singh, J.K. Juneja, Chandra Prakash and K.K. Raina, Ceramics International, **37**, 1697, 2011.

Work not included in thesis

11. *Structural, Dielectric and Ferroelectric Properties of Mn doped $Ba_{0.80}Pb_{0.20}Ti_{0.90}Zr_{0.10}O_3$ ceramics*, Parveen Kumar, Sangeeta Singh, J.K. Juneja, Chandra Prakash and K.K. Raina, Ferroelectric Letters, **37**, 110-115, 2010.

12. *Effect of Two-Stage Sintering on Dielectric and Ferroelectric Properties of $Ba_{0.80}Pb_{0.20}TiO_3$ Ceramics*, Parveen Kumar, Pratibha Singh, Sangeeta Singh, J.K. Juneja, Chandra Prakash and K.K. Raina, Ferroelectric Letters, **36**, 92-101, 2009.

13. *Dielectric and Ferroelectric Properties of BST and Ni-Zn Ferrite Composites*, Renu Rani, Parveen Kumar**,** Sangeeta Singh, J.K. Juneja, Chandra Prakash and K.K. Raina, Integrated ferroelectrics, **122**, 38-44, 2010.

14. *Improved Properties of $BaTiO_3$ Ceramics Prepared by Ultrasonic mixing*, Parveen Kumar, Pratibha Singh, Sangeeta Singh, J.K. Juneja, Chandra Prakash and K.K. Raina, Integrated ferroelectrics, **122**, 114-118, 2010.

15. *Ferroelectric Properties of Microwave Processed PZT-NiZn Ferrite Composites*, Rekha Rani, Parveen Kumar**,** Sangeeta Singh, J.K. Juneja, Chandra Prakash and K.K. Raina, Integrated ferroelectrics, **122**, 45-51, 2010.

16. *Improved properties of Li-Mn-Ti ferrites by microwave sintering*, Mamata Maisnam, Sumitra Phanjoubam, Parveen Kumar**,** JK Juneja, Ashok Kumar and Chandra Prakash, Integrated ferroelectrics, **122**, 31-37, 2010.

17. *Dielectric Properties of La Doped 0.95PZT-0.05NZF Composites,* Rekha Rani, Parveen Kumar**,** J.K. Juneja, Chandra Prakash and K.K. Raina, Advances in Condensed Matter Physics, *In press.*

18. *Influence of Zr Substitution on Ferroelectric Properties of BST ceramics,* Renu Rani, Parveen Kumar, Sangeeta Singh, J.K. Juneja, K.K. Raina and Chandra Prakash, Ferroelectric Letters, *In Press.*

19. *Improved Dielectric Properties via Mechano-Chemical Activation in* $Ba_{0.80}Pb_{0.20}TiO_3$ *Ceramics*, Parveen Kumar, Renu Rani, Sangeeta Singh, J.K. Juneja, K.K. Raina and Chandra Prakash, AIP Proceedings, *Accepted.*

20. *Improved Properties of Pb Based BLZT Ferroelectric Ceramics,* Parveen Kumar, Sangeeta Singh, J.K. Juneja, K.K. Raina and Chandra Prakash, AIP Proceedings, *Accepted.*

21. *Structural, Dielectric and Ferroelectric Properties of* $Ba_{0.9}Sr_{0.1}TiO_3$ *and Mn doped Ni-Zn Ferrite Composites,* Renu Rani, Parveen Kumar, Sangeeta Singh, J.K. Juneja, K.K. Raina and Chandra Prakash, Ceramics International, *Under final review*.

22. *Dielectric and Ferroelectric Properties of Strontium Substituted* $BaTiO_3$ *and Mn-doped Ni-Zn Ferrite Composites*, Renu Rani, Parveen Kumar, Sangeeta Singh, J.K. Juneja, K.K. Raina and Chandra Prakash, Bulletin of Material Sciences, *Communicated.*

Conferences Attended:

1. *Electrical Properties of Ti Substituted Lithium Ferrites Prepared by Mechanical Alloying*, Kavita Sharma, Parveen Kumar, Sangeeta Singh, J.K. Juneja and Chandra Prakash, International Conference on Magnetic Materials-2008, NPL, New Delhi

2. *Structural and Dielectric Properties of BST Ceramics Prepared by Microwave Processing*, Renu Dahiya, Rekha Gandhi, Parveen Kumar, Sangeeta Singh, J.K. Juneja, Chandra Prakash, K.K. Raina, International Symposium on Nano Materials-2009, Jalandhar

3. *Effects of samarium doping on the ferroelectric properties of modified lead zirconate titanate ceramics*, Pratibha Singh, Parveen Kumar, Sangeeta Singh, J.K. Juneja, Chandra Prakash and K.K. Raina, International Conference on Electroceramics, 13-17 December-2009, New Delhi**.**

4. *Structural and Dielectric Properties of BPZT ceramics*, Parveen Kumar, Sangeeta Singh, J.K. Juneja, Chandra Prakash and K.K. Raina, NSE-2007, GVMGC, Sonipat.

5. *Two-Stage Sintered substituted Barium Titanate Ceramics*, Parveen Kumar, Sangeeta Singh, J.K. Juneja, Chandra Prakash and K.K. Raina, NSFD-2008, Thapar University, Patiala.

6. *Effect of La doping on the dielectric properties of BPZT Ceramics*, Parveen Kumar, Sangeeta Singh, J.K. Juneja, Chandra Prakash and K.K. Raina, NCPMS-2008, GJU, Hissar.

7. *Synthesis and Dielectric Behavior of Sm Substituted Barium Titanate Based Ceramics*, Parveen Kumar, Sangeeta Singh, J.K. Juneja, Chandra Prakash and K.K. Raina, EPSDP-2009_Abhohar.

TABLE OF CONTENTS

LIST OF FIGURES

Chapter 1

Chapter 2

Chapter 3

Chapter 4

Chapter 5

LIST OF TABLES

Chapter 1

Chapter 3

Chapter 4

Chapter 5

Chapter 1

Introduction

This chapter includes a brief introduction about electroceramics which includes dielectric, ferroelectric and piezoelectric materials. Barium titanate is the most investigated ferroelectric material due to its large number of applications like Multi Layered Ceramic Capacitors (MLCC), actuators and PTCR. Still there is a large scope for further investigations and improvements in its properties as the properties extensively depends on the substitution and processing techniques used. Recent developments on the substituted barium titanate are reviewed here. Emphasis is on the discussion on the effect of substitution on the structural, electrical and ferroelectric properties of substituted barium titanate which is the subject of investigation in the present thesis.

1.1 Background

There are approximately 100 elements, each possessing a unique electronic configuration determined by its atomic number Z, and the spatial distribution and energies of their electrons. These can be classified as metallic, gaseous, or nonmetallic elemental solids. A very few of them are used in their pure form; most often they are alloyed or reacted with other elements to form engineering materials. The later can be broadly classified as metals, polymers, semiconductors, or ceramics. Each class has its distinctive properties that reflect the differences in the nature of the bonding. In metals, the bonding is metallic in nature, where delocalized electrons provide force that holds the positive ions together. Polymers consist of very long C-based chains to which other organic atoms and molecules are attached. Semiconductors are covalently bonded solids which includes Si, Ge, GaAs, CdTe, and InP. The presence of strong covalent bonds holding semiconductors together make their mechanical properties quite similar to those of ceramics which are brittle and hard. Ceramics can be defined as solid compounds that are formed by the application of heat, and sometimes heat and pressure. Due to the large number of chemical, electrical, biological, and mechanical properties of ceramics, they are used extensively in many domestic and industrial applications. In the electronic and manufacturing industries, which require materials sustaining extremely high temperatures and corrosive environments, high-tech ceramics play important role [1-4].

Ceramics are different from glasses and single crystals as they are composed of an aggregate of randomly oriented crystallites intimately bonded together to form a solid and have anisotropic character and are polycrystalline materials. All the crystals, existing in nature, can be grouped into seven crystal systems as shown in figure 1.1.

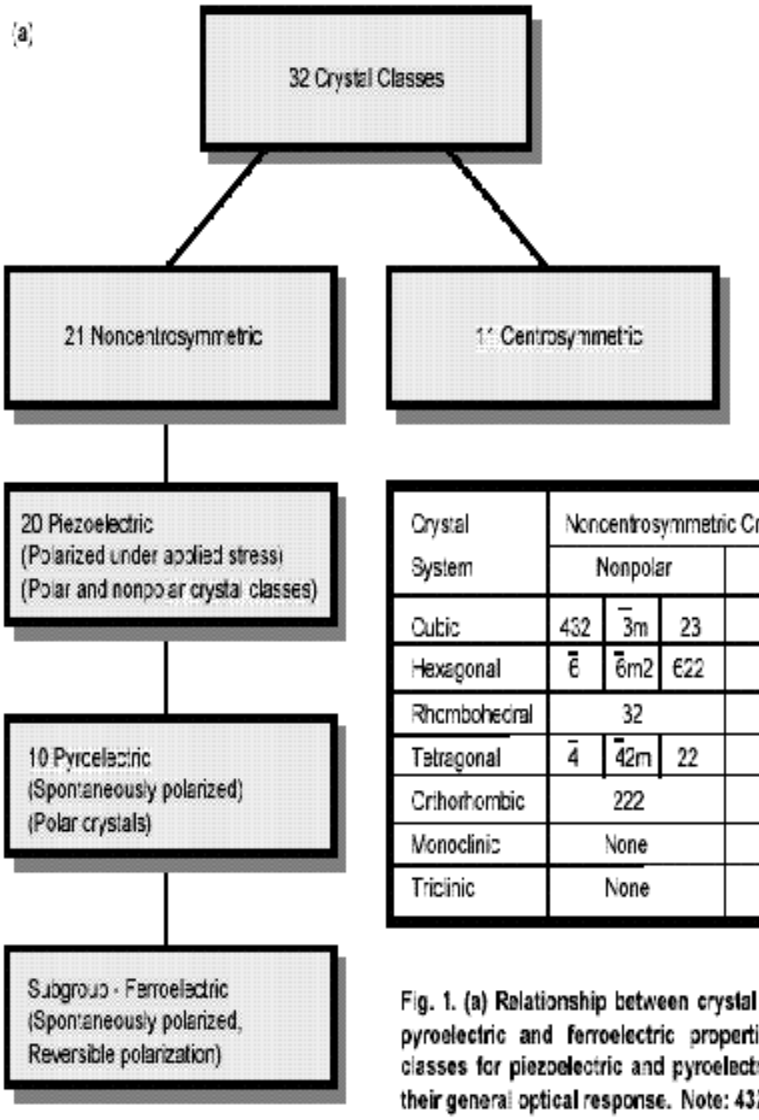

(b)

Crystal System	Noncentrosymmetric Crystal Classes					Optic Axes
	Nonpolar			Polar		
Cubic	432	$\bar{3}$m	23	None		Isotropic
Hexagonal	$\bar{6}$	$\bar{6}$m2	622	6	6mm	Uniaxial
Rhombohedral	32			3	3m	
Tetragonal	$\bar{4}$	$\bar{4}$2m	22	4	4mm	
Orthorhombic	222			mm2		Biaxial
Monoclinic	None			2	m	
Triclinic	None			1		

Fig. 1. (a) Relationship between crystal classes and piezoelectric, pyroelectric and ferroelectric properties. (b) Specific crystal classes for piezoelectric and pyroelectric materials together with their general optical response. Note: 432 is not piezoelectric.

Depending on the symmetry elements, these seven crystal systems can be subdivided into 32 point groups, where a point group is a combination of symmetry elements. Out of these, only 21 belong to non-centrosymmetric classes. All but one are piezoelectric, means they exhibit electrical polarity when subjected to stress. Again out of 20 piezoelectric crystal classes, 10 possess a spontaneous polarization, which is temperature dependent and these are known as pyroelectric materials. There exists a subclass of pyroelectric materials, which have two or more orientation states of polarization in the absence of an electric field. The

polarization in these materials can be switched from one state to other with the application of an electric field and are known as ferroelectric materials. The area of interest in the present work is related to substituted barium titanate ferroelectric ceramics, which are a highly specialized class of materials, termed as electroceramics. Their properties are predominantly controlled by their composition, microstructure and processing methodology.

1.1.1 Introduction to Ferroelectricity

Ferroelectricity discovered by P. Seignette in 1921 is one of the fastest-growing fields of Solid-State Physics. It has been also called Seignette electricity, as Seignette or Rochelle salt was the first material found to show ferroelectric properties. Unfortunately, the Rochelle salt loses its ferroelectric properties if the composition is slightly changed, which made it rather unattractive for industrial applications [5]. In 1945, ferroelectric behavior was reported in BaTiO3 which is a material of stable perovskite type, which is one of the fundamental crystal lattice structures. The main applications are high dielectric constant capacitors, piezoelectric sonar and ultrasonic transducers, radio and communication filters, pyroelectric security surveillance devices, medical diagnostic transducers, stereo tweeters, buzzers, gas ignitors, positive temperature coefficient (PTC) sensors and switches, ultrasonic motors, electrooptic light valves, thin-film capacitors, and ferroelectric thin film memories. Several excellent articles on the history of ferroelectricity have been written [6-8].

1.1.2 General Features of Ferroelectrics

1.1.2a Definition

The materials which possess the spontaneous polarization even in the absence of an electric field and the direction of spontaneous polarization can be changed by an applied electric field are called ferroelectric materials and this phenomena of switching of polarization is called ferroelectricity [9]. According to the nature of chemical bonds, crystalline ferroelectrics may be classified into four types:

(i) Tungston Bronze ($PbNb_2O_6$)

(ii) Pyrchlore ($Cd_2Nb_2O_{7)}$

(iii) Layer Structure ($Bi_4Ti_3O_{12}$)

(iv) Oxygen Octahedral {BaTiO3, PZT, PLZT, PMN, (Na,K)NbO3}

Most of the useful ferroelectrics, such as barium titanate (BT), barium zirconate titanate (BZT), barium strontium titanate (BST), lead titanate ($PbTiO_3$), lead zirconate titanate (PZT) and potassium niobate ($KNbO_3$), have perovskite structure. Perovskite is the mineral name of calcium titanate ($CaTiO_3$). A brief explanation about ferroelectric materials with perovskite structure is given in the next section.

1.1.2b Perovskite Crystal Structure

Its simplest structure is cubic, which is the high temperature form for many mixed oxides of ABO_3 type, where A is a large radius cation, which occupies the empty sites between O_2 octahedra, while B is a small radius cation, which occupies the center of the octahedron, formed by O_2^- ions.

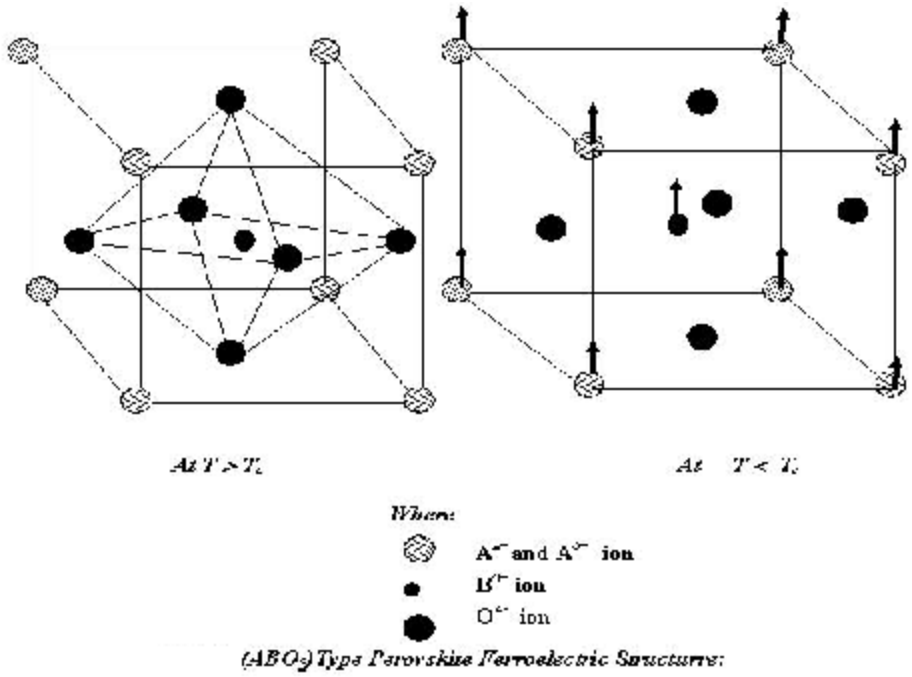

Figure 1.2. A cubic ABO_3 perovskite-type unit cell

Most perovskite-type ferroelectrics are compounds with either $A^{2+}B^{4+}O_3^{2-}$ or $A^{1+}B^{5+}O_3^{2-}$type formula. The structure is also very tolerant to cation substitution to both A and B sites of lattice, and hence may lead to more complex compounds, such as $(K_{1/2}Bi_{1/2})TiO_3$, $Pb(Fe_{1/2}Ta_{1/2})O_3$, $Pb(Mg_{1/3}Nb_{2/3})O_3$, and $Pb(Zn_{1/3}Nb_{2/3})O_3$ [10,11]. The most important member of the tetragonal phosphates is potassium dihydrogen phosphate (KH_2PO_4), commonly abbreviated as KDP. But in Rochelle and KDP, ferroelectricity is present at low temperatures due to their T_c points, +23 and -150 ^oC, respectively. Thus for study of the ferroelectric effect, these crystals are ideal materials. However, from the device application point of view, water solubility, low T_C points, and low polarization values are limiting factors [12,13]. In 1945, when ferroelectric behavior was observed in barium titanate ($BaTiO_3$), due to its perovskite structure, better ferroelectric properties, chemical and

mechanical stability, barium titanate (BT) became one of the most extensively studied ferroelectric material, it was considered not only as a model system for ferroelectricity, but also for practical applications. In addition, it also exhibits ferroelectric properties at and above room temperature and can be easily prepared and used in the form of polycrystalline samples [14].

Ferroelectricity is characteristics of compounds with distorted perovskite structure. The distortion of oxygen octahedra, leading to ferroelectricity is shown in figure 1.2.There exits a characteristic temperature known as Curie Temperature (T_c), below which the perovskite unit cell is non-centrosymmetric and at $T > T_c$, perovskite unit cell becomes symmetric and the material is in paraelectric state. The explanation of transition temperatures is given in the next section.

1.1.2c Ferroelectric Phase Transitions

In most cases, ferroelectrics have a transition temperature called, the Curie points, T_c. For temperature $T>T_c$, the crystal does not exhibit ferroelectricity, while for $T<Tc$ it is ferroelectric. On decreasing the temperature through Curie point, a phase transition from a non-ferroelectric phase to a ferroelectric phase occurs. If there are more than one ferroelectric phases, the temperature at which the crystal transforms from one ferroelectric phase to another is called the transition temperature. Near the Curie point or phase transition temperatures, properties including dielectric, elastic, optical, and thermal constants show an anomalous behavior. The temperature dependence of the dielectric constant above the Curie point (T>Tc) in most ferroelectric crystals is governed by the Curie- Weiss law [15-17].

$$\varepsilon = \varepsilon_o + \frac{C}{(T - T_o)} \qquad \text{...1.1}$$

where ε is the permittivity of the material, ε_o is the free space permittivity, C is the Curie constant and T_o is the Curie-Weiss temperature. The Curie-Weiss temperature T_o is, different from the Curie point T_c. There are three types of phase transitions on the basis of behavior of dielectric constant with temperature; first order, second order and diffused phase transition (relaxor behavior). These are shown in figure 1.3. For first order transitions, $T_o < T_c$ while for second order phase transitions, $T_o = T_c$ [17]. The order of the phase transition is defined by the discontinuity in the partial derivatives of the Gibbs free energy (G) of the ferroelectric at the phase transition temperature [18]. For the nth-order phase transition, *n*th-order derivative of G is a discontinuous function at the transition temperature.

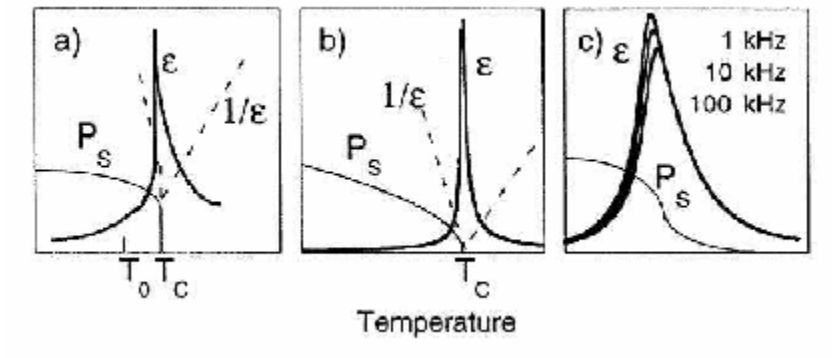

Figure 1.3. Schematic temperature dependence of the dielectric permittivity (ε) and spontaneous polarization P_s for (a) a first-order, (b) a second-order ferroelectric and (c) a relaxor ferroelectric **[18]**

Thus, spontaneous polarization and strain change continuously at the phase transition for a ferroelectric with the second order phase transition, and are discontinuous at the phase

transition temperature for first-order ferroelectrics. Many ferroelectrics show diffuse phase transition behavior. These ferroelectrics are known as relaxor ferroelectrics. General property changes with ferroelectric phase transitions and are summarized in figure 1.3, schematically. The dielectric anomaly is not a definite proof of ferroelectricity, which is normally confirmed by hysteresis loop.

1.1.2d Ferroelectric Domains and Hysteresis Loop Behavior

Ferroelectrics possess regions with uniform polarization called ferroelectric domain. With-in a domain all the electric dipoles are aligned in the same direction. There may be many domains in a crystal separated by interfaces called domain walls [19]. A single domain can be obtained by domain wall motion, which can be possible, by the application of an electric field. A very strong field could lead to the reversal of the polarization in the domains known as domain switching. Thus, the most distinguishing feature between pyroelectric and ferroelectric material is that the direction of the spontaneous polarization in ferroelectrics can be switched by an applied electric field. The polarization reversal can be observed by measuring the ferroelectric hysteresis [20] as shown in figure 1.4. The starting point is assumed to be at A. As the electric field strength is increased, the domain starts to align in the positive direction, giving rise to rapid increase in the polarization (curve A). At very high field levels, the polarization saturates. The polarization does not fall to zero when the external field is removed. At zero external fields, some of the domains remain aligned in the positive direction hence the crystal will show a remnant polarization P_r. The crystal cannot be completely depolarized until a certain field is applied in the reverse direction. The external field needed to reduce the polarization to zero is called the coercive field strength, E_c. If the field is increased further to more negative value, the direction of polarization flips and hence

a hysteresis loop is obtained. The value of spontaneous polarization P_s, is obtained by extrapolating the curve of saturated polarization at point C, onto the polarization axis [20].

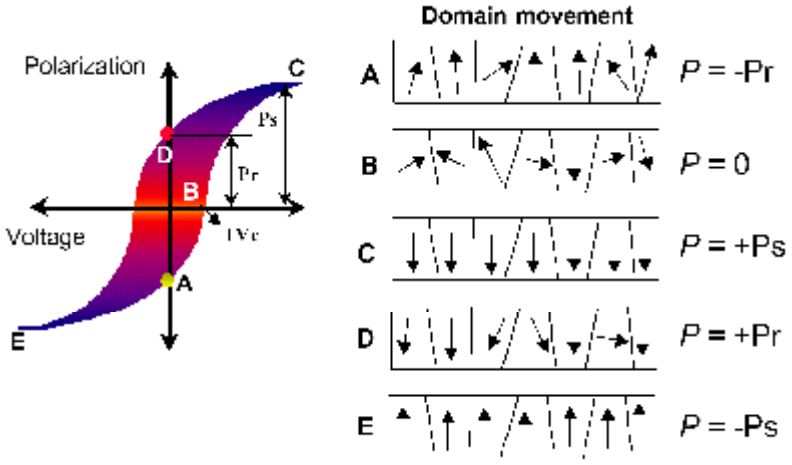

Figure 1.4. Ferroelectric (P-E) hysteresis loop

1.1.2e Poling

As the ceramics are polycrystalline material and posses no net polarization and hence can be used for applications exploiting its piezoelectric or pyroelectric properties. In order to put the materials for practical applications, domains are aligned in one direction by applying high electric field. This process is called poling. In this process, a high electric field is applied on the ferroelectric ceramic samples to force the domains to reorient in the direction of the applied electric field. Poling is possible only in ferroelectric materials and the various poling steps are shown in figure 1.5. Before poling, the ferroelectric ceramic does not possess any piezoelectric and pyroelectric properties because of the random orientation of the ferroelectric domains in the ceramics. For domain reorientation, a poling field must be applied on the sample and maintained for certain duration of time. As crystalline anisotropy and coercive field, E_c, of the ferroelectric materials decreases with the increase in poling

temperature. Thus, for a given field and poling time, better domain rearrangement results at higher temperature, but lower than T_c. Also, with increasing temperature, space charges, which act against domain motion, decreases in ceramic materials. However, when the poling temperature is too high, problems arise as the electrical conductivity increases and the consequent increase in leakage current would result in sample breakdown during the poling process. For poling the sample is heated to a suitable temperature and high d.c. electric field is applied for an hour. Then sample is allowed to cool to room temperature in the presence of applied and field is removed at room temperature. After poling, a remnant polarization and remnant strain are maintained within the material, and it starts exhibiting piezoelectric and pyroelectric effects [21].

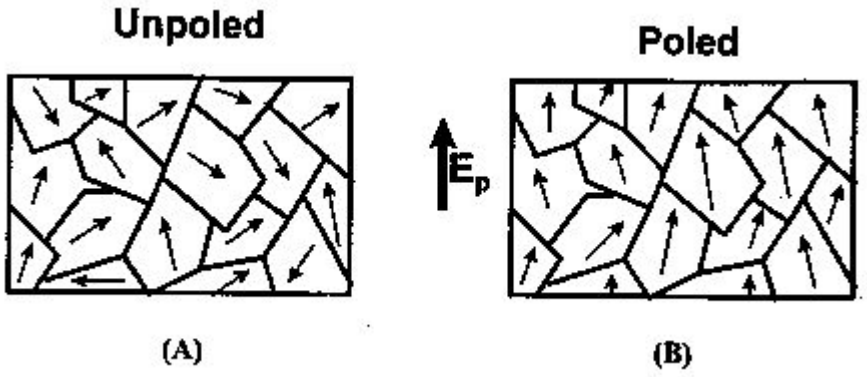

Figure 1.5. Poling of a ferroelectric material

1.1.3 Piezoelectricity

Piezoelectricity**,** a property possessed by selected group of material as discussed in section 1.1, was discovered in 1880 by Jacques and Pierre Curie during their systematic study of the effect of pressure on the generation of electrical charge by crystals, such as quartz, zincblende, and tourmaline. The name "piezo" is a Greek word, meaning, "pressure," hence; piezoelectricity is the generation of electricity as a result of a mechanical pressure [22]. It follows that a piezoelectric material develops a potential across its boundaries when subjected to a mechanical stress (or pressure), called direct piezoelectric effect. This property is exploited to make sensors. Conversely, when an electric field is applied to piezoelectric material, a mechanical deformation takes place. This is called converse piezoelectric effect and the material can be used to make actuator. Thus the piezoelectric material can be used as sensor and actuator both and hence often called as smart material. These materials are being used extensively in smart systems, which consist of a sensor, actuator and control system. Ferroelectricity is a subgroup of piezoelectricity. It is a linear effect that is related to the microscopic structure of the solid. The microscopic origin of the piezoelectric effect is the displacement of ionic charges within a crystal structure. In the absence of the external stress, the charge distribution within the crystal is symmetric and the net electric dipole moment is zero. However, when an external stress is applied, the charges are displaced and the charge distribution is no longer symmetric. A net polarization develops and results in an internal electric field. A material can only be piezoelectric if the unit cell has no center of inversion.

1.1.3a Piezoelectric Parameters and Relations

A piezoelectric ceramic is anisotropic in nature i.e. their physical properties are different in different directions. A piezoelectric can be represented by different constants that relate to both the direction of applied mechanical or electrical force and to the directions perpendicular to the applied force. Consequently, each constant has two subscripts that refer to the directions of two related quantities. The direction of positive polarization usually is made to coincide with the z-axis of a rectangular system of X, Y, Z axes [Figure 1.6]. Direction X, Y, Z is represented by the subscripts 1, 2, or 3, respectively, and shear about one of these axes is represented by the subscripts 4, 5, or 6, respectively.

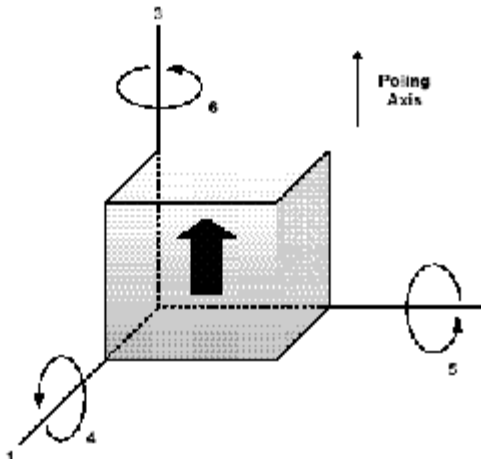

Figure 1.6. Direction of force affecting a piezoelectric element

Two effects are operative in piezoelectric crystals. The direct effect (designated as a generator) is identified with the phenomenon whereby electrical charge (polarization) is generated from mechanical stress, whereas the converse effect (designated as a motor) is

associated with the mechanical movement generated by the application of an electrical field. The basic equations that describe these two effects in regard to electric and elastic properties are

$$D = dE + \varepsilon^T E \quad \text{(generator)} \quad \ldots 1.2$$

$$S = s^E T + dE \quad \text{(motor)} \quad \ldots 1.3$$

where, **D** is dielectric displacement (or polarization), **T** is stress, **E** is electric field, **S** is strain, **d** is piezoelectric coefficient, s is material compliance (inverse of modulus of elasticity), and ε is the dielectric constant. The superscript indicates a quantity held constant: in the case ε^T, stress is held constant, which means that the piezoelectric element is mechanically unconstrained, and in the case of $\mathbf{s}^E$, the electric field is held constant, which means that the electrodes on the element are shorted together.

1.1.3b Piezoelectric Charge Coefficient (d)

All the properties like **D** and **S** are directional quantities, e.g. $\mathbf{d_{31}}$ indicated that this piezoelectric charge coefficient relates to the generation of polarization (direct effect) in the electrode perpendicular to 3 or vertical direction and to the stress mechanically applied in 1 or lateral direction; $\mathbf{d_{33}}$ indicates the polarization generated in the 3 direction when the stress is applied in the 3 direction. They are related as:

$$D_3 = d_{33} T_3 \quad \text{(direct effect)} \quad \ldots\ldots 1.4$$

$$S_3 = d_{33} E_3 \quad \text{(converse effect)} \quad \ldots\ldots 1.5$$

The d coefficients are numerically equal in both equations. The d coefficients are usually expressed as $\times 10^{-12}$ Coulomb/Newton C/N for direct effect and $\times 10^{-12}$ m/V for converse effect.

1.1.3c Hydrostatic Charge Coefficient (d_h)

It corresponds to the effect of development of charge when a pressure is applied on the material. Hydrostatic charge coefficient (d_h) is related to d_{33} and d_{31} piezoelectric charge constants by the relation

$$d_h = d_{33} + 2d_{31} \qquad \textbf{…1.6}$$

and is measured in (C/N) units.

1.1.3d Piezoelectric Voltage Constant (g)

It gives the electric field produced by a stress in a piezoelectric material. Its usual units are meter volts / Newton and ‘g’ constant is related to the ‘d’ constant by the permittivity

$$\mathbf{g = d / (\varepsilon \varepsilon_o)} \qquad \textbf{…1.7}$$

where g is called the piezoelectric voltage coefficient, ε and ε_o are the dielectric constant of the material and permittivity of the free space, respectively. Corresponding to d_{33} and d_{31} piezoelectric constants, there exist g_{33} and g_{31} piezoelectric voltage coefficients.

High ‘g’ constant is desirable in materials intended to generate voltages in response to a mechanical stress, as in a phonograph pickup.

1.1.3e Hydrostatic Voltage Coefficient (g_h)

It gives the field produced by a pressure. It is related to the g_{33} and g_{31} piezoelectric charge coefficients by the relation

$$g_h = g_{33} + 2g_{31} \qquad \text{…1.8}$$

and its usual units are meter volts/Newton.

1.1.3f Electromechanical Coupling Factor (k)

The electromechanical coupling factor ($\mathbf{k_{33}}$, $\mathbf{k_{31}}$ and $\mathbf{k_p}$) represent the mechanical energy accumulated in a ceramic or crystal and is related to the total electric input (or vice versa). It is defined as the square root of the ratio of energy output in mechanical form to the total input electrical energy. These electromechanical coupling factors are material constants and they depend on degree of poling for piezoelectric ceramic. Electrical poling has little effect on these coupling factors, for relaxor material but they do get affected by reverse poling process. These coupling factors can be calculated for each individual vibration mode by using the resonant (f_r or f_m) and anti-resonant frequencies (f_a or f_n) from any immittance plots (Z″ vs frequency or Y″ vs frequency or ε vs frequency) and the application formula for ceramic disc are shown here [23,24]

$$k_{eff}^2 = \frac{(f_a^2 - f_r^2)}{f_a^2} \qquad \text{…1.9}$$

$$k_p^2 = 2.51x\frac{(f_a - f_r)}{f_r} \qquad \text{…1.10}$$

$$k_{31}^2 = 0.5(1-\sigma) \times k_p^2 \quad \text{...1.11}$$

$$k_t^2 = k_{33}^2 = r \times Cot(r)\, r \times \tan\left(\frac{\pi}{2} - r\right) \text{ where } r = (\pi \times f_r)/(2f_a) \quad \text{...1.12}$$

Where k_{eff} is the effective electromechanical coupling coefficient, k_p is the planar or radial mode coupling coefficient, k_{31} is the coupling coefficient for length wise vibration (direction of vibration is perpendicular to the direction of polarization) and k_{33} (or k_t) is the coupling coefficient for longitudinal or thickness vibration (direction of vibration and polarization is same). These electromechanical coupling factors are commonly used as a figure of merit for piezoelectric materials. High values of k values are most desirable and constantly sought in new materials.

1.1.4 Barium Titanate Based Ceramics

Lead based and barium based perovskites are known to show strong ferroelectricity. Among these, $BaTiO_3$ is the most investigated ferroelectric material, which reveals many aspects of ferroelectricity. Discovered in 1940's, Barium titanate has been an interesting material as it is chemically and mechanically stable and shows ferroelectricity at and above room temperature. The detailed understanding of these materials was given by Cochran [25].

1.1.4a Crystal Structure

Barium titanate is a ferroelectric material with a Curie temperature (120 ^{o}C) at which the phase transition from the cubic paraelectric phase (above Curie temperature) to the tetragonal ferroelectric phase (below Curie temperature) occurs. It has perovskite-type structure and has the general chemical formula ABO_3, where O is oxygen, A represents a cation with a larger ionic radius (Ba) and B a cation with a smaller ionic radius (Ti). Being a larger ion Ba occupy A site whereas B site occupied by smaller Ti ion. Many ions satisfying conditions of radii and charge valence can replace the A and B-site ions.

1.1.4b Phase Transition in $BaTiO_3$

Below the 120 ^{o}C Barium Titanate under goes through a displacive transition to a tetragonal with point group 4mm. This is a polar phase with a spontaneous polarization along the tetragonal C axis, which is parallel to the <100> direction of the original cubic cell, making the material a ferroelectric at room temperature (Figure 1.7 b). The tetragonal phase of barium titanate has been the subject of most of investigations since the phase is structurally simple and also stable at room temperature. At lower temperatures, it undergoes two more structural transitions, which are in the ferroelectric state with different polar axis. Around 5 ^{o}C, the polar axis changes into the face diagonal and the structure becomes orthorhombic (Figure 1.7 c). At –90 ^{o}C, the polar axis again changes to body diagonal and the structure remains in the rhombohedral phase below this temperature (Figure 1.7 d) [13].

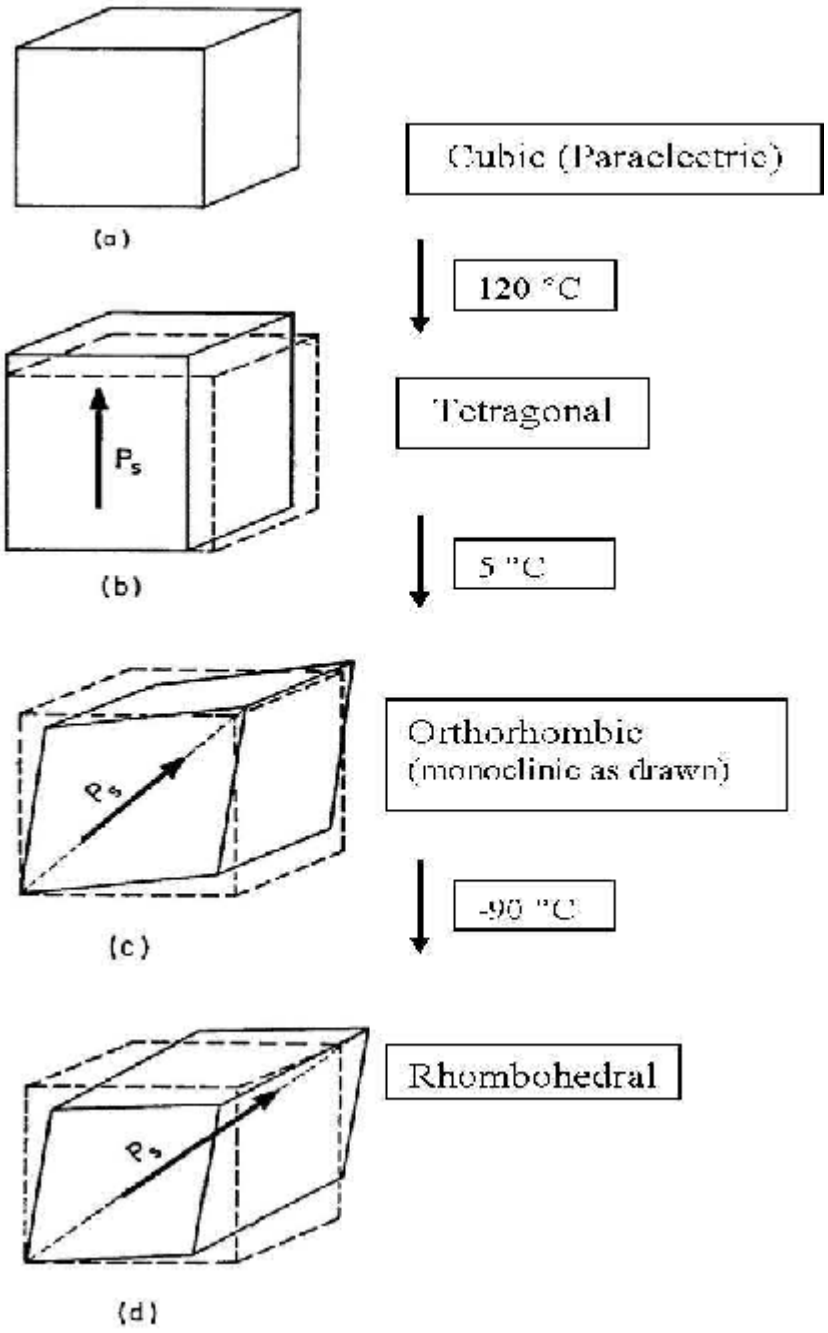

Figure 1.7. Phase transition in $BaTiO_3$

1.1.4c Effect of Substituents in $BaTiO_3$

A lot of research activity has been driven by the need for improved materials with enhanced properties, and to a great extent the required improvements have been achieved by careful optimization to enhance a desired property through appropriate substitutions and, modifications in the processing conditions. Much of the earlier reported studies emphasize that the observed changes in the $BaTiO_3$ based compositions depend on both: substitution and the composition, and accordingly different types of behaviour have been noticed in some of the binary systems derived from $BaTiO_3$. Isovalent dopants are commonly used to alter T_c and the lower temperature orthorhombic/tetragonal [O/T] and rhombohedral /orthorhombic [R/O] phase transition temperatures, hereafter referred as $T_{O/T}$ and $T_{R/O}$ respectively. A-site doping with cations of the same valence as Ba causes the Curie temperature T_c (120^{o}C in $BaTiO_3$) to either decrease (Sr substitution) or increase (Pb substitution), without any significant broadening of phase transition. With B-site doping, the ferroelectric domains, which are associated with a cooperative off-centre displacement of Ti^{4+} ions in their TiO_6 octahedra are disrupted, which often leads to a broadening of transition peak at T_c. Partial replacement of titanium by tin (Sn), Zirconium (Zr) or hafanium (Hf) generally leads in reduction in T_c.

Amongst all the compositions investigated so far $Ba(Zr_xTi_{1-x})O_3$ (BZT) has attracted a lot of interest. An increase in the Zr content induces a reduction in the average grain size, decreases the dielectric constant and provides greater stability and lowers the leakage current level.

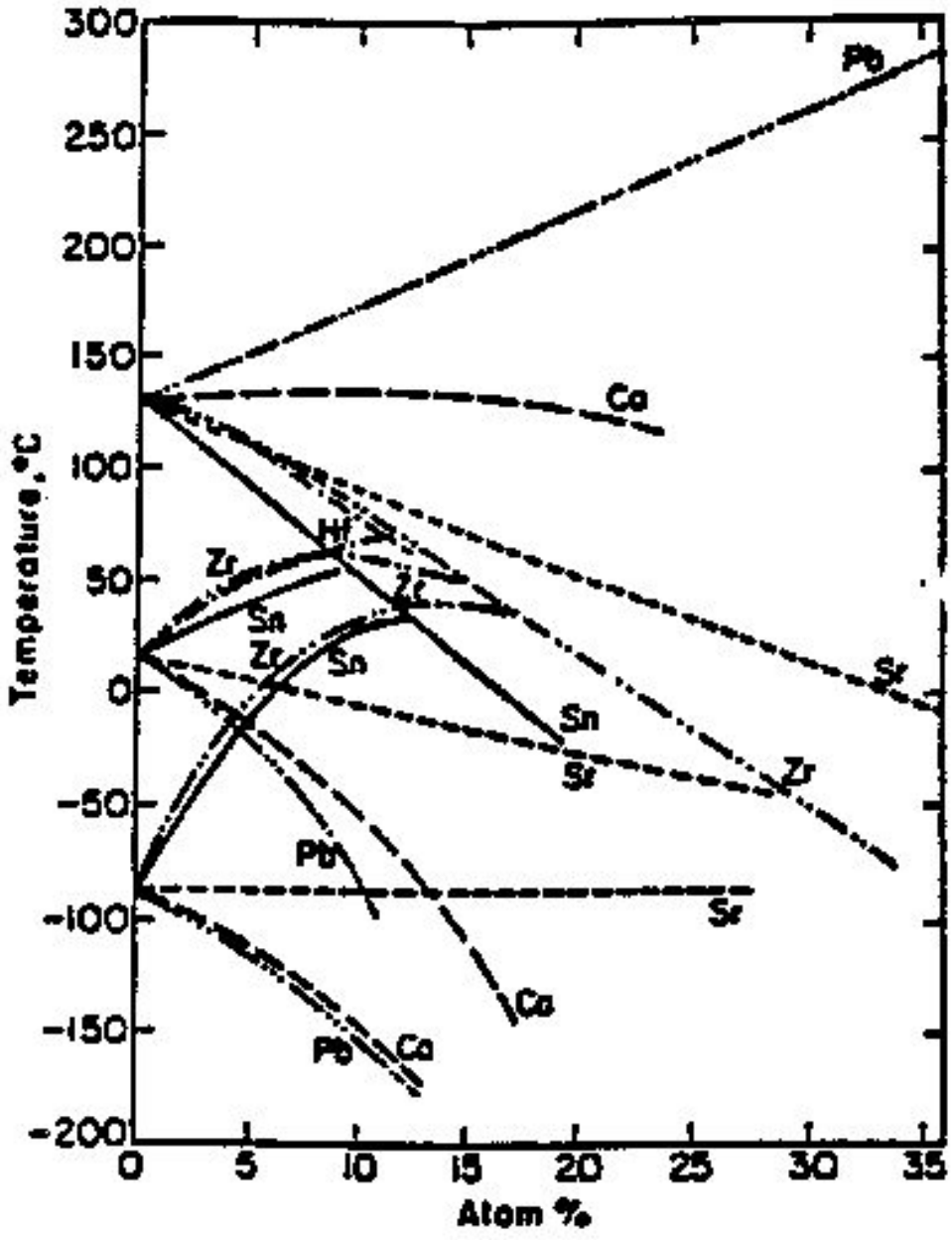

Figure 1.8. Dependence of Curie temperature of $BaTiO_3$

upon various additions

Zr is found to play an interesting role here because a different character of dielectric response with respect to the ferroelectric-to-paraelectric phase transition can be achieved by the substitution of Zr for Ti in $BaTiO_3$. The Zr^{4+} (0.72Å) ion is chemically more stable than

the Ti^{4+}(0.60Å) and high dielectric constant values of this material make it useful for device application. BZT is the solid solution of $BaTiO_3$ and $BaZrO_3$ [$Ba(Zr_xTi_{1-x})O_3$] and has been identified as one of the most attractive compositions for dielectric applications in multilayer ceramic capacitor (MLCs) applications [26]. The effect of some A and B-site isovalent dopants on the phase transition temperatures are summarized in Fig.8. A-site doping with Sr^{2+} results in decrease of both T_c and $T_{O/T}$ whereas $T_{R/O}$ is unaffected. T_c increases linearly with Pb^{2+} substitution, however Ca^{2+} doping has negligible effect upto ~10 mole %. The behavior observed with Sr^{2+} doping is normally explained as a cation size effect, whereby the smaller ionic radius of Sr^{2+} compared to Ba^{2+} stabilizes the cubic polymorph, thus decreasing T_c. The effect of A-site doping with Pb^{2+} or Ca^{2+} on T_c, however, cannot be explained on the basis of cation radii. Although many isovalent A-site dopants are effective in displacing or "shifting" T_c they do not have a dramatic effect on the value of ε_{max} and on the profile of $d\varepsilon/dT$. The introduction of isovalent cations on B-site, however, can have significant effect on ε_{max} and $d\varepsilon/dT$. Common B-site dopants such as Zr^{4+} and Sn^{4+} causes a linear decrease in T_c, whereas both $T_{O/T}$ and $T_{R/O}$ increase. The reduction in T_c is essentially accompanied by an increase in ε_{max}, but with continuous substitution ε_{max} decreases and becomes increasingly broad. This behavior is commonly called as "pinching" and it's attributed to the coalescence of the three phase transition temperatures at a certain dopant amount and thus overlaps of three permittivity maxima associated with the individual phase transition [21].

1.2 Substituted Barium Titanate ($BaTiO_3$) – A literature survey

F.W. Perry and G.A. Hutchins investigated the compositional inhomogeneity of (Ba,Pb)TiO_3 crystals [27]. In the year of 1971, Yu. N. Venevtsev studied a ferroelectric family of barium titanate ceramics [28]. Brajer and Kulscar showed that increasing Zr content increases the orthorhombic-tetragonal phase transition temperature, while tetragonal-cubic phase transition temperature decreases [29,30]. The first observation on the influence of Zr content on the rhombohedral-cubic phase transition temperatures was reported by Hellicar and Verbiskaja et al. for Zr contents of >15% [31,32]. Other authors have assumed a coexistence of both the orthorhombic and tetragonal phase within a small temperature interval at the Curie point T_c. Hennings et al. gave an explanation of the temperature characteristics of the permittivity. This observation leads to a change from first order to second order transitions at low zirconium contents. Further increase in the amount of Zr results in a stimulated broadening of the dielectric constant versus temperature curve. This phenomenon is due to the increased sensitivity of the ceramic, relative to local structural transitions in the vicinity of the T_c, which leads to a distribution of curie maximum and, thus, a broad resulting envelope. This phenomenon is called a diffuse phase transition (DPT) and appears for zirconium content of >13 % [33]. Recently, many researchers have concentrated on studying the normal ferroelectric to relaxor behavior of BZT ceramics. Due to its low leakage current it proved to be an important material for micro-electro-mechanical systems (MEMS) [34-36]. Yu et al. reported the ferroelectric relaxor behavior in $Ba(Ti_{1-x}Zr_x)O_3$ (x=0.30) ceramics and its dielectric properties in the temperature range from -123 to 177^oC. Thus, for higher value of x > 0.25 it shows relaxor behavior that is useful for capacitor application [37]. H. Kishi et al investigated the effect of substitution of rare earth and Mn on

dielectric properties of barium titanate ceramics. The lattice parameters and electrical resistivity results indicated that La ions occupied A sites and Ho ions occupied both A and B-sites. In the case of Ho-Mn substituted samples, the decrease in lattice parameter and a shift of the Curie point to high temperatures by re-oxidation treatment were observed in the range in which Ho ions predominantly occupy B-site (act as acceptors) [38]. D. Makovee et al [39] and T. Wang et al [40] studied PTCR effect in highly donor doped barium titanate and dielectric characteristics and tunability of barium stannate titanate respectively. Microstructure and electrical properties of porous $(Ba,Sr)TiO_3$ ceramics were investigated by K. Park et al [41]. The crystalline structure of the porous $(Ba,Sr)TiO_3$ ceramics was strongly dependent on the oxygen content. X.M. Chen et al studied the effect of Ca substitution on the dielectric and their field dependence of $(Ba_{1-x},Ca_x)TiO_3$ ceramics. The barium titanate based solid solution with tetragonal structure was obtained for x = 0.1 and a tetragonal to cubic phase transition was observed with increasing x since $CaTiO_3$-based solid solution phase with cubic structure appeared for x = 0.3 and became the major phase for x = 0.7. The dielectric constant decreased with increasing x, while the dielectric loss and temperature dependence are significantly suppressed [42]. Studies on the dielectric properties of $Ba_{1-x}Sr_xTiO_3$ ceramic solid solutions have shown that the compositions with $x < 0.8$ exhibited normal ferroelectric behavior while a relaxor characteristic was observed in the $SrTiO_3$ region ($x > 0.8$) [43, 44]. Effect of bismuth doping on the dielectric properties of $Ba_{1-x}Sr_xTiO_3$ ceramics were investigated and a relaxor behavior was observed. The degree of diffuseness and the relaxation increases as x increases [45]. Tunable microwave device application such as electronically tunable mixer, delay lines, filters and phase shifters, demand low dielectric constant (ε_r); large tunability $K = ((\varepsilon_{r(0)} - \varepsilon_{r(app)})/\varepsilon_{r(0)}$, low loss

tangent (tanδ); and good thermal stability. Currently the most studied solid solution includes (Ba, Sr) TiO_3 with some additives such as MgO, $MgTiO_3$ or Al_2O_3, but their reproducibility, as well as their stability needs to be improved [46-48]. Zhai et al. reported that BZT could be a promising material for microwave frequency application in thin film forms which is grown by sol-gel process on Pt-coated silicon substrates [49]. Other researcher also presented the tunability of $Ba(Zr_{0.2}Ti_{0.8})O_3$ by sol-gel process on the basis of grain size. According to them as the grain size decreases, the maximum dielectric constant and transition temperature both decrease and fine grain samples showed a better relaxor behavior. They followed the Vogel-Fulcher relation which is a typical characteristic of a relaxor, and determined the activation energy (E_a = 0.032 eV), T_{VF} = 253.2K, and $\nu_o = 2.63\times10^{13}$Hz. The value of tunability and tanδ was 82% and 0.0034 respectively [50]. Electrical properties and relaxation characterizations for undoped and ZnO-doped $Ba(Ti_{1-x}Zr_x)O_3$ have been studied via complex impedance measurements. The results suggest that the grain interior Zn^{2+} substitute Ti^{4+} and serves as an acceptor dopant [51]. Shrabanee Sen and R.N.P. Choudhary studied that for polycrystalline samples of $Ba_{1-x}Ca_xSn_{0.05}Ti_{0.95}O_3$ the resistance decreases with the increase in temperature [52]. Structural and electrical properties of cerium $Ba(Ti_{1-x}Zr_x)O_3$ thin films with the mole fraction of x = 0.2 had been investigated by Won Seok Choi et al. The dissipation factor and the leakage current were lower in Ce-doped BZT thin films [53]. The effect of the mole concentrations of precursor solution on the microstructure and dielectric properties of sol-gel deposited $BaZr_{0.35}Ti_{0.65}O_3$ thin films have been investigated by Zhai Jiwei et al. The BZT thin film showed a very stable and highly insulative characteristic against applied field. Thus they are better than barium strontium titanium films for application in tunable microwave

devices [54]. The polycrystalline samples of $Ba_{1-x}Sr_xZr_{0.05}Ti_{0.95}O_3$ have good electrical properties in the range of 31-500^oC. The imaginary part of the complex impedance as a function of frequency shows Debye-like relaxation in the materials. Bulk ac conductivity varies with frequency and shows that the compounds exhibit Arrhenius-type of electrical conductivity [55,56].

In literature (**table** 1.1) it is found that barium titanate (BT) is useful as a dielectric material for capacitor applications and for tunable devices. Earlier reported works have been mostly focused on ceramics substituted at either A-site (e.g., Pb, Ca, La and Sm) or B-site (Zr, Sn, Mn and Nb). Barium titanate based ceramics with simultaneous substitutions are very rare in the past work. Especially, earlier investigations with substitutions of Zr have not been systematically correlated with the accompanying structural changes, and have been rather commonly investigated for the changes in the dielectric properties. In the study of electroceramics, doping is an effective way to further improve the properties and since no reports are available in the literature on further doping in the BZT system, an attempt has been made in the present thesis to investigate the influence of some selected dopants in the BZT system. In the present thesis a systematic study has been taken up to investigate the structural, electrical and ferroelectric properties for the BZT based ceramics with simultaneous substitution on the both sites.

Table 1.1 Literature survey on $BaTiO_3$ and $BaZr_xTi_{1-x}O_3$ ceramic

Sr. No.	Authors	Major Observations	Method Composition	Dielectric properties	Ferroelectric and piezoelectric	
					P_r ($\mu C/cm^2$), E_c (kV/cm^2)	d_{33} and k_p
1.	Henning et al.[33] (1982)	Studied ε′-temp characteristic for capacitor application	**Conventional**, $BaZr_xTi_{1-x}O_3$. 0<x0.25. Emphasis on dielectric properties	Normal to relaxor behaviour	--	--
2.	Yu et al. (2002)	Prepared composition to see relaxor behaviour	**Conventional**,$BaTi_{0.70}Zr_{0.30}O_3$,	5000	10 (175K)	4.3
3.	Tang et al. (2004)	Tunable application with effect of grain size and got (k)=82% (60μm)	**Sol-gel technique,** $BaZr_{0.2}Ti_{0.8}O_3$,	1800, 5000 & 7500	-	-
4.	Boyeong Woo Lee et al.[57] (2005)	Preparation of $BaZr_xTi_{1-x}O_3$ by the hydrothermal process from peroxo-precursors	**Hydrothermal,** $BaZr_xTi_{1-x}O_3$	Relaxor behavior	--	--
5.	X.P. Jiang et al.[58] (2006)	Relaxor behavior and tunability in $BaZr_{0.35}Ti_{0.65}O_3$ ceramics	**Conventional**, $BaZr_{0.35}Ti_{0.65}O_3$	Relaxor behavior	--	--
6.	H.Y. Tian et al.[59] (2007)	Structural and piezoelectric properties	**Conventional**, Hf doped barium titanate	Normal ferroelectric propeties	--	d_{33}; 180 – 315
7.	Y. Wang et al.[60] (2007)	Structural and dielectric properties of Nb-Zn co-doped $Ba(Ti,Zr)O_3$ ceramics	**Hydrothermal,** Nb-Zn co-doped $Ba(Ti,Zr)O_3$	8000-15000	--	--
8.	Shan et al. (2007)	Studied structural properties of Y3+ doped BZT & explain site occupancies with doping	**Conventional,** $Ba(Zr_{0.25}Ti_{0.75})O_3+xY_2O_3$	16000-1200	-	-
9.	Reddy et al (2007)	Prepared BZT10 with Ho and studied its ε′-temp variation	**Conventional**, $BaZr_{0.10}Ti_{0.90}O_3$ with Ho substitution	25000-9000	-	-
10.	T. Badapanda et al. (2009)	Phase formation and dielectric study of Bi doped $BaTi_{0.75}Zr_{0.25}O_3$ ceramics	**Conventional**, $BaTi_{0.75}Zr_{0.25}O_3$	Relaxor behavior	--	--

1.3 Objectives of the Present Work

Present work entails the following objectives: -

- A barium titanate composition substituted with zirconium (BZT) would be identified for studies.
- To synthesize identified BZT composition with varying amount of substituents e.g. Pb, Sm and Ca.
- To characterize systematically the materials for physical, structural and electrical properties (dielectric, ferroelectric and piezoelectric) and,
- Composition-structure-property relationships in synthesized titanate materials.

References

[1] M.W. Barsoum, Fundamentals of Ceramics, McGraw-Hill Companies, New York, 1997.

[2] D.W. Richerson, Modern Ceramic Engineering, Marcel Dekker, New York, 1992.

[3] J.S. Reed, Principles of Ceramic Processing, John Wiley and Sons, Inc., New York, 1995**.**

[4] I.D. Marinescu, H.K. Tonshoff and I. Inasaki, Handbook of Advanced Ceramics Machining, Taylor and Francis, Philadelphia, 2007.

[5] H.D.Megaw, Ferroelectricity in crystals (Methuen, London, 1957).

[6] G. Busch, Ferroelectrics, **74** (1987) 267.

[7] W. Kanzig, Ferroelectrics, **74** (1987) 285.

[8] G. Busch, Ferroelectrics, **71** (1987) 43.

[9] A.J. Maulson and J.M. Herbert, Electroceramics, Chapman and Hall, 1990, U.K.

[10] Y. Xu, Ferroelectric Materials and Their Applications, North-Holland Elsevier Sci. Publ., Amsterdam, 1991.

[11] L.E. Cross, Ferroelectrics, **151** (1994) 305.

[12] H.D. Megaw, Ferroelectricity in Crystals, Methuen and Co., London, 1957.

[13] F. Jona and G. Shirane, Ferroelectric Crystals, Pergamon Press, Oxford, 1962.

[14] B. Wul and I.M. Goldman, C.R. Acad. Sci. U. R. S. S., **46** (1945) 177.

[15] R.E. Nettleton, Ferroelectrics, **1** (1970) 221.

[16] R.E. Nettleton, Ferroelectrics, **2** (1971) 73.

[17] A. Safari, R.K. Panda, and V.F. Janas, Key Eng. Mater., **35** (1996) 122.

[18] D. Damjanovic, Rep. Prog. Phys. **61** (1998) 1267.

[19] F. John and G. Shirane, Ferroelctric crystals (New York: Pergamon, 1962).

[20] B.T. Batthais and A.Von. Hippel, Phy. Rev., **73** (1998) 1378.

[21] B. Jaffe, W. Cook and H. Jaffe, Piezoelectric Ceramics, Academic Press, London, (1971).

[22] W.G. Cady, Piezoelectricity; pp 1-20. McGraw-Hill, New York, 1946.

[23] ANSI/IEEE standards on piezoelectricity, **176** (1987) 1.

[24] V. K. Katiyar and S.L. Srivastava, J. Appl. Phys., **76** (1994) 455.

[25] W. Cochran, Phys. Rev. Lett., **3**, 412 (1959); Adv. Phys., **387** (1960).

[26] U. Weber, G. Greuel, U. Boettger, S. Weber, D. Hennings and R. Waser, J. Am. Ceram. Soc., **84** (2001) 759.

[27] F.W. Perry and G.A. Hutchins, Mat. Res. Bull., **2** (1967) 409.

[28] Yu. N. Venevtsev, Mat. Res. Bull., **6** (1971) 1085.

[29] E.J. Brajer, "Polycrystalline Ceramic Material," U.S. Pat. No. 2 708 243, 1955.

[30] F. Kulscar, "Fired Ceramic Barium Titanate Body" U.S. Pat. No. 2 735 024, 1956.

[31] R.C. Kell and N.J. Hellicar, Acustica, **6** (1956) 235.

[32] T.N. Verbitskaja, G.S. Zhdanow, Yu. N. Venevtsev and S.P. Soloviev, Sov. Phys.-Crystallogr., **3** (1958) 182.

[33] D. Hennings and A. Schell, J. Am. Ceram. Soc., **65** (1982) 539.

[34] Z. Yu, R. Guo, A.S. Bhalla, Appl. Phys. Lett., **77** (2000) 1535.

[35] Z. Yu, C. Ang, R. Guo and A.S. Bhalla, Appl. Phys. Lett., **81** (2002) 1285.

[36] P.S. Dobal, A. Dixit, and R.S. Katiyar, Z. Yu, R. Guo and A.S. Bhalla, J. Appl. Phys., **89** (2001) 8085.

[37] Zhi Yu, Chen Ang, Ruyan Guo and A.S. Bhalla, J. Appl. Phys., **92** (2002) 2655.

[38] H. Kishi, N. Kohzu, Y. Iguchi, J. Sugino, M. Kato, H. Ohsato and T. Okuda, J. Eur. Ceram. Soc., **21** (2001) 1643.

[39] D. Makovee, N. Ule and M. Drofenik, J. Am. Ceram. Soc., **84** (2001) 1273.

[40] T. Wang, X.M. Chen and X.H. Zheng, J. Electroceramics, **11** (2003) 173.

[41] K. Park, J.G. Kim, J. Kim and W.S. Cho, Mat. Sci. Eng. B, **88** (2002) 9.

[42] X.M. Chen, T. Wang and J. Li, Mat. Sci. Eng. B, **113** (2004) 117.

[43] V.V. Lemanov, E.P. Smirnova, P.P. Syrnikov and E.A. Tarakanov, Phys. Rev. B, **54** (1996) 3151.

[44] L. Zhou, P.M. Vilarinho and J.L. Baptista, J. Eur. Ceram. Soc., **19** (1999) 2015.

[45] L. Zhou, P.M. Vilarinho and J.L. Baptista, J. Eur. Ceram. Soc., **21** (2001) 531.

[46] X.F. Liang, W.B. Wu and Z.Y. Meng, Mater. Sci. Eng. B00 (2003) 11.

[47] M.W. Cole, P.C. Joshi, M.H. Ervin, M.C. Wood, R.L. Pfeffer, Thin Solid Films, **374** (2000) 43.

[48] D. Li, M.A. Subramanian, Solis State Sci., **2** (2000) 507.

[49] J. Zhai, X. Yao, L. Zhang and B. Shen, **84** (2004) 3136.

[50] X.G. Tang, J. Wang, X.X. Wang, and H.L.W. Chan, Solid State Communication **131** (2004) 163.

[51] Yongli Wang, Longtu Li, Jianquan Qi and Zhilun Gui, Mat. Chem. Phys., **76** (2002) 250.

[52] Shrabanee Sen and R.N.P. Choudhary, Mat. Lett., **58** (2004) 661.

[53] Won Seok Choi, Junsin Yi and Byungyou Hong, Mat. Sc. and Eng. B, **109** (2004) 146.

[54] Zhai Jiwei, Yao Xi, Zhang Liangying, Shen Bo and Haydn Chen, J. of Crystal Growth, **262** (2004) 341.

[55] J. Nowotny and M. Rekas, Ceram. Int., **17** (1991) 227.

[56] Shrabanee Sen and R.N.P. Choudhary, Mat. Chem. Phys., **87** (2004) 256.

[57] Byeong Woo Lee and Seung-Beom Cho, J. Eur. Ceram. Soc., **25** (2005) 2009.

[58] X.P. Jiang, M. Zeng, H.L.W. Chan and C.L. Choy, Mat. Sc. and Eng. A, **438** (2006) 198.

[59] H.Y. Tian, Y. Wang, J. Miao, H.L.W. Chan and C.L. Choy, J. Alloys and Comp., **431** (2007) 197.

[60] Y. Wang, Z. Zhuang and J. Zhou, Mat. Sci.-Poland, **25** (2007) 121.

Chapter 2

Experimental Aspects

This chapter presents a brief background on the methods of sample preparation and characterization techniques used for studying various properties (such as structural, dielectric, ferroelectric and piezoelectric) of $BaZr_{0.10}Ti_{0.90}O_3$ *doped ceramic. The details on experimental techniques and the characterization equipment used in the present work are presented in this chapter. Synthesis of ceramic by conventional solid state reaction method is described.*

2.1 Introduction

Ferroelectric ceramics are important electronic materials that have wide range of industrial and commercial applications. The performances of ferroelectrics are closely related to the ways they are processed because synthesis methods play an important role in determining the microstructural, electrical and optical properties of ferroelectric ceramics. Therefore it is important to understand the various processes take place during material synthesis. Various routes have been developed to synthesize ferroelectric ceramics. For the present work, conventional solid state route was adopted. This requires high calcination and sintering temperature resulting in loss of lead, lithium due to their high volatilities, thus affecting the microstructure and subsequently the electrical properties of the ferroelectric materials [1-3]. So study of calcination and sintering temperature is very essential. The electrical characterization of ferroelectric ceramics includes electrical conductivity, dielectric constant and tangent loss, ferroelectric hysteresis loop and piezoelectric properties etc. Discussion on each one of the processes and the parameters is presented in following sections. Also a brief description about the synthesis and characterization parameters adopted for the material synthesis is given.

2.1.1 Synthesis of materials (*Solid state reaction method)*

A number of techniques (conventional and non-conventional) are normally used to synthesize ceramic materials [4]. Some of them are listed below:

i) Hydrothermal synthesis

ii) Spray drying techniques

iii) Wet chemical methods

iv) Sol-gel route

v) Solid State reaction route

Solid state route has been adopted for the material synthesis for the present work which is a conventional and simplest way to prepare ceramic material compositions of required shapes and electrical properties with cost effectiveness. Usually, polycrystalline materials are prepared by the solid state route, since it is better, cheaper and productive [5].The various steps used in solid state reaction route are shown below in the form of flow chart.

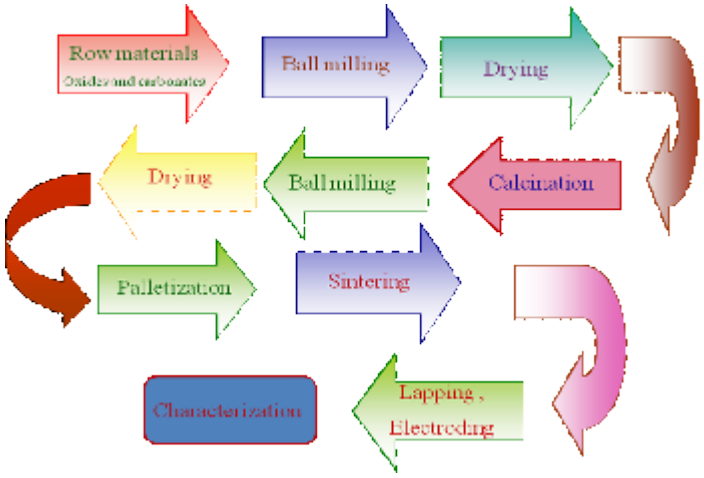

Figure 2.1. Flow- Chart for conventional solid state route

2.1.2 Raw Chemicals and Ball Milling

Chemical composition is only one aspect of the specification of raw materials. Raw materials are evaluated on the basis of their purity and particle size. Impurities of raw materials affect the reactivity as well as the dielectric and conductive properties of the fired ceramics, and through these the piezoelectric properties [6]. One aspect of the composition

that is difficult to specify exactly is the moisture content. It depends on the ambient humidity, the method of storage and particle size. In this solid state methodology of preparation, the metal oxides/carbonates of analytical grade (AR grade) were taken as starting materials. The raw materials used for the present work were $BaCO_3$, PbO, ZrO_2, TiO_2, La_2O_3, Sm_2O_3 and $CaCO_3$. These oxide materials were weighed in desired stoichiometric ratio and ball milled for mixing the raw materials, eliminating aggregates and/or reducing the particle size. The ball mill used for the present work was conventional ball milling shown in figure 2.2. Here maximum speed goes upto 80 r.p.m. This can reduce the particle size to 1-10 μm range [5]. High density zirconia balls and distilled water were used as milling media. For all the samples the ball milling was done for 16 hours followed by drying at 130^{o}C. After that dried powder was subjected to calcination [7] (see 2.1.3). The calcined powder was again ball milled for 8 hours to reduce the particle size which enhances the densification during sintering (see 2.1.5).

Figure 2.2. Conventional ball milling

2.1.3 Calcination

Solids usually do not react at room temperature and in order to facilitate the reaction, they are heated to higher temperature. Solid-state reaction is usually slow because during the reaction, a large amount of bonds break, and the ions migrate through a solid unlike gas phase. The limiting factor in a solid state reaction is usually diffusion. So the rate-controlling step in a solid-state reaction is the diffusion of the cations through the product layer. **Calcination** causes the constituent solids to interact by inter diffusion of their ions and so reduces the extent of the diffusion that must occur during sintering in order to obtain a homogeneous body. It can therefore be considered to be part of the mixing process. The calcination conditions are important factor controlling shrinkage during sintering [5]. In general, four physical processes are involved in the calcination of the raw materials: (i) Linear expansion of the particles (< 400^0C) (ii) Solid phase reaction (400-750^0C) (iii) Contraction of product (750-850^0C) and (iv)Grain growth (>850^0C). Synthesis of the phase of a compound takes place by solid-phase reaction, which involves the chemical reaction through atomic diffusion among grains at temperature below the melting points of the raw materials [8]. It also helps in removing the unwanted gases (CO_2 in case of carbonates) and products during the decomposition of the constituent compounds. Usually, the calcination temperature is chosen high enough to cause reaction, but low enough to facilitate subsequent grinding. In the materials, having volatile constituents, the calcination temperature must be kept low enough to avoid loss of the volatile parts.

2.1.4 Compaction

After calcination, the powders are ball milled again for better homogeneity. Further it is compacted to the desired shape by several compaction techniques. Generally, an organic binder is incorporated into the powder, for giving sufficient strength to dry shapes, so that handling between shaping and sintering may not be difficult. One of the most important requirements of the binder is that it should be possible to remove the binder from the pressed shapes without any disruptive effect. For the present work, dilute solution of polyvinyl alcohol (PVA) was used as binder.

The following techniques can be used in forming ceramic powders into a desired shape*:*

- Uniaxial (Die) Pressing
- Isostatic Pressing
- Injection Molding
- Extrusion
- Slip Casting
- Gel Casting
- Tape Casting

Among these different shaping techniques uniaxial pressing was used for the present work shown in figure 2.3. Uniaxial pressing is carried out in a die with movable top and bottom punches shown in figure. It is used for giving small simple shapes to the calcined powder. A cavity is formed at the bottom in lower portion. This cavity is filled with free flowing granulated powder and then it is struck with the top of the die. With the help of the top-punch, pressure in the range of 10 ton/sq.in is applied. A lot of care at various levels of

mixing is needed while using this pressing technique, as samples prepared by this technique show the mechanical cracks after sintering.

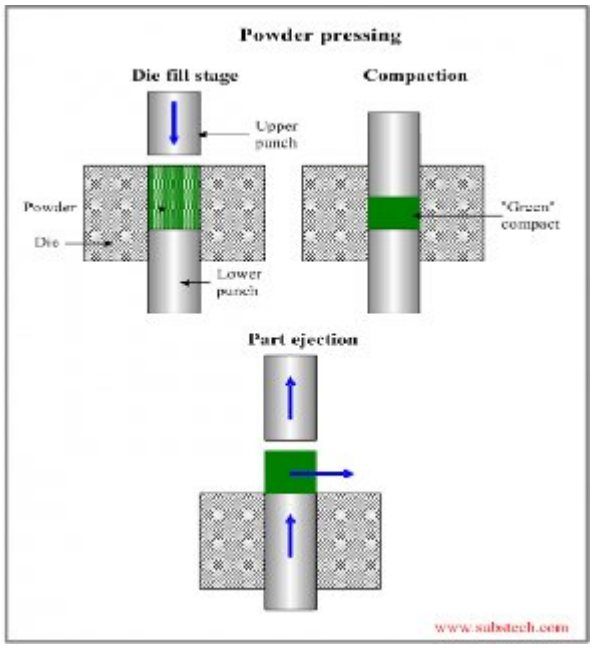

Figure 2.3. Uniaxial pressing

2.1.5 Sintering

Sintering converts a compacted powder into a denser structure of crystallites joined to one another by grain boundaries shown in figure 2.4. During sintering, at an appreciable temperature, the atomic motion is more violent and the area between grains in contact increases due to the thermal expansion of the grains and finally only one interface between two grains remains. This corresponds to a state with much lower surface energy. In this state, the atoms on the grain surfaces are affected by neighboring atoms in all directions, which results in densified ceramic [9]. At the beginning of the sintering process, the lattice distortion and internal strain are reduced by atomic diffusion which is called as 'the recovery processes. With further increase in temperature, a recrystallization process takes

place through atomic diffusion. During recrystallization, new crystal nuclei form and grow at grain boundaries and in other regions inside the grain with higher free energies. Meanwhile, some grains grow by swallowing up other smaller grains. In the recrystallization stage, grain growth is usually realized through the motion of grain boundaries. In general, higher the sintering temperature, larger the grains would grow, as the grain growth is caused by atomic diffusion, which increases with the increase in sintering temperature. Since, the grain growth is caused by atomic diffusion, a higher sintering temperature and a larger hold time would result in larger grains and result in highly densed ceramics [10]. The oxide ceramics should be sintered in an oxidizing atmosphere or in air. Further, in ferroelectric ceramics containing lead, evaporation of PbO takes place above 800^{o}C and creates a Pb vacancy which affects the material properties considerably [11]. Thus in order to avoid lead loss, sintering is done in a closed and lead rich atmosphere.

The factors that affect sintering process are

1. Temperature.
2. Green density.
3. Uniformity of green microstructure.
4. Atmosphere.
5. Impurities
6. Size distribution.
7. Particle size.

A programmable high temperature resistive furnace using silicon carbide heating elements was used to sinter the ceramic samples. The working area (inside heating zone) is 12″

Depth × 6″ Height × 6″ Width and maximum operating temperature is 1550 ^{o}C. The sensor used to measure temperature is a R-type thermocouple. A conventional sintering furnace was used for the present work shown in figure 2.4. In conventional heating, the cycle time is often dominated by slow heating rates that are chosen to minimize steep thermal gradients, which in turn minimize processing induced stresses.

a)

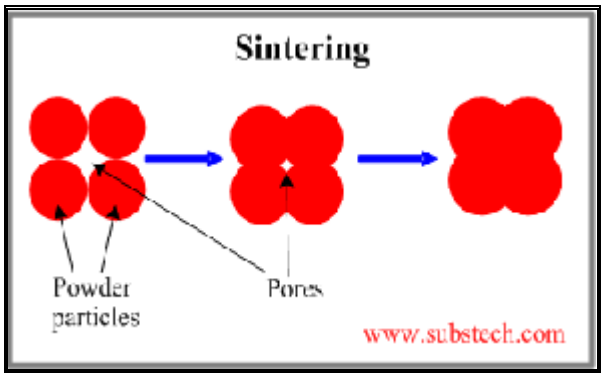

b)

Figure 2.4 a) Grain growth during sintering and b) sintering furnace

2.2 Characterization

The samples prepared by conventional solid state reaction technique were characterized for their structural, dielectric, ferroelectric and piezoelectric properties. The description about characterization techniques are given below:

2.2.1 Density

In the majority of electrical applications sintered ceramics are required to have minimum porosity i.e. maximum density. From the application point of view properties reach their optimum values at the highest density, while porosity in excess of 25-30% allows the ingress/entrance of moisture leading to many serious problems. However, there are cases where porosity is desirable: for example, in humidity and gas sensors and where thermal shock resistance is of overriding importance. Keeping in view the application potential of these materials for electrical/piezoelectric devices, the compositions developed in this work have been optimized to obtain a maximum density. For all the samples experimental density was measured by Archimedes principle shown in figure 2.5.

According to this principle

$$d_{ex} = W_a / (W_a - W_w) \quad g/cc \qquad \textbf{…2.1}$$

Where W_a and W_w is the weight in air and water respectively.

For this, the sample was weighed in air and then it was attached to very thin thread and immersed in water to determine W_w.

With the help of unit cell volume, theoretical or X-ray density (d_{th}) was calculated using the relation,

$$d_{th} = (Z \cdot M)/(N \cdot V) \quad g/cc \qquad \textbf{…2.2}$$

where *Z* is the number of molecules in a unit cell and is equal to 1 for the present system, *M* is the molecular weight of the compound, *N* is the Avogadro's number value and *V* is the volume of unit cell.

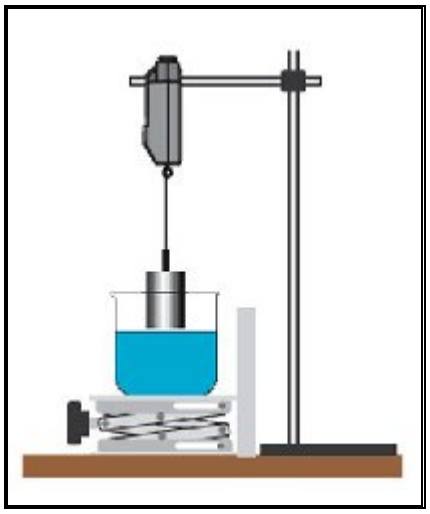

Figure 2.5. Density measurement by Archimedes principle

After calculating X-ray density (d_{th}), experimental density (d_{exp}), relative density was calculated using the relation

$$P = [(d_{th}-d_{ex})/d_{th}] \times 100\ (\%) \qquad \textbf{… 2.3}$$

Where (100 – P) gives percentage densification or relative density (d_{rel}).

2.2.2 X-ray Diffraction (XRD)

X-ray crystallography is a method of determining the arrangement of atoms within a crystal, in which a beam of X-rays strikes a crystal and diffracts into many specific directions. For diffraction applications, only short wavelength x-rays (hard x-rays) in the range of a few angstroms to 0.1 Å (1 keV-120 keV) are used. Because the wavelength of x-rays is comparable to the size of atoms, they are ideally suited for probing the structural arrangement of atoms and molecules in a wide range of materials. The energetic x-rays can penetrate deep into the materials and provide information about the bulk structure [12-13].From the angles and intensities of these diffracted beams, a crystallographer can produce a three-dimensional picture of the density of electrons within the crystal. From this electron density, the mean positions of the atoms in the crystal can be determined, as well as their chemical bonds, their disorder and various other information. The basic principle emphasizes that for a fixed wavelength (λ), the constructive interference occurs for a fixed set of an inter planer spacing (d) and at an incidence angle (θ) shown in figure6. According to Bragg's condition of diffraction:

$$n\lambda = 2d \sin\theta. \qquad \textbf{…2.4}$$

For a cubic system, the inter planar distance (d) is given by

$$\frac{1}{d^2} = \frac{h^2 + k^2 + l^2}{a^2} \qquad \textbf{…2.5}$$

Combining the above two equations we get a relation, which predict the diffraction angle for any set of planes, For any set of planes, for a given 'λ' if the following condition is

satisfied, we can calculate the h,k and l values for at different Sinθ and find out the unit cell parameter.

$$\mathrm{Sin}^2\theta = \frac{\lambda^2}{4a^2}(h^2+k^2+l^2) \qquad \textbf{…2.6}$$

Similarly, the relation for a tetragonal and orthorhombic system is

$$Sin^2\theta = \frac{\lambda^2}{4}\left(\frac{h^2+k^2}{a^2}+\frac{l^2}{c^2}\right) \qquad \textbf{…2.7}$$

$$Sin^2\theta = \frac{\lambda^2}{4}\left(\frac{h^2}{a^2}+\frac{k^2}{b^2}+\frac{l^2}{c^2}\right) \qquad \textbf{…2.8}$$

For the present work, XRD patterns were recorded using Bruker, D-8 Advance model at room temperature. Cu-K_α (λ = 1.54056 Å) radiations were used for recording the diffraction pattern. The diffraction angle, 2θ was varied from 20^o to 70^o. All the Lattice parameters ('a' and 'α') were calculated using the standard formula (2.5) and Powder X software.

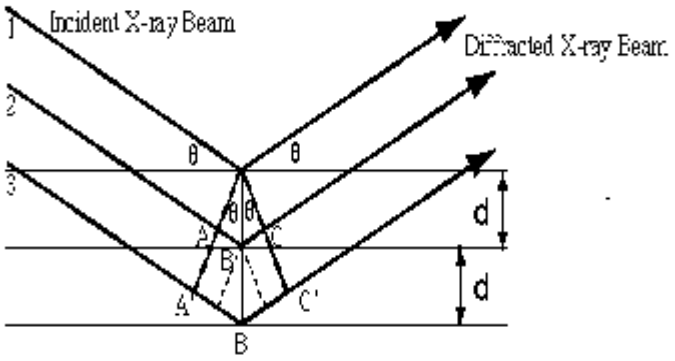

Figure 2.6. Bragg diffraction condition

2.2.3 Scanning Electron Microscopy (SEM)

The scanning electron microscope (SEM) is a type of electron microscope that images the sample surface by scanning it with a high-energy beam of electrons in a raster scan pattern. The electrons interact with the atoms that make up the sample producing signals that contain information about the sample's surface topography, composition and other properties such as electrical conductivity. For the present study, this technique has been used to study the grain size of the ceramic samples. The micrographs also help in studying and identifying the porosity and uniformity of the samples. Microstructural study for the fractured surfaces of the studied samples was done using SEM (ZEOL).

2.2.4 Dielectric Properties

Ferroelectric materials are also good dielectrics. For most of the applications of ferroelectric materials, the relative dielectric constant (ε) and dielectric loss (tanδ) are important practical parameters and dielectric properties provide a great deal of information about the suitability of the material for various applications.

The dielectric constant (ε) is the ratio of the capacity of a condenser with that of a condenser capacity in vacuum. It is a measure, therefore, the amount of electrical charge a given substance can withstand at a given electric field strength.

The capacitance (C) for a parallel plate capacitor with air being the medium between plates is given by:

$$C = \varepsilon_0 A/t \qquad \ldots 2.9$$

Where ε_0 is the permittivity of free space and is equal to 8.854 x 10^{-12} F/m, A is the area of electrode and t is the separation between two parallel plate electrodes. When a dielectric (electrical insulator) is inserted between the plates, the capacitance of the capacitor is increased by a factor ε which is called the dielectric constant of the dielectric material. Therefore, for a parallel plate capacitor with a dielectric between the capacitor plates, the capacitance (C) is given by:

$$C=\varepsilon\varepsilon_0 A/t \qquad \ldots 2.10$$

Thus the energy stored in a capacitor of a given volume at a given voltage is increased by the factor of the dielectric constant when the dielectric material is present. For an alternating electric field, the dielectric constant can be expressed in terms of real and imaginary quantities as:

$$\varepsilon_r = \varepsilon_{real} - i\varepsilon_{imag} \qquad \ldots 2.11$$

Where, ε_{real} is the real component of the dielectric constant, in phase with the applied field. ε_{imag} is the imaginary component and is 90^o out of phase with the applied field, caused by either resistive leakage or dielectric absorption. For normal substances, the value of ε is low, usually under 5 for organic materials and under 20 for most inorganic materials. Generally, ferroelectric ceramics have much higher ε, typically several hundreds to several thousands [14]. In the present study the dielectric constant (ε) was measured as a function of frequency and temperature. Dielectric constant (ε) was determined from measured value of capacitance.

The charging current in an ideal dielectric leads the applied voltage by 90^o shown in figure 2.7. However, in real dielectrics, in addition to the charging current associated with the storage of electric charge by the dipoles, a loss current must also be considered. The loss current arises from the long-range migration of charges, e.g., dc ohmic conduction and the dissipation of energy associated with the rotation or oscillation of dipoles [6]. As the dielectric is not loss free, it is generally represented by a complex quantity. The total current in the real dielectric is a complex quantity which leads the voltage by an angle (90-δ), where δ is called the loss angle. Dielectric loss (tanδ) also known as dissipation factor is defined as $\tan\delta = \varepsilon_{imag}/\varepsilon_{real}$. For present study measurement of capacitance and loss tangent (tanδ) of the materials were done as a function of ac frequency (20Hz to 1MHz) at room temperature. These were carried out using Agilent 4284A LCR meter while; measurements with temperature from (30^oC to 300^oC) were carried out by using Agilent 4263B LCR meter interfaced with a PC and programmable temperature controller which is shown in figure 2.8**.** The dielectric constant (ε) of the materials at different frequencies were calculated using the relation $\varepsilon = t\ C_p/\varepsilon_o A$, where A is the area of the electrode, t is the thickness of the material, C_p is the capacitance measured in parallel mode and ε_o is the permittivity of the free space (8.854×10^{-12} F/m).

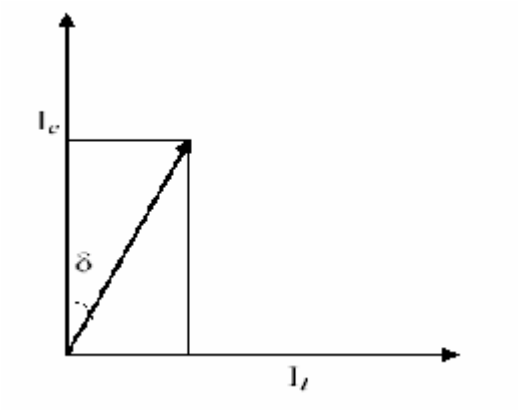

Figure 2.7. The vector resolution current in a capacitor

Figure 2.8. Experimental Setup for dielectric of ac measurement system

2.2.5 Ferroelectric Properties

Ferroelectric domains are the regions of the material with uniformly oriented spontaneous polarization. A very strong field could lead to the reversal of the polarization in the domain, known as polarization (or domain) switching. This dynamic characteristic of a ferroelectric domain is anisotropic and depends on temperature and on the applied electric field [14-15]. The polarization reversal takes place by the growth of existing

antiparallel domains, by domain-wall motion and by nucleation and growth of new antiparallel domains [16-17]. The observation of hysteresis loops (e.g., with a modified Sawyer-Tower circuit [18]) is frequently used for the identification of ferroelectrics is shown in figure 2.9 and figure 2.10 represents the ferroelectric tracer used in present study. The system consists of PC, software, programmable voltage source (up to 3 kV) and silicone oil bath. The set up is shown in figure 2.10. For measurement, specimen is kept in a spring-loaded jig and immersed in silicon oil. The loop is recorded by the system and the software computes all the parameter e.g. P_s, P_r E_c and E_{max}.

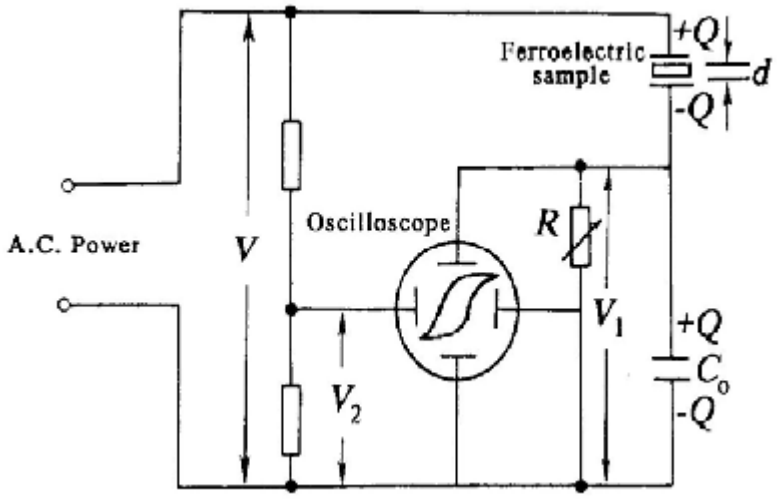

Figure 2.9. Schematic of modified sawyer-Tower circuit

Figure 2.10. Experimental setup for ferroelectric hysteresis measurement system

2.2.6 Poling

Poling is a process during which a high electric field is applied on the ferroelectric ceramic sample to force the domains to reorient in the direction of the applied electric field. The poling is possible only in ferroelectric materials and poling steps are shown in figure 2.11. Before poling, the ferroelectric ceramic doesn't possess any piezoelectric and pyroelectric properties owing to the random orientation of the ferroelectric domains in the ceramics. For domain reorientation, a poling field must be applied on the sample and maintained for a certain length of time. For a given field and poling time, better domain rearrangement results at higher poling temperature. This happened because with the increase in poling temperature, crystalline anisotropy and coercive field, Ec, of the ferroelectrics decreases. Also, with increasing temperature, space charges, which act against domain motion, decreases in the ceramic.

Figure 2.11. Poling steps of a ferroelectric material

However, when the poling temperature is too high, problems arise as the electrical conductivity increases and the consequent increase in leakage current would result in sample breakdown during the period of poling. After poling, the electric field is removed and a remnant polarization and remnant strain are maintained in the material, and the sample starts exhibiting piezoelectric and pyroelectric effects [6]. In the present study the sample, immersed in oil, was heated to 150^{o}C and an electric field ~ 25 kV/cm was applied and was kept for 1hr. After that the sample was allowed to cool by switching off the heater in applied electric field and the field was removed at room temperature.

2.2.7 Piezoelectric Properties

Piezoelectric charge coefficients, d_{33} and d_{31} were measured using Piezometer system of Concord Electroceramics Ind., India. shown in figure 2.13.

Conventionally, d_{33} is defined as charge per unit force, both in the direction of polarization of a piezoelectric material i.e.

$$d_{33} = (\partial D_3)/(\partial T_3)_E \qquad \textbf{…2.12}$$

where D is the dielectric displacement vector and T is the applied stress vector.

Most powerful measurement of the strength of the piezoelectric effect is the electromechanical coupling factor k, which reflects the efficiency of a material. It gives us the measure of the part of the applied electrical energy converted into mechanical energy or vice-versa and measured by the resonance–antiresonance method using impedance-frequency data [19].

$$k^2 = \frac{\text{Mechanical energy converted into electrical energy}}{\text{Input Mechanical energy}}$$

or

$$k^2 = \frac{\text{Electrical energy converted into mechanical energy}}{\text{Input electrical energy}}$$

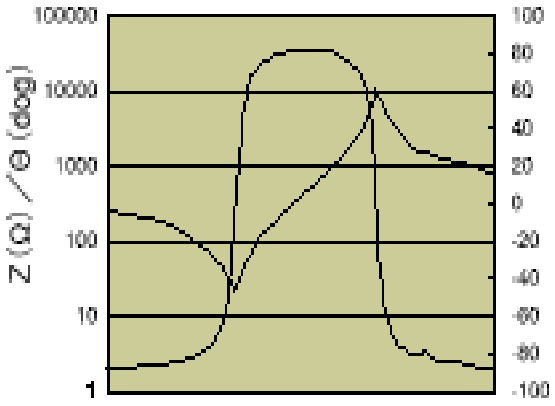

Figure 2.12. Resonance and antiresonance frequencies of a piezoelectric material

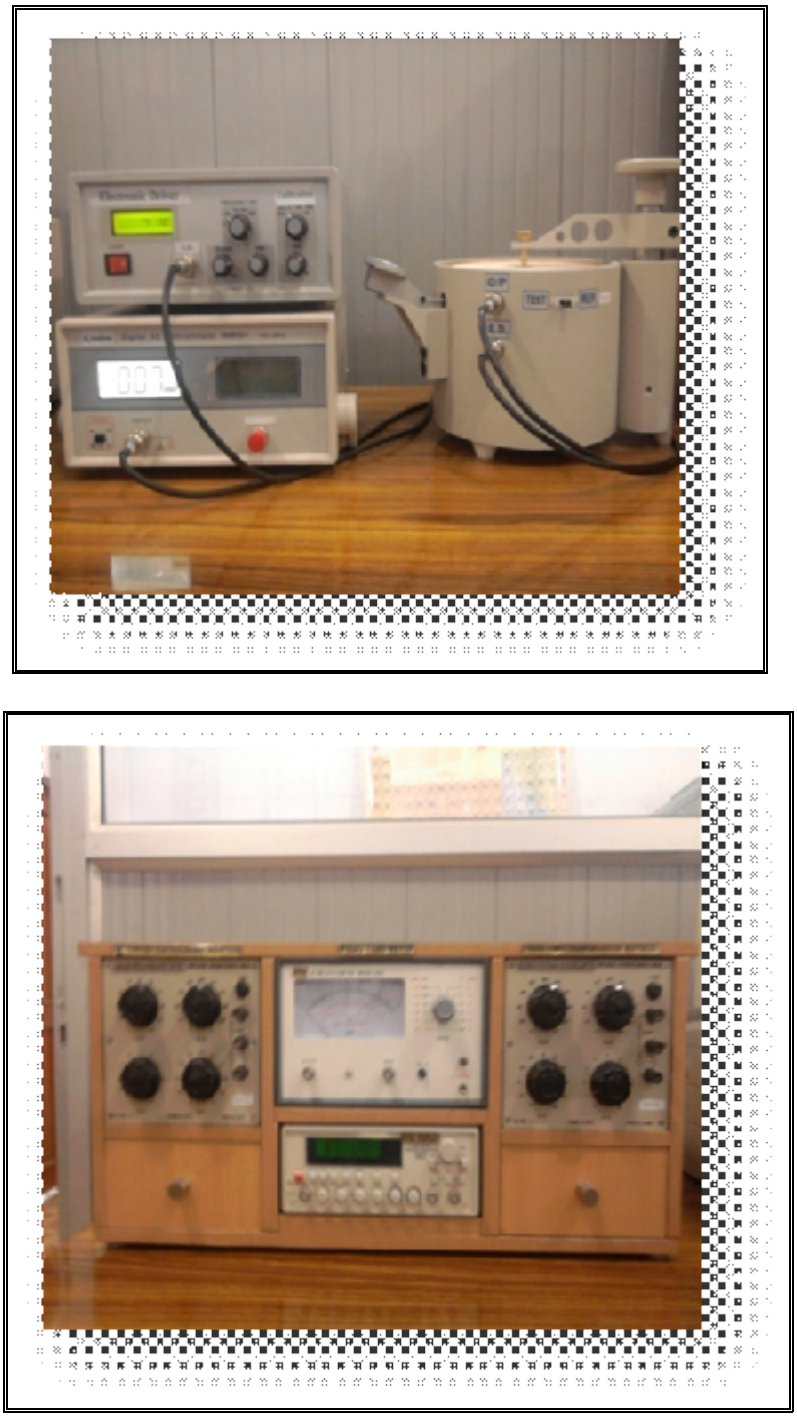

Figure 2.13. Piezoelectric Measurement set-up

References

[1] K. Keizer, E.H. Janssen, K.J. Devries, A.J. Burggraaj, Material Res. Bull., **8** (1973) 533.

[2] T. Yamamoto, Am. Ceram. Soc., **71** (1992) 978.

[3] G. Arlt, Ferroelectrics, **104** (1990) 217.

[4] P. Consin et.al., Mater. Sci. and Engg. A, **130** (1990) 119.

[5] A.J. Moulson, J.M. Herbert, Electroceramics, Chapman and Hall, UK, (1990).

[6] B. Jaffe, W. Cook and H. Jaffe, Piezoelectric Ceramics (Academic Press, London, 1971).

[7] M.H. Lente, A.L. Zanin, S.B. Assis, I.A. Santos, J.A. Eiras and D. Garcia, J Eur. Ceram. Soc., **24 (**2004) 1529.

[8] Y. Xu, Ferroelectric Materials and Their Applications, Elsevier Science Pub. Co. New York, USA, (1991).

[9] M.W. Barsoum, Fundamental of ceramic, 1997.

[10] K. Uchino, Processing of ceramics, 1982.

[11] A. H. Webster, T. B. Weston and N. E. H. Bright, J. Am. Ceram. Soc. Bull., **50** (1967) 490.

[12] S.K. Chatterjee, Prentice-Hall of India Private Limited, New Delhi, 1999.

[13] B.D. Cullity, Addison-Wesley Publication Company, Reading, Massachusetts,Menlo Park, California.

[14] B.T. Batthias and A. von Hippel, Phys. Rev., **73** (1948) 1378.

[15] W.J. Merz, Phys. Rev., **95** (1954) 690.

[16] ME Lines and A. M. Glass, Principles and Applications of Ferroelectrics and Related Materials, Oxford, Clarendon, (1979).

[17] V. Shur and E. Rumyantsev, J. Korean Phys. Soc., **32** (1988) 727.

[18] C.B. Sawyer and C.H. Tower, Phys. Rev., **35** (1930) 269.

[19] P.R. Chowdhary and S.B. Deshpande, Ind. J. Pure. Appl. Phys.,**17** (1979) 571.

Chapter 3

Synthesis and Characterization BZT (10/90)

The chapter includes study of structural, dielectric and ferroelectric properties of modified BZT (10/90) electroceramics which is the subject of investigation in the present thesis. The effect of two-stage sintering on the structural, electrical and ferroelectric properties of BZT is also discussed.

3.1 Introduction to BZT:

Solid solutions of $BaTiO_3$ and $BaZrO_3$ ($BaTi_{1-x}Zr_xO_3$, or BTZ) have been established as one of the most important compositions for dielectrics in multilayer ceramic capacitors (MLCs). The high permittivity of the $BaTiO_3$ ceramic is increased more by the addition of zirconium. The dielectric behavior of $BaTi_{1-x}Zr_xO_3$ ceramics has been discussed widely in the literature. In the mid-1950s, Brajer [1] and Kulscar [2] showed that, as the zirconium content increases, the orthorhombic– tetragonal phase transition increases and the tetragonal– cubic phase transition decreases. The first dependence of the phase transition temperatures on the zirconium content was shown by Kell and Hellicar [3]. Verbitskaja et al. [4] reported a direct rhombohedral– cubic phase transition for zirconium contents of, 15%. Other authors have assumed a coexistence of both the orthorhombic and tetragonal phases within a small temperature interval at the Curie point (T_C). The latter has been confirmed via detailed investigation [5]. In addition, a broadening of this temperature range of coexisting crystal structures, relative to decreasing zirconium content, and a subsequent separation of the structural phases, relative to further decreases in the amount of zirconium, was observed. Hennings et al. [5] gave an explanation of the temperature characteristics of the permittivity. Calorimetric measurements at the T_C value showed a clear decrease in the latent heat, disappearing at a zirconium content of; 10%. This observation leads to a change from first-order to second-order transitions at low zirconium contents. Further increases in the amount of zirconium results in a stimulated broadening of the $C(T)$ curve. This phenomenon is due to the increased sensitivity of the ceramic, relative to local structural transitions in the vicinity of T_C, which leads to a distribution of Curie maxima and, thus, a broad, resulting envelope. This phenomenon is called a diffuse phase

transition (DPT) and appears at zirconium contents of, 13%, according to Hennings et al. [5] in regard to the dielectric properties, great importance is given to aging by investigators. Aging is known as the change—generally, a decrease—in electric parameters (permittivity, loss factor) in the absence of any electrical or mechanical stress. In poled ceramics, aging occurs in the form of a constriction or shifting of the hysteresis along the field axis by the internal field [6]. Those aging effects commonly can be reversed completely by heating at temperatures greater than T_C. The explicit aging behavior of ferroelectric ceramics is dependent on several experimental parameters (temperature, frequency, field amplitude, electrical conditions, etc.), as well as material parameters (composition, dopants, grain size, thermal treatment, etc.). Generally, aging is assumed to be caused by the decreasing mobility of the domain walls, which obviously leads to a decrease in the permittivity (ε) and loss factor (tanδ) with time. Pinning of the domain wall can be achieved via two different mechanisms: (i) migration of the domain walls to defects, where they get pinned in extensive potential minima [7,8], or (ii) diffusion of defects to the domain walls, thereby decreasing their electrostatical and mechanical energy [9,10]. Arlt and co-workers [11-13] developed the volume model, which involves the alignment of defect dipoles. The alignment of electrical-defect dipoles, which consist of oxygen vacancies and acceptors, in the environment of the volume polarization leads to clamping of the domain walls.

Thus, several authors studied the effect of Zr on different properties in $BaZr_xTi_{1-x}O_3$ but there has been no single study correlating all the properties. Yu et al. [14-15] studied the piezoelectric and strain properties in the range of x = 0-0.3 for ceramic and in single crystal for x = 0.05 and 0.08. Moura et al. [16] has recently observed the polarization vs electric field behaviour of $BaZr_xTi_{1-x}O_3$ for x = 0.05, 0.10 and 0.15. Nanakorn et al. [17]

also studied its dielectric and ferroelectric properties in ceramic for x = 0.02, 0.05 and 0.08. Maiwa et al. [18] studied the dielectric and electromechanical properties for x= 0.10 prepared by conventional and spark plasma sintering. Yu at al. [15] measured highest value of remnant polarization (22 $\mu C/cm^2$) in the orthorhombic state for ⟨110⟩ directions. Moura et al. [16] obtained maximum value of polarization for its rhombohedral state (x = 0.15). Further more, the Electrical properties of the BT-based ceramics depend strongly on the microstructure as well as composition. The microstructure of BT can be controlled by two approaches. First one is by using additives to prohibit the grain growth for obtaining highly dense ceramics, while the other is using the novel processing technique to modify the microstructure. Numerous studies on the sintering of barium titanate and thermal expansion of similar materials have been reported in the literature [19-24]. Substitution of other ions for host cations at the A or B site in $BaTiO_3$ perovskite cell leads to remarkable changes of its characteristics [25]. By adding oxide groups of softeners, hardeners and stabilizers one can modify it. Softeners (donors) reduce the coercive field strength, elastic modulus and the aging effects and increase the permittivity and dielectric constant and mechanical losses. Doping of hardeners (acceptors) gives higher conductivity, reduces dielectric constant and increases mechanical quality factor and aging effect [26]. As other BT based systems, Barium Zirconate Titanate (BZT) solid solutions are also electric field- tunable dielectrics with potential use in devices for wireless communications as variable capacitors, phase shifters and voltage-controlled oscillators [27]. The ferroelectric properties of BZT are largely dependent on the amount of Zr substitution [28].

In this work a study on the structural, dielectric and ferroelectric properties of $BaTi_{0.90}Zr_{0.10}O_3$ ceramic is carried out to explore their properties and applications. All

samples were prepared by conventional solid state reaction method. Sintering was done at four different temperatures (1200, 1250, 1300, 1350^{o}C for 4h) with a uniform heating rate of 5^{o}C/min. Effect of Two-stage sintering on various properties of the BZT ceramics is also discussed.

3.2 XRD analysis of BZT (10/90)

The X-ray diffraction patterns for BZT calcined at 1000^{o}C and sintered at 1200, 1250, 1300 and 1350^{o}C for 4 hrs are given in Figure 3.1. For calcined BZT powder, some extra peaks of $BaO.ZrO_2$ can also be observed along with the peaks indicating the formation of perovskite $BaTiO_3$. This is due to the chemical stability of the Zr^{4+} ion as compared to Ti^{4+}. The solubility can be enhanced by activating the reaction which can be done either by calcinations at some higher temperatures or sintering at high temperature until one get the single phase. In the present study, BZT powder calcined at 1000^{o}C was further sintered at four different temperatures from 1200 to 1350^{o}C. A different kind of reaction mechanism with many intermediate components was observed. BZT with perovskite rhombohedral phase was formed at 1350^{o}C.

3.3 Scanning Electron Microscopy (SEM)

Figure 3.2 shows the scanning electron micrographs (SEM) of BZT (10/90) sintered at four (1200, 1250, 1300 and 1350^{o}C) different temperatures. The SEM measurements were carried out on cross sectional part of the freshly broken samples. As it is very difficult to remove the porosity in case of ceramic samples prepared by oxides and carbonates but it can be controlled by changing processing parameters. In the present case the average grain size increases with increasing the sintering temperature.

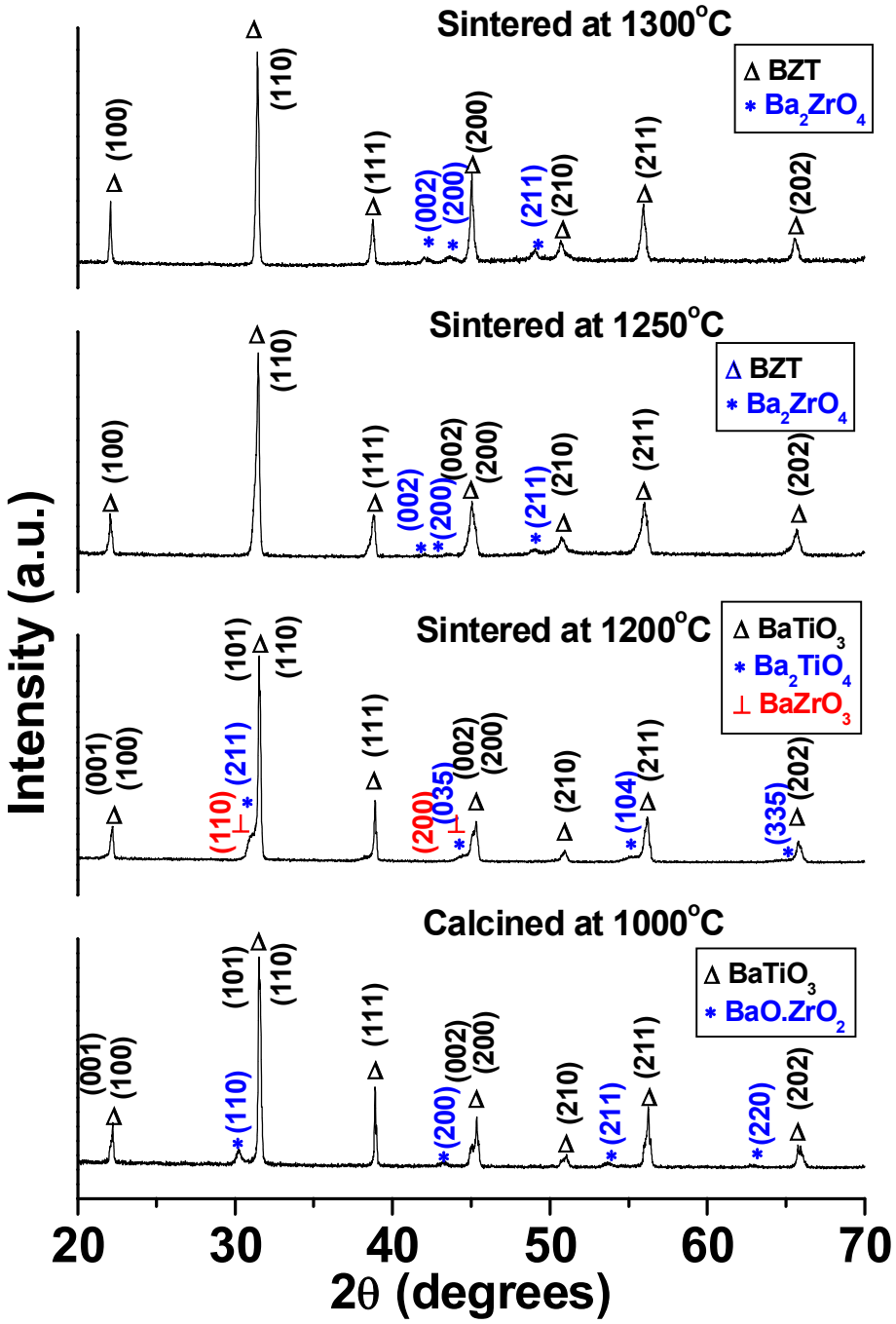

Figure 3.1(a). XRD patterns of BZT (10/90) sintered at different temperatures

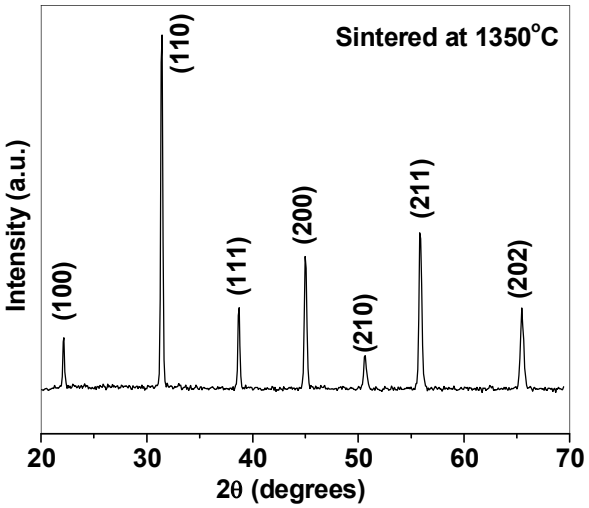

Figure 3.1(b). XRD patterns of BZT (10/90)

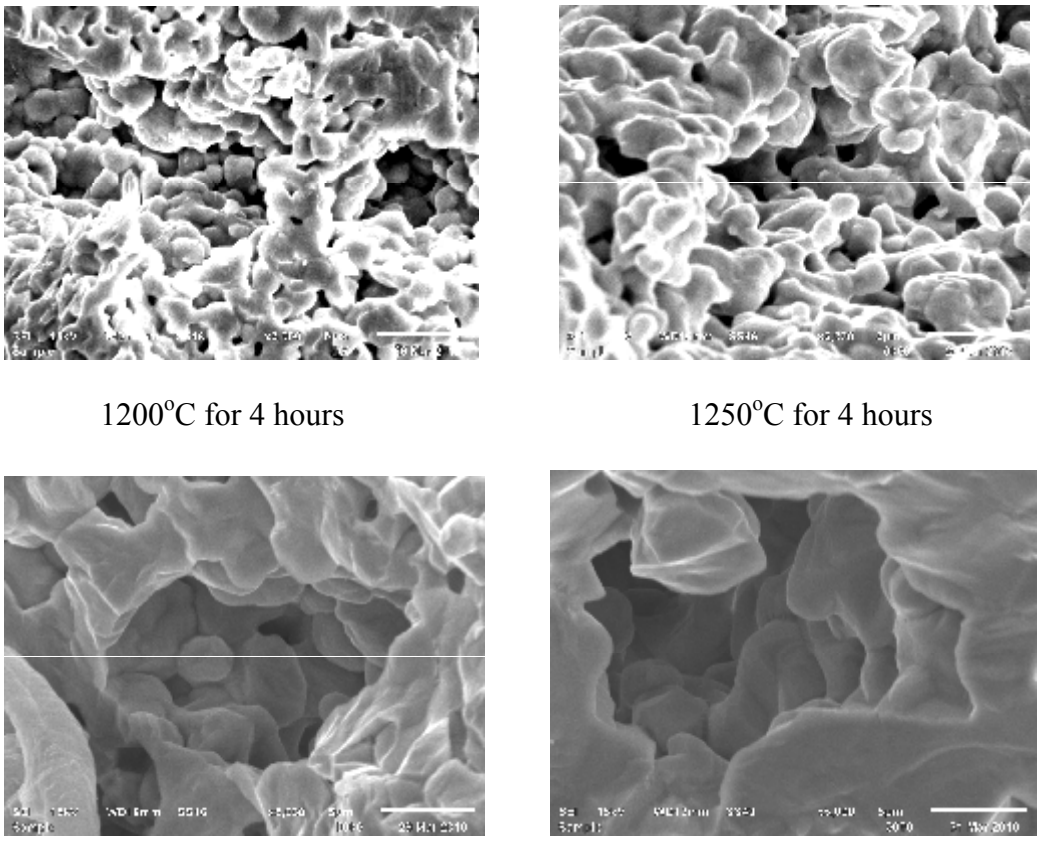

1200°C for 4 hours

1250°C for 4 hours

1300°C for 4 hours

1350°C for 4 hours

Figure 3.2 SEM micrographs for BZT sintered at different temperatures

3.4 Dielectric Properties

3.4.1 Variation of Dielectric Constant and tangent loss with frequency

Dielectric properties under the application of low alternating field were studied by using Agilent 4284A LCR meter. Figure 3.3 shows variation of dielectric constant (ε) and tangent loss (tanδ) over a frequency range (20Hz to 1MHz) for the ceramic samples sintered at different temperatures. Variation of ε and tanδ with frequency of the applied field shows a general trend as that for any ferroelectric. ε and tanδ decreases with increase in frequency and becomes approximately constant for frequencies greater than 10 kHz. A higher value of the dielectric constant at low frequency is due to the presence of all types of polarizations (i.e., electronic, ionic, dipolar, interfacial, etc.) in the material samples near room temperature. Since electronic polarization dominates over all other polarizations at higher frequencies, the value of dielectric constant decreases with increase in frequency [38]. Large dispersion in ε and tanδ can be observed for BZT samples sintered at temperatures lower than 1350^{o}C. The high value of dielectric constant at lower frequencies is attributed to the effect of heterogeneity of the samples like pores, impurities and grain structure etc [39].

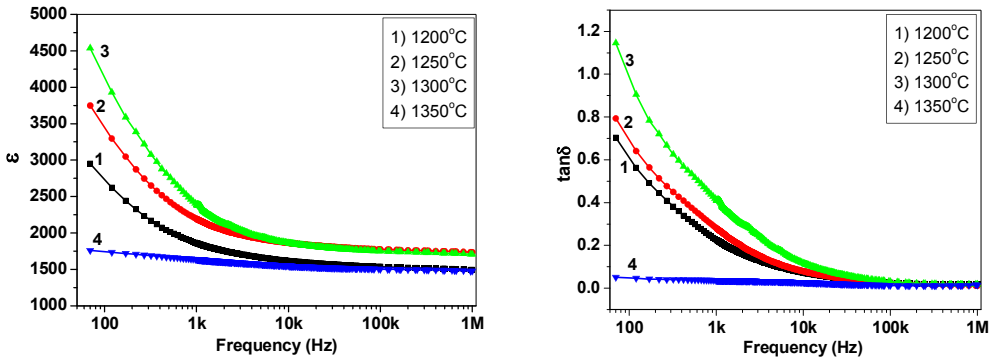

Figure 3.3 Variation of ε and tanδ with frequency

3.4.2 Variation of ε and tanδ with temperature

Figure 3.4 shows the variation of ε with temperature in the range of 30^{o}C to 160^{o}C at four different frequencies (100Hz, 1, 10 and 100 kHz). Dielectric maxima peaks can be observed at a certain temperature 'T_{max}' showing the ferroelectric to paraelectric transition. In case of BZT samples sintered at temperature lower than 1350^{o}C, a small hump in the dielectric vs temperature graph can also be observed. This corresponds to the ferroelectric to ferroelectric transition (orthorhombic-tetragonal; T_{o-t}). In barium titanate based ceramics, lower transition temperatures orthorhombic/tetragonal 'T_{o-t}' and rhombohedral/orthorhombic 'T_{r-o}' occurs at 0^{o}C and -90^{o}C respectively. Substitution of chemically stable and larger zirconium 'Zr^{4+}' for smaller titanium 'Ti^{4+}' affects the various transition temperatures in different fashions. It increases 'T_{o-t}' and 'T_{r-o}' at a rate of 7^{o}C and 18^{o}C per mol % respectively where as decreases T_{max} at a rate 5.3^{o}C per mol% [37]. Due to its larger ionic radius, Zr^{4+} ions need higher energy to get activated for diffusion. This can be done by increasing the sintering time or temperature. In the present case, small hump in dielectric constant and T_{max} approaches each other as the sintering temperature increases. Finally one can observe only one dielectric peak at 92^{o}C for BZT sample sintered at 1350^{o}C as per literature. This can be attributed to the increase in diffusivity of Zr^{4+} ion with increase in sintering temperature. As the sintering temperature increases more and more Zr^{4+} ions get fit into the Ti-site and increase the unit cell volume and lattice parameter. Also the B-O bonds get weaken resulting in decreased stresses and finally decreases the T_{max} from 128^{o}C to 92^{o}C.

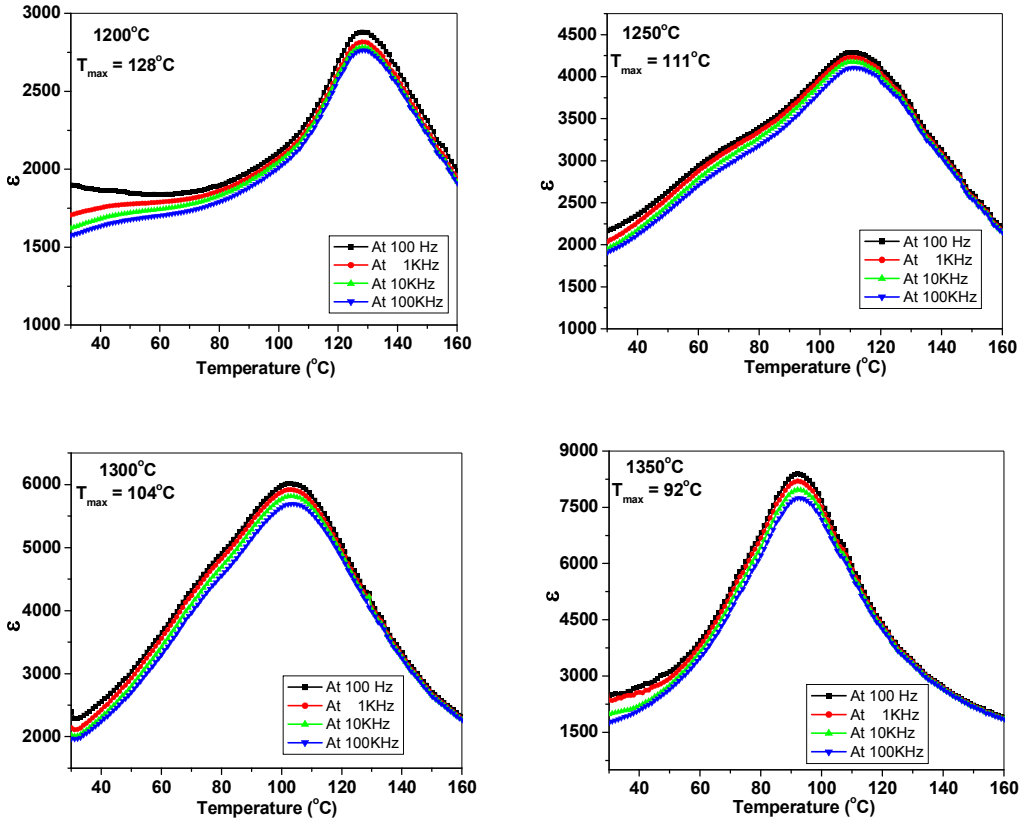

Figure 3.4 Temperature dependence of ε for BZT samples

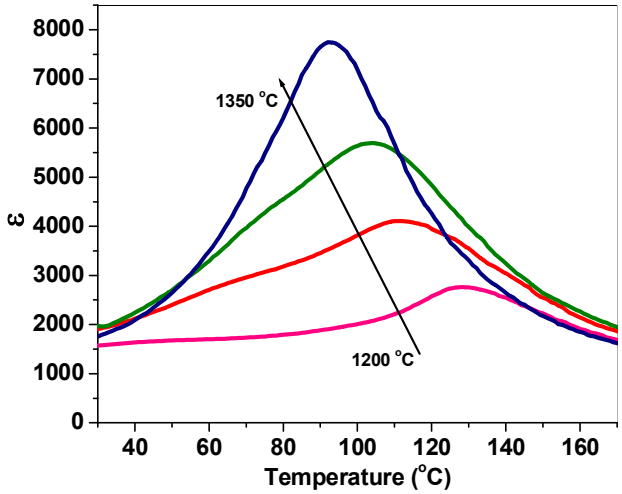

Figure 3.5 ε vs temperature of BZT (10/90) sintered at 100 kHz

The room temperature dielectric constant increases with increase in sintering temperature upto 1300^{o}C while decreases for sample sintered at 1350^{o}C. This is due to the shifting of lower transition temperature T_{o-t} towards higher temperature. Increase in ε_{max} can be related to increased grain size [40]. Figure 3.5 shows the comparative dielectric behavior of BZT sintered at different temperatures under low alternating field of frequency 100 kHz.

3.5 Ferroelectric Properties

The PE loops recorded for BZT samples sintered at different temperatures are shown in figure 3.6. Various ferroelectric parameters like coercive field (E_c), remenance (P_r) and maximum polarization (P_{max}) are given in Table 3.1. It was observed that E_c decreases as sintering temperature increases whereas P_r and P_{max} increases with increase in sintering temperature. All this can be attributed to the increase in grain size with increase in sintering temperature. Because for finer grains (grain diameter around 1.5μm), under the same electric field, the absolute value of the strain decreases and the hysteresis becomes smaller [40]. This is explained by the increase in coercive field for 90^{o} domain rotation with decreasing grain size. The grain boundaries "pin" the domain walls and do not allow them to move easily. For BZT ceramics sintered at 1200 and 1250^{o}C grains are very small, thus they have comparatively larger E_c. The increase in P_r and P_{max} may be due to the development of multidomains inside the grains as the grain size increases. Also the diffusion of Zr to the lattice site is enhanced as the sintering temperature increases. Thus the compositional in-homogeneity decreases with increase in sintering temperature, which results in better ferroelectric properties.

Table 3.1. Ferroelectric properties of BZT sintered at different temperatures

Sintering Temperature (^oC)	1200	1250	1300	1350
E_c (kV/cm)	1.6	1.53	1.50	1.18
P_r ($\mu C/cm^2$)	0.71	1.50	2.07	2.90
P_{max} ($\mu C/cm^2$)	6.96	9.83	10.45	12.44

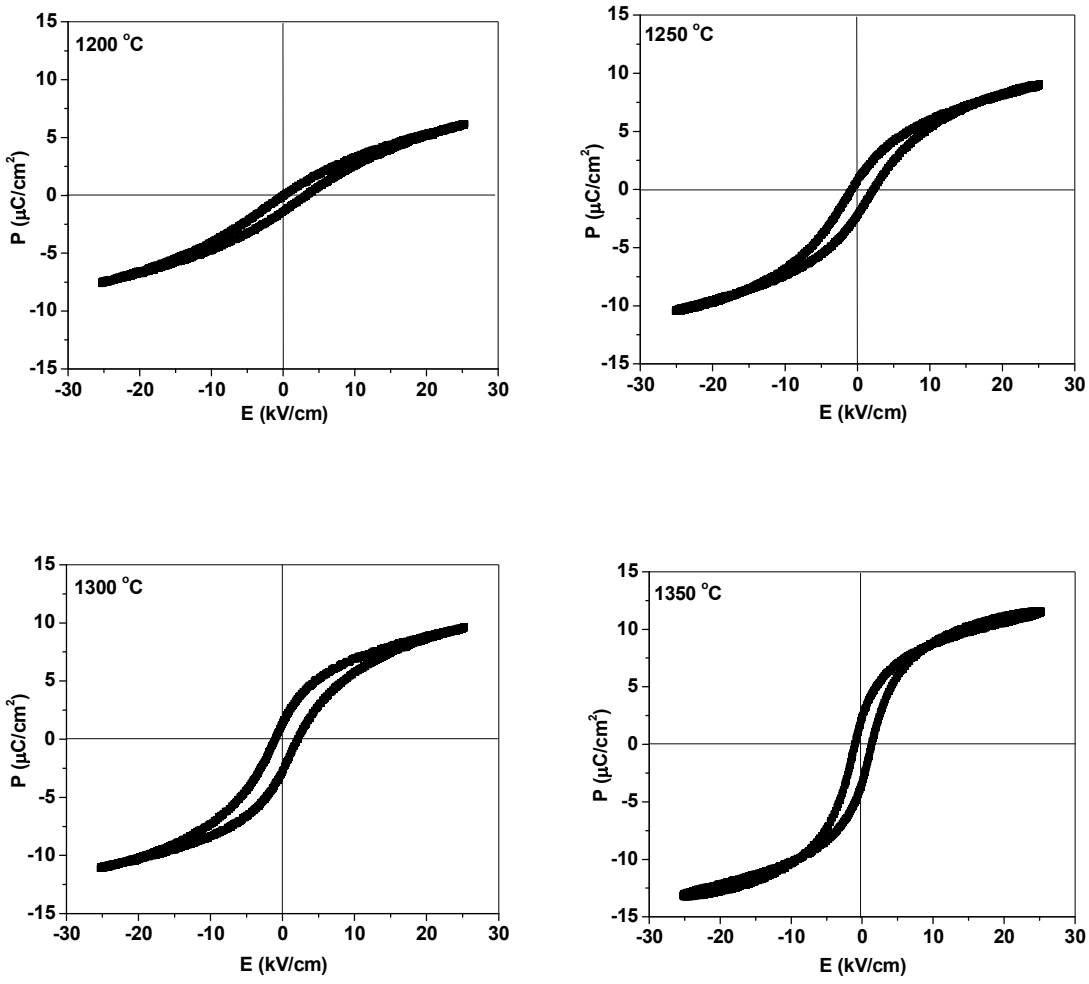

Figure 3.6 PE hysteresis loops for BZT (10/90) sintered at different temperatures

3.6 Two-stage Sintering of BZT (10/90)

The electrical properties of the BT-based ceramics depend strongly on the microstructure as well as composition. The microstructure of these ceramics can be controlled by two approaches. First one is by using additives to prohibit the grain growth for obtaining highly dense ceramics, while the other is using the novel processing technique to modify the microstructure. Numerous studies on the sintering of these ceramics and thermal expansion of similar materials have been reported in the literature [41-43]. Being a simple and low-cost technique the two-stage technique is opted for the fabrication of the $BaZr_{0.10}Ti_{0.90}O_3$ ceramics. The effect of two-stage sintering on densification, microstructure, dielectric and ferroelectric properties of the ceramics is investigated along with the comparison to the normal sintering technique. Normal sintering was done in alumina crucibles at temperature 1350^{o}C with a heating rate of 5^{o}C/min. In two stage sintering, sintering was done firstly at 1150^{o}C (t_1) and then followed by different firing temperature (t_2) 1350^{o}C. The two sintering profiles are shown in figure 7 (a)-(b).

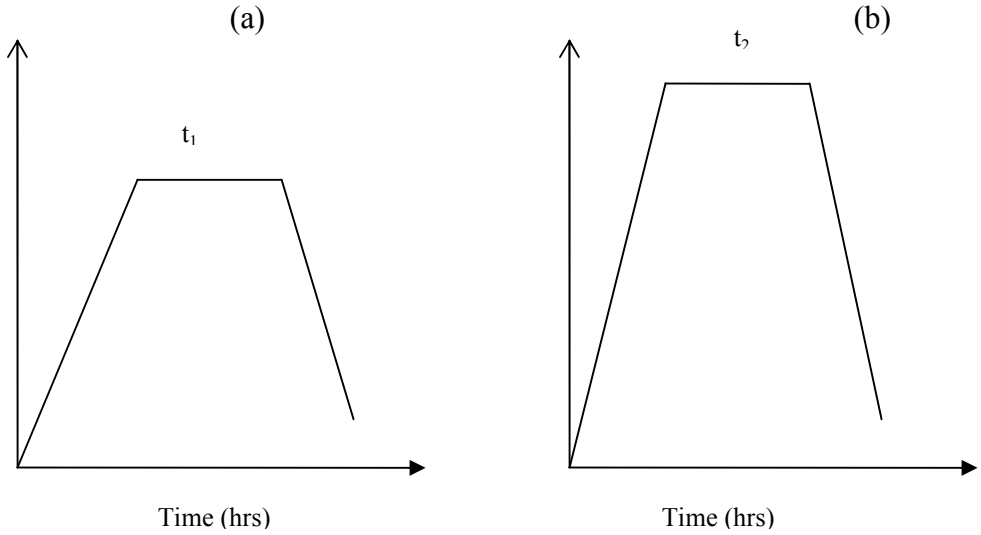

Figure 3.7 (a) First Sintering Step (b) Second Sintering Step

3.6.1 Effect on Structural Properties

Samples prepared by normal and two stage sintering were subjected to X-ray diffraction analysis in order to confirm single phase formation. Figure 3.8 shows the X-ray diffraction patterns for both the samples and confirms the pure perovskite phase with rhombohedral structure. The crystallite size of the polycrystalline samples was calculated from the FWHM ($\beta_{1/2}$) of the predominant reflections in the XRD pattern using Scherrer's formula:

$$P = 0.89\lambda/(\beta_{1/2}\cos\theta)$$

The values of lattice constant (a), broadening ($\beta_{1/2}$) and crystallite size (P) for both samples are given in table 3.2 for comparison. Microstructural features of normally and two stage sintered samples are shown in figure 3.9.

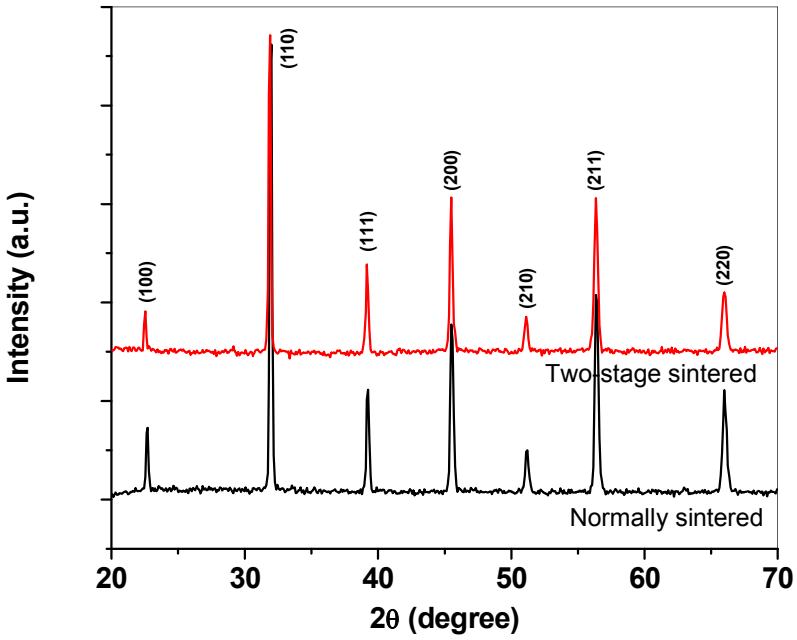

Figure 3.8 XRD patterns for normally and Two-stage sintered BZT (10/90)

Table 3.2 Structural and electrical parameters of normally and two-stage sintered samples

Parameters	Normal sintering 1350°C	Two-stage sintering 1150/1350°C
Lattice constant, a (Å)	3.9808	3.9839
FWHM, $\beta_{1/2}$ (degrees)	0.8272	0.9191
Particle size (Å)	104	94
X-ray density (g/cc)	6.25	6.24
Experimental density (g/cc)	5.49	5.85
Relative density (%)	87.8	93.8
T_c (°C)	92	82
ε_r	1912	2036
ε_{max}	7748	7884
$\tan\delta_r$	0.045	0.019
$\tan\delta_{max}$	0.036	0.030
γ	1.78	1.59
E_a (eV) ($T<T_c$)	0.42	0.45
E_a (eV) ($T>T_c$)	0.67	0.90

3.6.2 Effect on Dielectric Properties

Variation of dielectric constant at four different frequencies (100 Hz, 1, 10 and 100 kHz) with temperature for normally and two stage sintered samples is shown in figure 3.9. Both the samples show dielectric dispersion at low temperatures and large dispersion for

normally sintered sample was observed as compare to that for two stage sintered sample. For both the samples, dielectric constant first increases with increase in temperature, reaches to a maximum value at Curie temperature and then decreases with further increase in temperature indicating ferroelectric-paraelectric phase transition. Comparison of dielectric constant and tangent loss at 100 kHz is shown in figure 3.10. From figure, it is clear that two stage sintering results in enhanced room temperature dielectric constant. Also, there is improvement in tangent loss value for two stage sintered sample as shown in figure 3.10. Figure 3.11 shows the frequency dependence of dielectric properties for both the samples. The dielectric constant decreases with increase in frequency and this decrease is rapid for lower frequency region because as the frequency increases, ionic and orientation polarizations decrease. The variation of tangent loss with frequency shows similar dispersion as that of dielectric constant with frequency. Values of T_c, room temperature dielectric constant (ε_r), dielectric maxima (ε_{max}) and maximum dielectric loss ($\tan\delta_{max}$) for both samples are given in table 3.2.

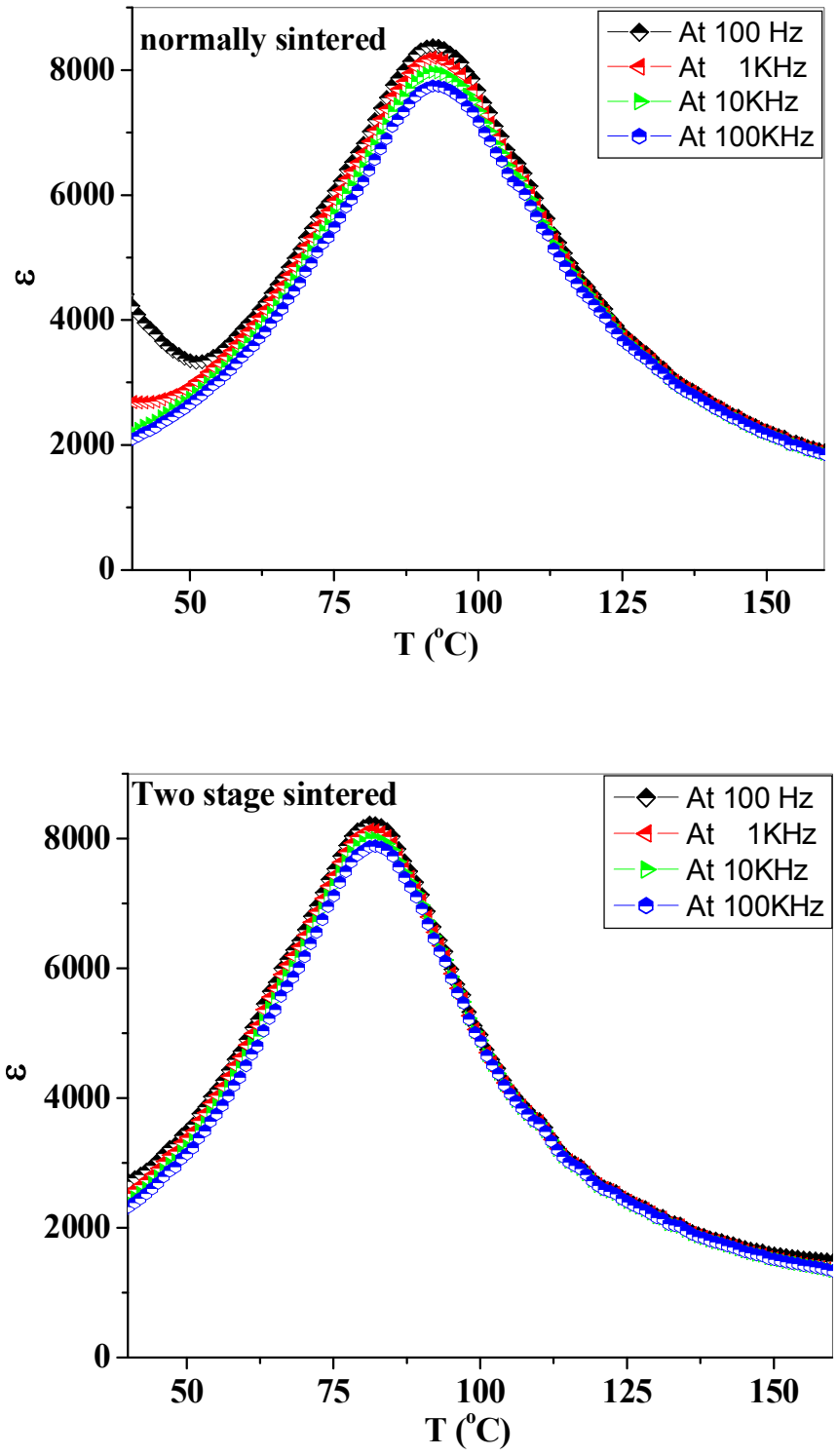

Figure 3.9. Variation of dielectric constant with temperature

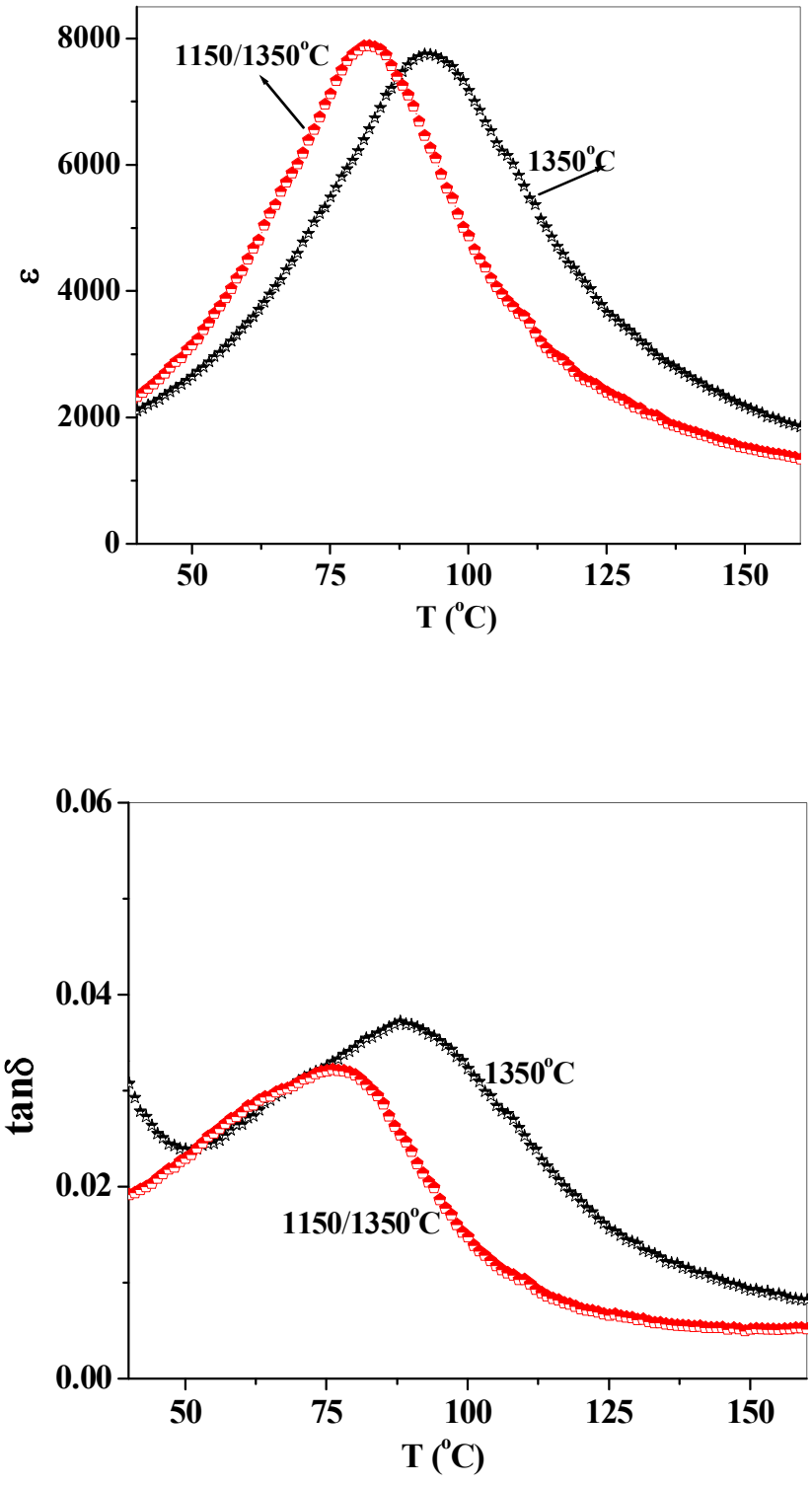

Figure 3.10. Variation of ε and tanδ with temperature at 100 kHz

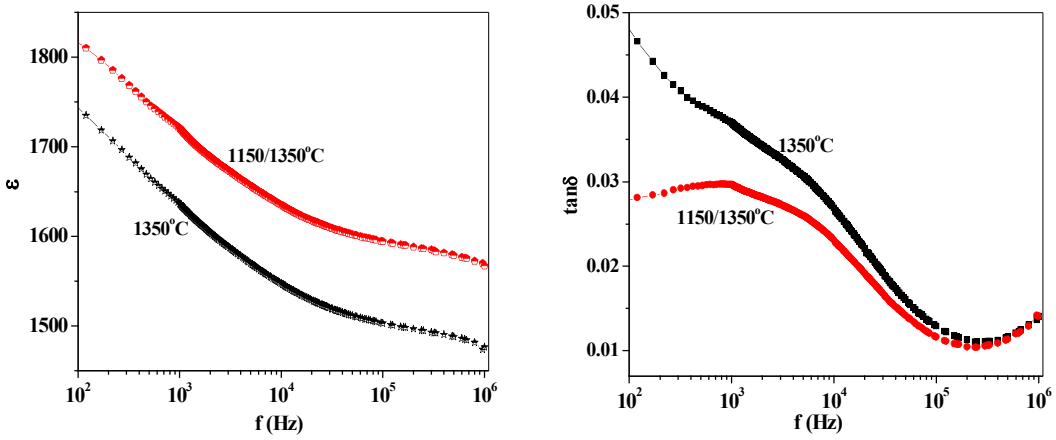

Figure 3.11. Variation of ε and tanδ with frequency at room temperature

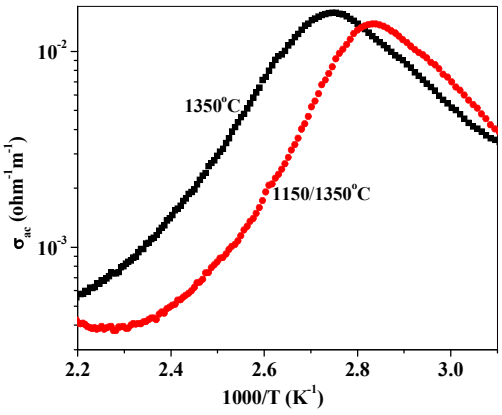

Figure 3.12. Temperature dependence of ac conductivity at 100 kHz

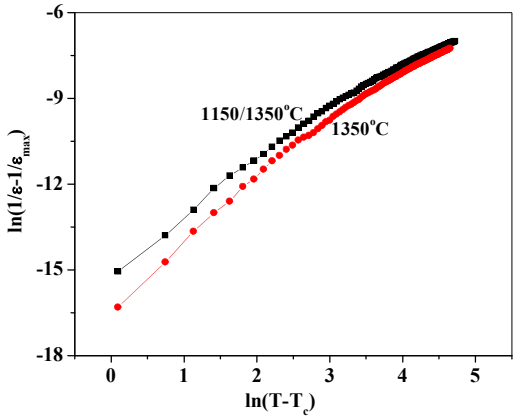

Figure 3.13. $\ln(1/\varepsilon-1/\varepsilon_{max})$ vs. $\ln(T-T_c)$ at 100 kHz

The ac conductivity (σ_{ac}) of both samples at different temperatures was calculated from the dielectric data using the relation:

$$\sigma_{ac} = \varepsilon\varepsilon_o\omega\tan\delta$$

where ω is angular frequency and ε_o is the permittivity of free space. The temperature dependence of σ_{ac} at 100 kHz is shown in figure 3.12. It exhibits an increase in conductivity with increase in temperature up to T_c, which may be due to increase in polarizability and above T_c, there is a fall in σ_{ac} data which indicates a typical behavior of the dc component in the conductivity [44]. The activation energy (E_a) required for charge conduction was obtained by Arrhenius relation

$$\sigma_{ac} = \sigma_o\exp(-E_a/kT)$$

Where σ_o is temperature independent constant and k is Boltzmann constant. The values of activation energy of both samples are given in table 3.2. The degree of diffusiveness for both the samples was calculated using the formula

$$\ln(1/\varepsilon-1/\varepsilon_{max}) = \gamma \ln(T-T_c) + a$$

where, ε_{max} is the value of dielectric constant at T_c. The value of γ lies between 1 and 2, where $\gamma = 1$ is for ideal Curie-Weiss behavior and lies between 1 and 2 for diffused phase transitions [14, 45]. The calculated values of γ are given in table 3.2 and it is observed that γ is small for two stage sintered sample i.e. degree of disorderness decreases.

References

[1] E.J. Brajer, "Polycrystalline Ceramic Materials," U.S. Pat. No. 2 708 (1955) 243.

[2] F. Kulscar, "Fired Ceramic Barium Titanate Body," U.S. Pat No. 2 735 (1956) 024.

[3] R.C. Kell and N.J. Hellicar, Acustica, **6** (1956) 235.

[4] T.N. Verbitskaja, G.S. Zhdanow, Yu.N. Venevtsev and S.P. Soloviev, Sov. Phys.–Crystallogr. (Engl. Transl.), **3** (1958) 182.

[5] D. Hennings, A. Schnell and G. Simon, J. Am. Ceram. Soc., **65** (1982) 539.

[6] U. Robels, J.H. Calderwood and G. Arlt, J. Appl. Phys., **77** (1994) 4002.

[7] K.W. Plessner, Proc. Phys. Soc., London, **69** (1956) 1261.

[8] B. Lewis, Proc. Phys. Soc., London, **73** (1960) 17.

[9] Z. Pajak and J. Stankowski, Proc. R. Soc. London *A*, **72** (1958) 1144.

[10] A. Misarova, Solid State Phys., **2** (1960) 1276.

[11] H. Neumann and G. Arlt, IEEE Spectrum, **76** (1987) 303–10.

[12] R. Lohkamper, H. Neumann and G. Arlt, J. Appl. Phys., **68** (1990) 4220–24.

[13] U. Robels and G. Arlt, J. Appl. Phys., **73**, (1993) 3454–60.

[14] Yu. Zhi, R. Guo and A.S. Bhalla, J. Appl. Phys., **88** (2000) 410.

[15] Yu. Zhi, R. Guo and A.S. Bhalla, Appl. Phys. Lett., **77** (2000) 1535.

[16] F. Moura, A.Z. Simoes, B.D. Stojanovic, M.A. Zaghete, E. Longo and J.A. Varela, J. Alloys Comp., **462** (2008) 129-132.

[17] N. Nanakorn, P. Jalupoom, N. Vaneesorn and A. Thanaboonsombut, Ceram. Int., **45** (2007) 452.

[18] Hiroshi Maiwa, Jap. J. Appl. Phys., **46** (2007) 7013.

[19] W. Chaisan, R. Yimnirun and S. Ananta, Ferroelectrics, **346** (2007) 84.

[20] J.S. Choi and H.G. Kim, J. Mater. Sci., **27** (1992) 1285.

[21] H.T. Kim and Y.H. Han, Ceram. Int., **30** (2004) 1719.

[22] J.K. Lee, K.S. Hong and J.W. Jang, J. Am. Ceram. Soc., **84** (2001) 2001.

[23] S. Wongsaenmai, R. Yimnirun, S. Ananta, R. Guo and A.S. Bhalla, Mater. Lett., **62** (2008) 352.

[24] R. Wongmaneerung, R. Guo, A.S. Bhalla, R. Yimnirun and S. Ananta, J. Alloys Comp., **461** (2008) 565.

[25] U. Bottger, Dielectric properties of polar oxides, properties, characterization and imaging, ed. R. Waser, U. Bottger and S. Tiedke, Wiley-VCH Verlag GmbH&Co. KGaA, Weinheim, 2005.

[26] M. Aparna, T. Bhimasankaram, G. Prasad, S.V. Suryanarayana and G.S. Kumar, Bull. Mater. Sci., **24** (2001) 497.

[27] Y. Zhi, C. Ang, R. Guo and A.S. Bhalla, Appl. Phys. Lett., **81** (2002) 1285.

[28] A. Simon, J. Ravez and M. Maglione, Solid State Sci., **7** (2005) 925.

[29] F.W. Perry, G.A. Hutchins and L.E. Cross, Mat. Res. Bull.**, 2** (1967) 409.

[30] S.M. Pilgrim, A.E. Sutherland and S.R. Winzer, J. Am. Ceram. Soc., **73** (1990) 3122.

[31] Powder-X for Windows by Cheng Dong (Institute of Physics, Chinese Academy of Sciences, P.O. Box 603, Beijing 100080, P.R. China.

[32] K. Watanabe, H. Ohsato, H. Kishi, Y. Okino, N. Kohzu, Y. Iguchi and T. Okuda, Solid State Ion., **108** (1998) 129.

[33] M.T. Buscaglia, V. Buscaglia, M. Viviani, P. Nanni and M. Hanuskova, J. Eur. Ceram. Soc., **20** (2000) 15.

[34] M. W. Barsoum, Fundamentals of Ceramics, The McGraw Hill, New York, 1997.

[35] I. Bunget and M. Popescu, Physics of Solid Dielectrics, Elsevier, New York, 1984.

[36] L.L. Hench and J.K. West, Principles of Electronic Ceramics, John Wiley & Sons, New York ,1989.

[37] B. Jaffe, W. Cook and H. Jaffe, Piezoelectric Ceramics, Academic Press, London, 1971.

[38] O.P. Thakur and C. Prakash, Phase Transitions, **76** (2003) 567.

[39] C.M. Kanamadi, L.B. Pujari and B.K. Chougule, J. Magn. Magn. Mater. **295** (2005) 139.

[40] K. Uchino, Ferroelectric Devices, Marcel Dekker, Inc., New York 2000.

[41] D.F. Rushman and M.A. Strivens, Trans. Faraday Soc., **42** (1946) 231.

[42] G. Shirane and K. Suzuki, J. Phys. Soc. Japan, **6** (1951) 274.

[43] Yu.N. Venevtsev, G.S. Zhdanov, S.P. Solov'ev and V.V. Ivanova, Kristallografiya **4** (1959) 255; Soriet Phys. Cryst., **4** (1959)235.

[44] M.E. Lines and A.M. Glass, Principles and applications of ferroelectrics and related materials, Gharendon, Oxford, 1977.

[45] B. Vaidhyanathan, A.P. Singh, D.K. Agrawal, T.R. Shrout, R. Roy and S. Ganguly, J. Am. Ceram. Soc., **84** (2001) 1197.

Chapter 4

Synthesis and Characterization of Substituted BZT 10/90 Ceramics

BZT 10/90 ceramics substituted with Pb^{2+}, Zr^{4+} and Ca^{2+} were synthesis by conventional solid state reaction method. Samples were sintered at 1300^{o}C and subjected to XRD and SEM analysis to get structural information. The prepared samples were also studied for their dielectric, ferroelectric and piezoelectric properties. The obtained results were correlated and discussed in this chapter.

4.1 Introduction

$BaTi_{1-x}Zr_xO_3$ (BZT) ferroelectric ceramics with low dielectric loss are used in the fabrication of ceramic capacitors as Zr^{4+} is chemically more stable than Ti^{4+} [1-3]. It has been observed that a suitable substitution at different atomic sites of any ferroelectric structure usually has a dramatic effect on physical properties of materials. By selecting suitable substituent ions for Ba site or Ti site, many physical and electrical properties can be modified which can be useful for device fabrication such as computer memory and display, sensors, modulator, etc. The nature of ferroelectric phase transition at the transition temperature of BZT bulk ceramics is known to change strongly with Zr content. For $x > 0.08$, $BaTi_{1-x}Zr_xO_3$ ceramics show a broad dielectric constant temperature curve near transition temperature [4-8]. It has been reported that Pb substituted BZT ceramics exhibit improvements in tangent loss, dielectric constant and ferroelectric properties. It is also reported that calcium substituted BZT ceramics exhibit a broad dielectric constant temperature curve near T_c with high value of dielectric constant [9].

4.2 Pb^{2+} Substituted BZT (10/90) (*A-site Substitution)*

Polycrystalline ceramic samples with compositions $Ba_{1-x}Pb_x\ Zr_{0.10}Ti_{0.90}O_3$ with $0 \leq x \leq 0.20$ in the steps of 0.05 were prepared by conventional solid state reaction technique. Since lead is volatile and hence in order to reduce the lead loss during sintering, Pb-substituted BZT ceramic samples were sintered at 1300^oC for 4 hours in lead rich environment.

4.2.1 Physical and Structural Properties

For all the samples, XRD patterns were recorded. Figure 4.1 shows the X-ray diffraction (XRD) patterns for all the sintered samples. The presence of sharp single peaks of varying intensity in the XRD pattern indicates formation of single phase polycrystalline samples. All the peaks in the XRD pattern could be indexed and the lattice parameters were determined using interplanar spacing 'd'. The lattice parameters were calculated using **powder "X"** software [10]. It has also been reported that there are mainly three stages of substitution of foreign ions in barium titanate based materials. In the first two stages, replacing ions replaces the original ions located in the lattice on the A or B site. In the third stage a secondary phase appears which indicates the insolubility of doped ions due to over limit of substitution [11,12]. The ionic radii of Ba^{2+} or Pb^{2+} in 12 coordinates are 1.75 Å and 1.63 Å respectively [13]. Therefore, Pb^{2+} can occupy A site in BZT solution. It can be observed from the XRD pattern that as the amount of Pb^{2+} is increased, the main peak (110) is shifting towards the lower angle side which indicates the increase in the lattice constants.

From figure 4.1, it can also be observed that the peak (at $2\theta \approx 45$ degree) is splitting as amount of Pb^{2+} ion increases which reveals that structure of material is changing and tetragonality is increasing with increasing amount of Pb^{2+}. The samples with $x = 0$ and 0.05 were found to have rhombohedral and orthorhombic structure, respectively. Further increase in x causes the change of structure from orthorhombic to tetragonal. Variations in lattice parameters (a, b and c) and tetragonality as a function of x are shown in figure 4.2. For all the compositions the calculated lattice parameters are shown in Table 4.1.

The experimental density 'd_{exp}', theoretical density 'd_{th}', relative density 'd_{rel}' and apparent porosity of Pb substituted BZT (10/90) are given in table 4.2. The relative density is found to increase with the increase in Pb substitution. This may be because of substitution of high density PbO to the selected $BaZr_xTi_{1-x}O_3$ matrix. However, the tetragonality and relative density is found to increase with increase in Pb substitution to BZT (10/90). The average grain size is found to increase upto 15 mol%, whereas, it decreases for x equal to 20 mol%. The SEM micrographs for all the samples are given in figure 4.3.

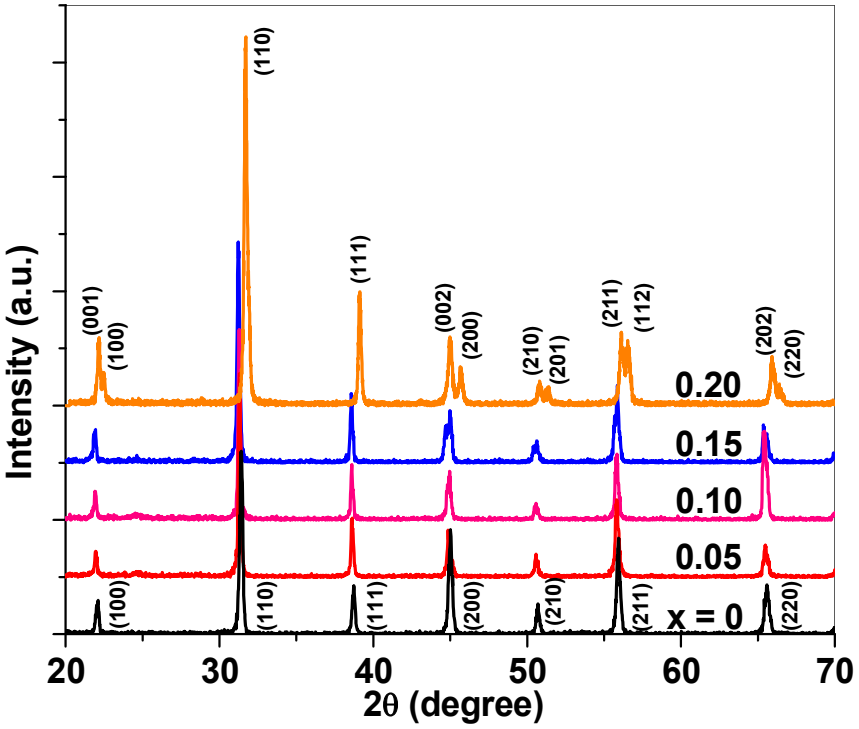

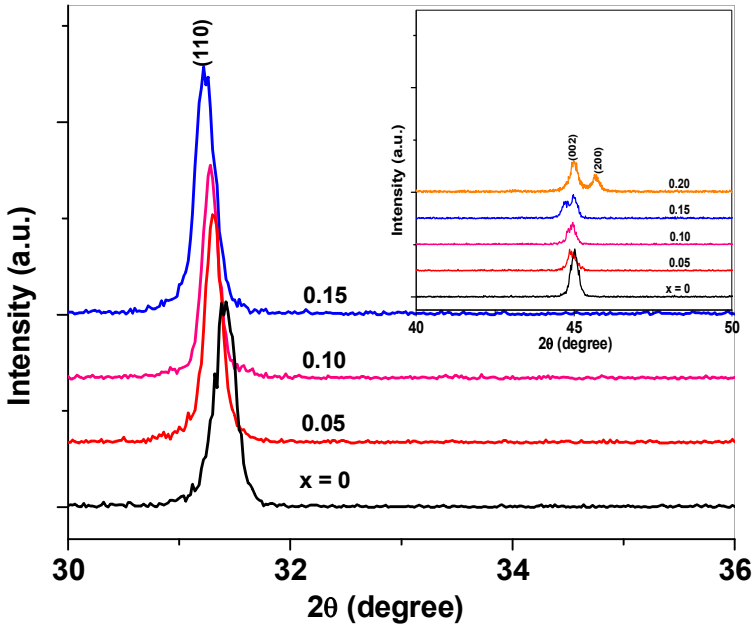

Figure 4.1 XRD patterns for Pb-substituted BZT ceramics

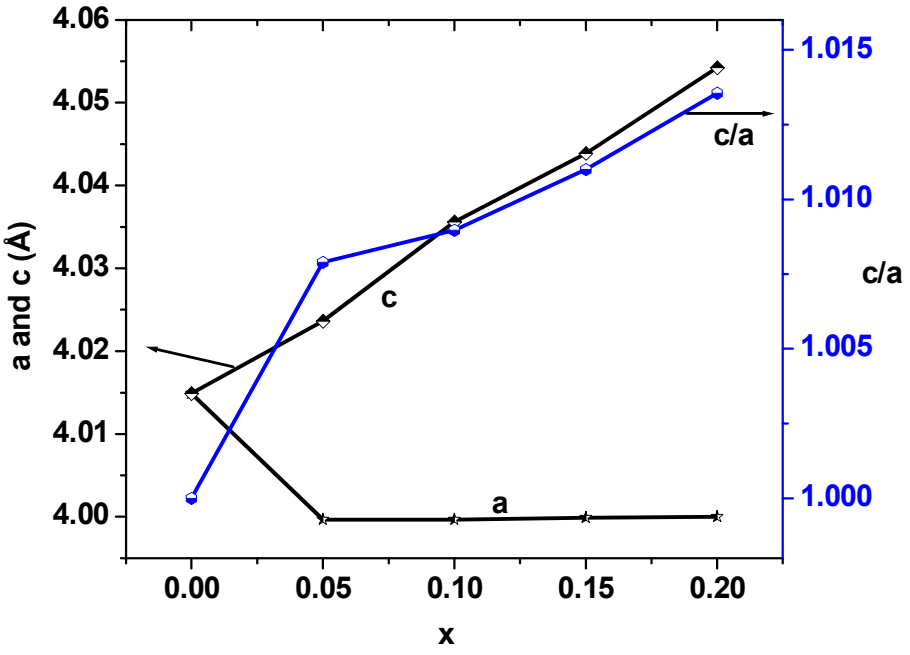

Figure 4.2 Variation of lattice parameters and c/a as a function of x

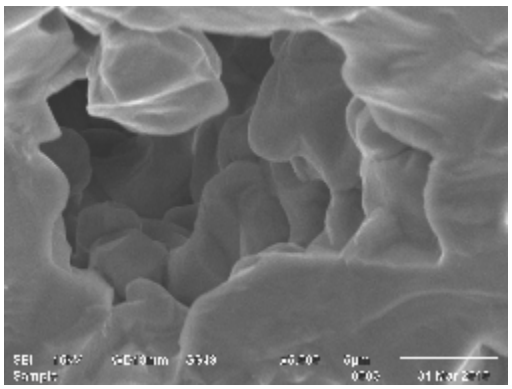

x = 0

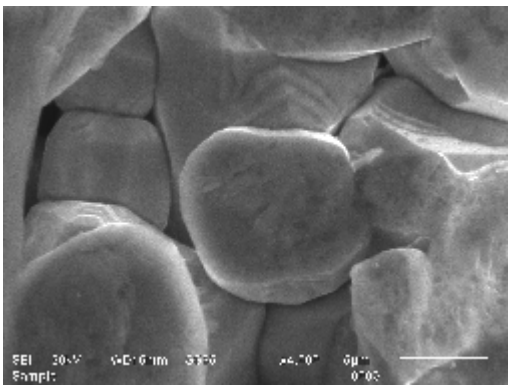

x = 0.05

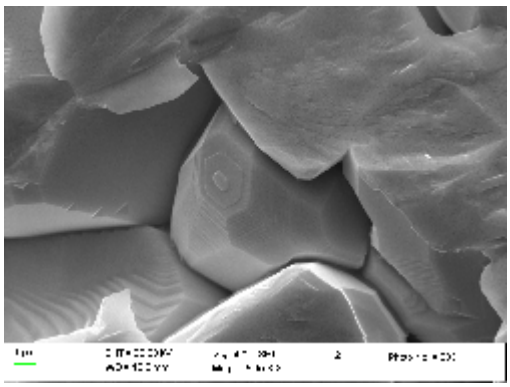

x = 0.10

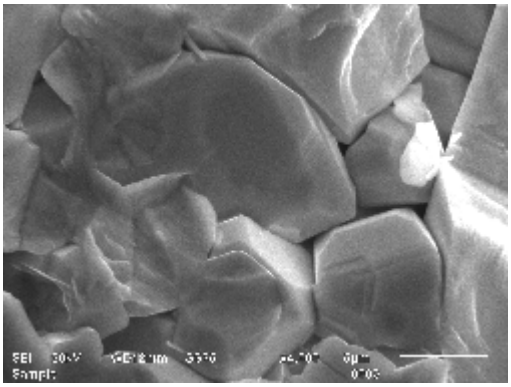

x = 0.15

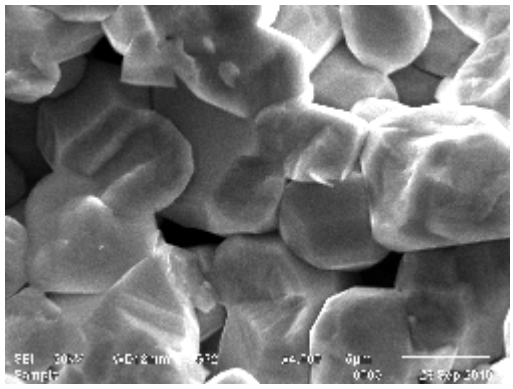

x = 0.20

Figure 4.3 SEM images of Pb-substituted BZT ceramics

Table 4.1 lattice parameters, c/a and structure for all values of x

x	α (degree)	a (Å)	b (Å)	c (Å)	Structure	c/a
0	89.59	4.0149	4.0149	4.0149	Rhombohedral	1.0000
0.05	90	3.9921	4.0119	4.0236	Orthorhombic	1.0079
0.10	90	3.9997	3.9997	4.0356	Tetragonal	1.0089
0.15	90	3.9999	3.9999	4.0439	Tetragonal	1.0110
0.20	90	4.0000	4.0000	4.0542	Tetragonal	1.0136

Table 4.2 Relative density (d_{rel}) and apparent porosity (*P*) of $Ba_{1-x}Pb_xTi_{0.90}Zr_{0.10}O_3$ for all values of x

x	d_{exp} (g/cc)	d_{th} (g/cc)	d_{rel} (%)	Porosity (%)	Av. Grain Size (μm)
0	4.83	6.09	79.3	20.7	6.37
0.05	5.32	6.21	85.7	14.3	8.79
0.10	5.41	6.29	96.0	14.0	10.21
0.15	5.55	6.37	87.13	12.87	12.12
0.20	5.78	6.44	89.75	10.25	6.7

4.2.2 Dielectric Properties

Figure 4.4 shows that dielectric constant (ε) and loss tangent (tanδ) decreases with increase in frequency, which is general behavior of a ferroelectric. A higher value of the dielectric constant at low frequencies is due to the presence of all types of polarizations (i.e. electronic, ionic, dipolar, interfacial etc.) in the material near room temperature. Since electronic polarization dominates over all other polarizations at higher frequencies, the

value of dielectric constant decreases with increase in frequency [14]. Figure 4.5 shows the variation of dielectric constant with temperature at four different frequencies (100 Hz, 1k, 10k and 100 kHz). The dielectric properties were measured as a function of temperature up to well above the transition temperature, T_c, of the corresponding samples. The dielectric constant increases with increasing temperature and shows a peak which is characteristic of ferroelectric materials. The dielectric constant does not show much dependence on frequency at temperatures below T_c but the effect of frequency becomes pronounced as the temperature approaches T_c. The temperature dependence of the dielectric constant and tanδ for all x measured at 100 kHz is shown in figure 4.6. For ceramic sample with x = 0.05 another smaller dielectric peak was observed at temperature lower than T_c. This hump corresponds to orthogonal to tetragonal phase transition for the material [15]. This may be attributed to the fact that substitution of Pb^{2+} for Ba^{2+} decreases ferroelectric to ferroelectric phase transitions (T_{r-o} or T_{o-t}) towards lower temperature. For samples with x > 0.05 no such peak is observed which indicates that material phase is tetragonal at room temperature [16]. The confirmation of the phase with different structures has already been discussed in Table 4.1. Increase in tanδ with increase in temperature may be due to conduction losses [17]. From the comparative plot of dielectric constant with temperature it can be observed that T_c shifts towards higher temperature with increase in x which is an expected result of Pb^{2+} substitution. Since sample with x = 0.05 have bigger grains, long range ordered polarization may occur resulting in dielectric peak with greater height as compared to samples with other values of x. Large sized grains can be achieved for other values of x by sintering the material samples at temperature higher than 1300^{o}C [18]. Volatile nature of lead is a limiting factor for sintering temperature. Greater stability of dielectric constant

over a certain range of temperature can also be observed for samples with higher values of x. This is also an expected result of Pb^{2+} substitution. Tangent loss is found to decrease with increase in Pb^{2+} content. Figure 4.7 shows the variation of room temperature (at $30^{o}C$) dielectric constant and T_c of the samples as a function of x. T_c increases with increase in x while room temperature dielectric constant increases upto x = 0.10 and then decreases for x greater than 0.10. Observed behavior of room temperature dielectric constant upto x = 0.10 because of shifting of T_{r-o} and T_{o-t} towards lower temperature.

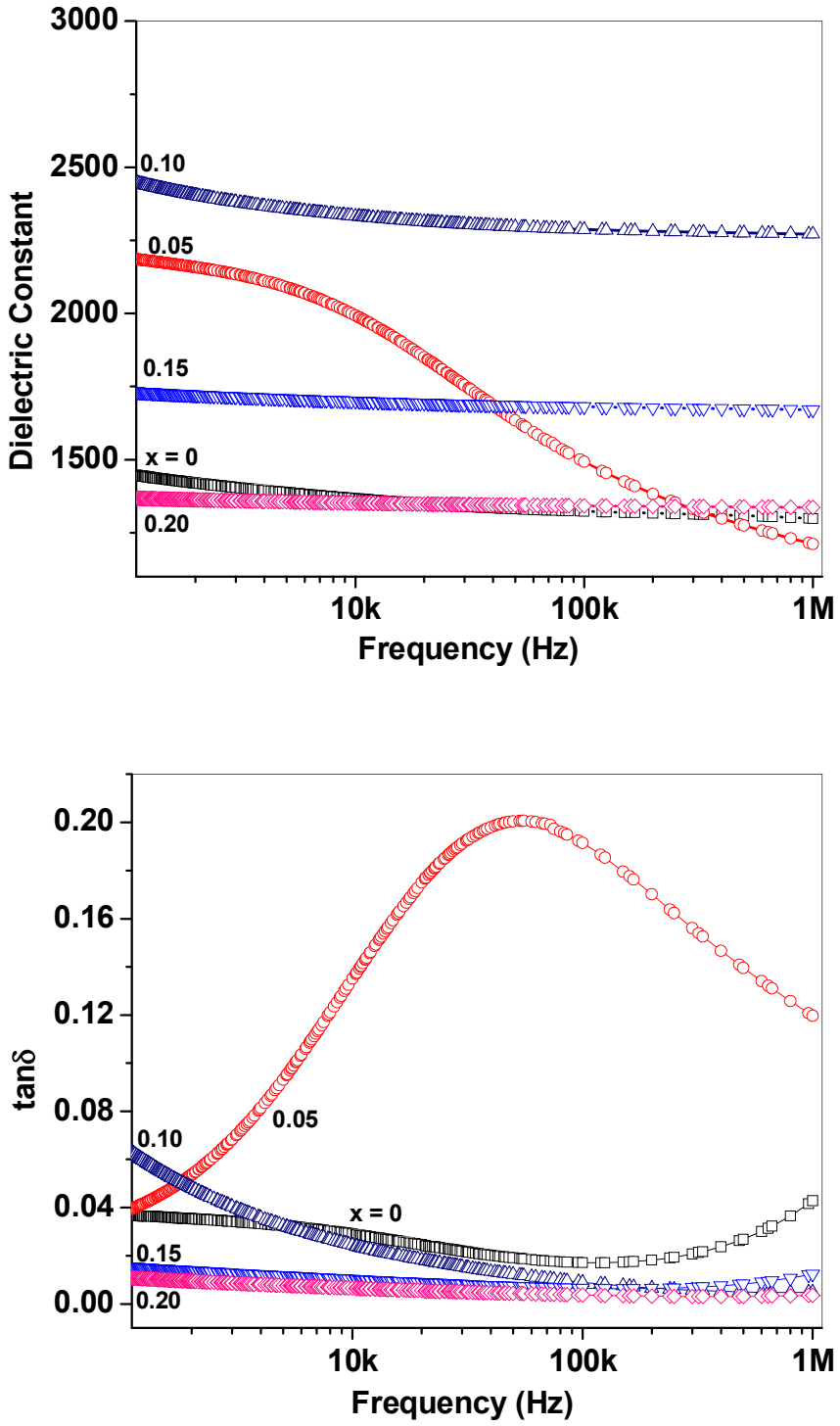

Figure 4.4 Variation of ε and tanδ with frequency for all x

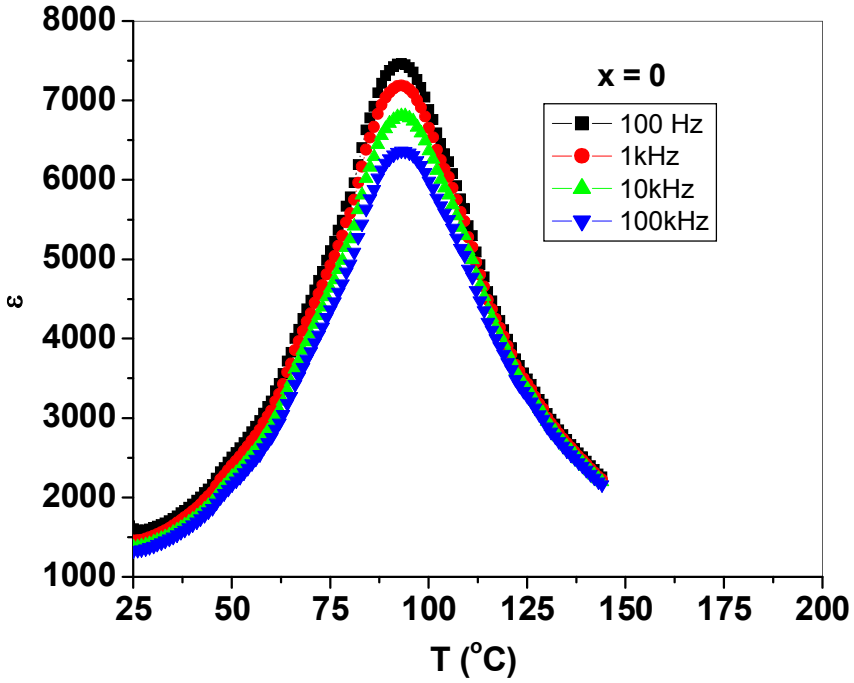
x = 0
100 Hz
1kHz
10kHz
100kHz
ε
T (°C)
8000
7000
6000
5000
4000
3000
2000
1000
25
50
75
100
125
150
175
200

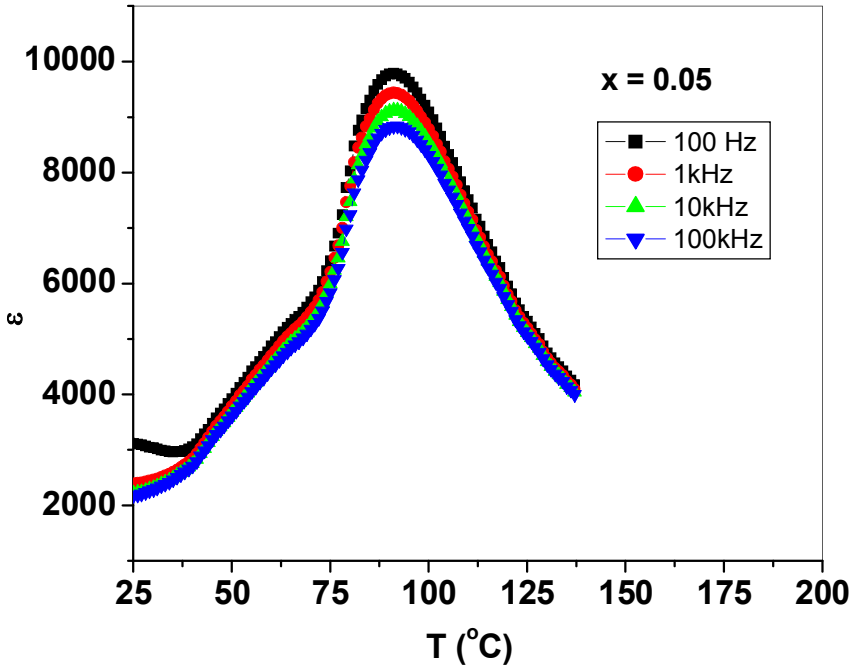
x = 0.05
100 Hz
1kHz
10kHz
100kHz
ε
T (°C)
10000
8000
6000
4000
2000
25
50
75
100
125
150
175
200

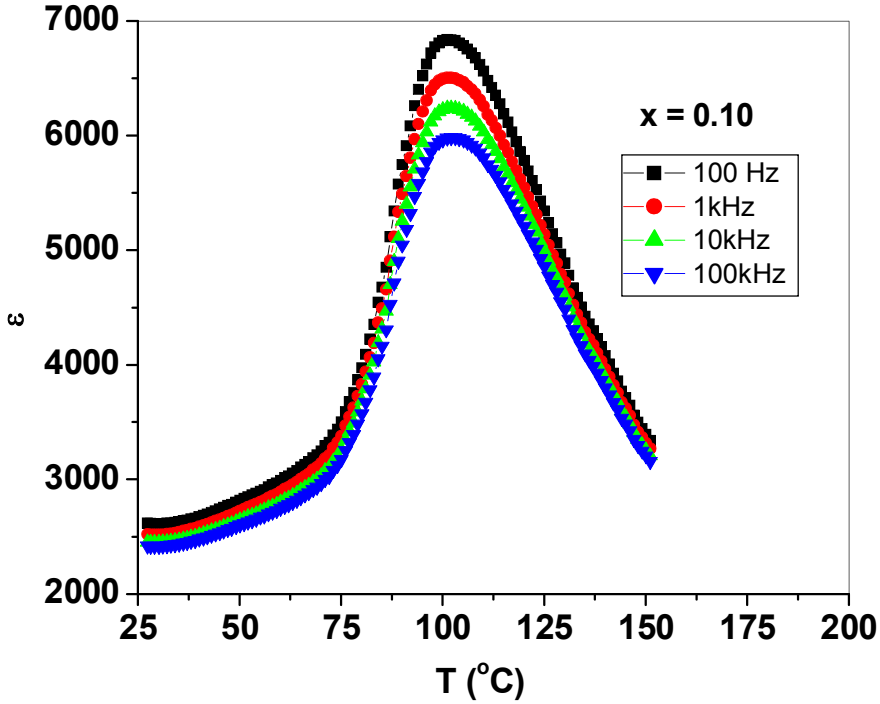
x = 0.10
100 Hz
1kHz
10kHz
100kHz
ε
T (°C)
7000
6000
5000
4000
3000
2000
25
50
75
100
125
150
175
200

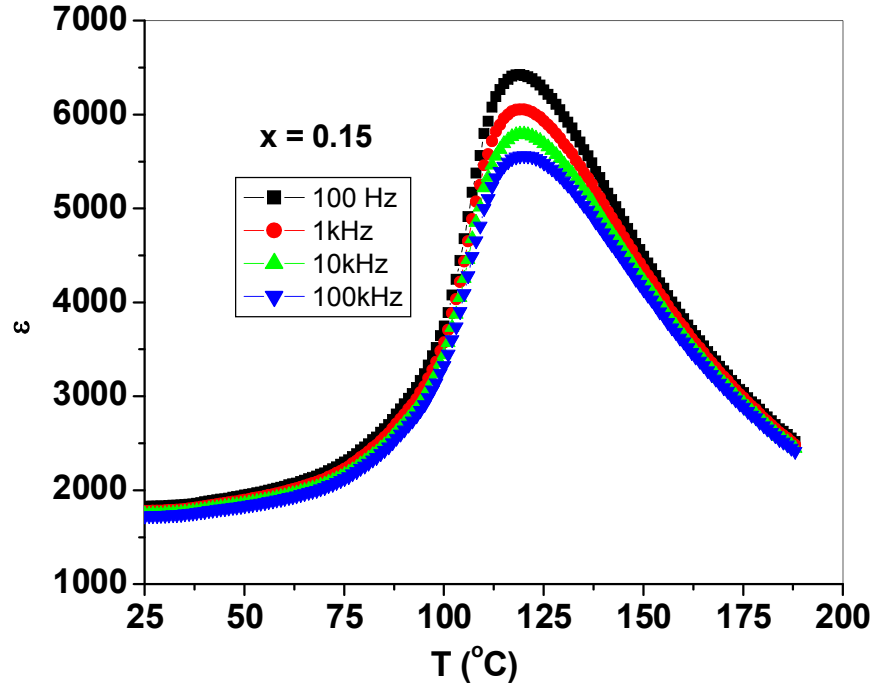
x = 0.15
100 Hz
1kHz
10kHz
100kHz
ε
T (°C)
7000
6000
5000
4000
3000
2000
1000
25
50
75
100
125
150
175
200

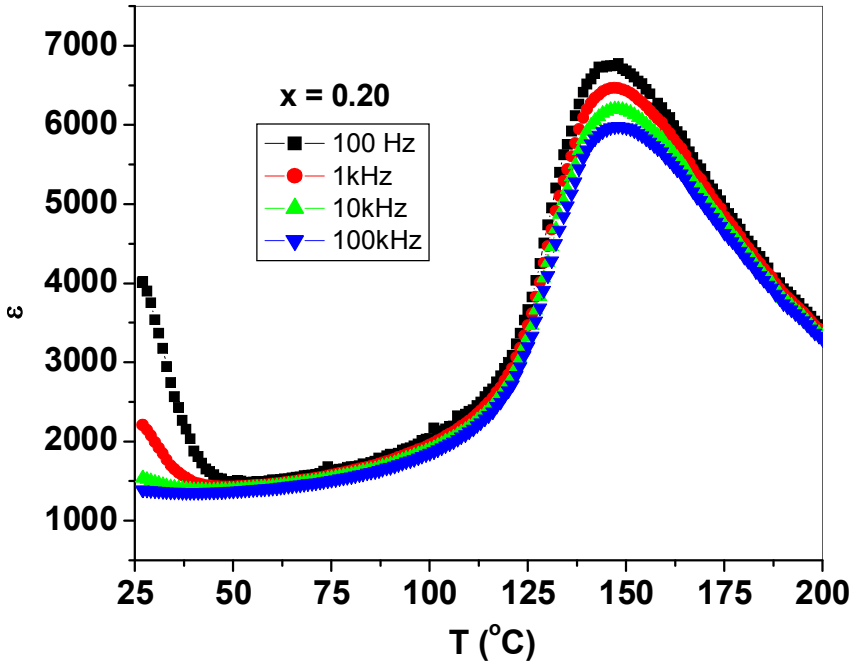

Figure 4.5 Variation of ε as a function of temperature at different frequencies

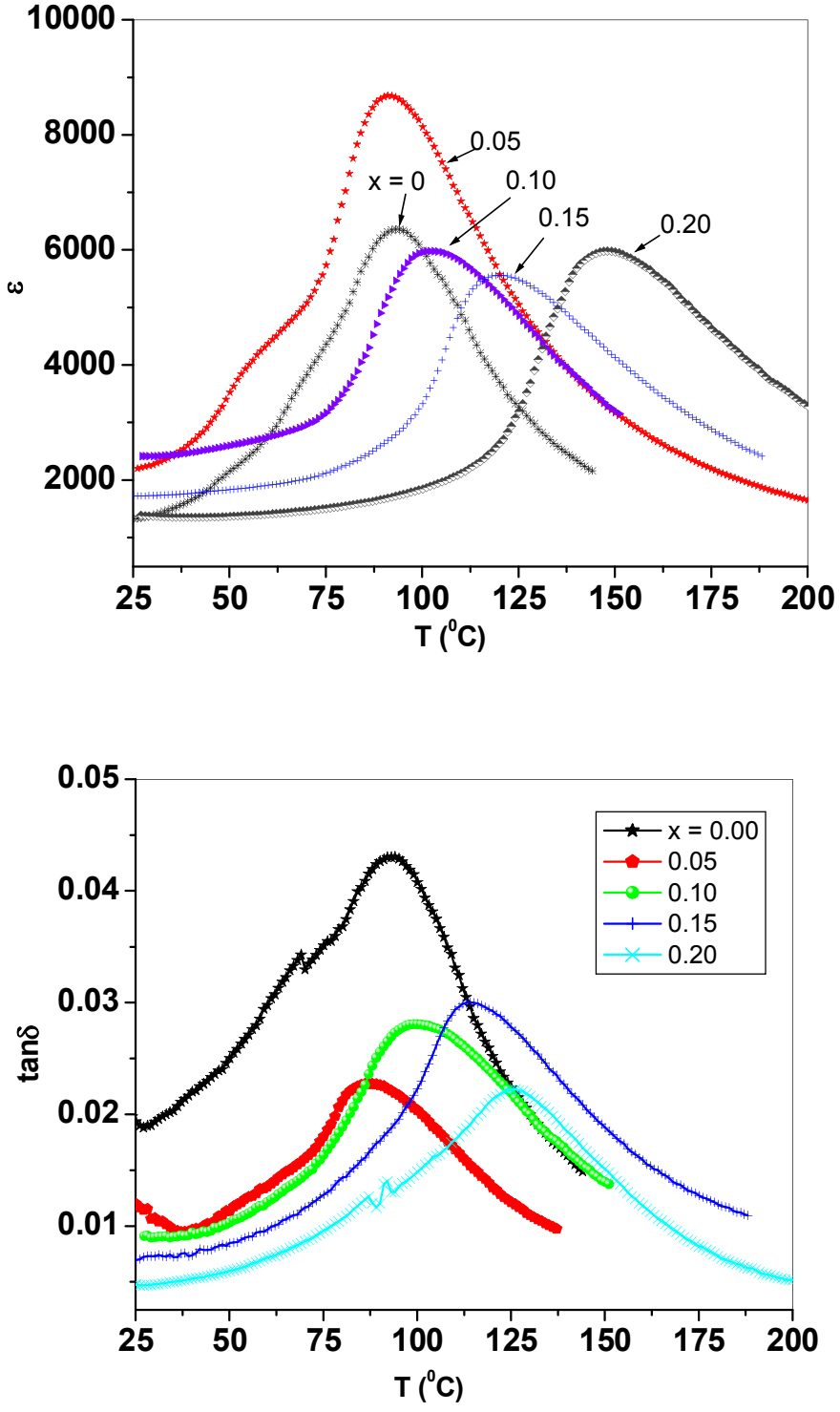

Figure 4.6 Variation of ε and tan δ as a function of temperature for all x at100 kHz

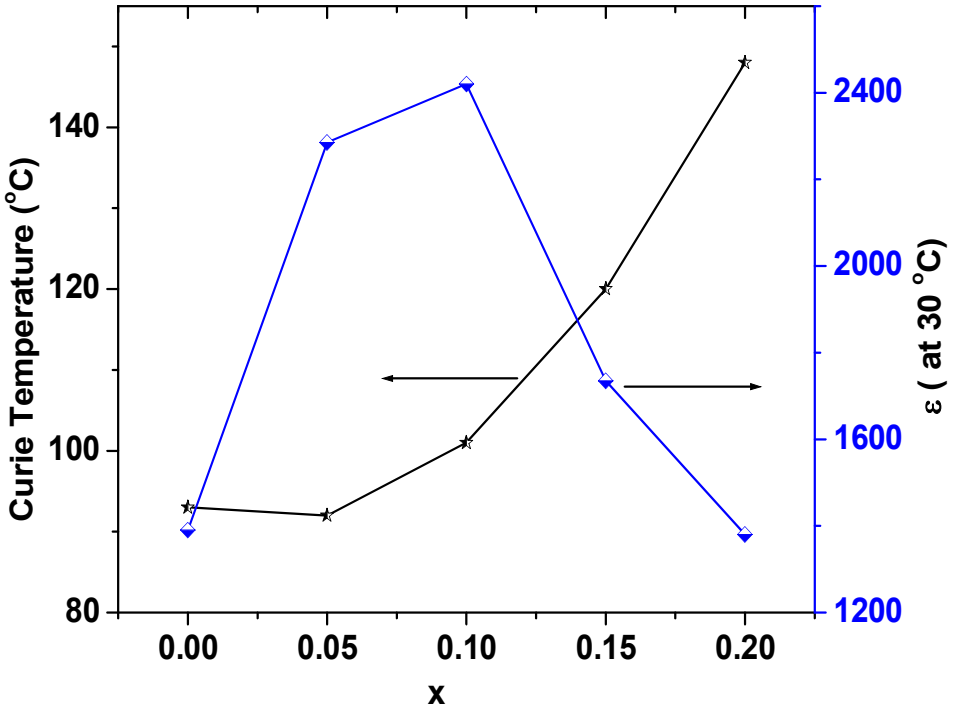

Figure 4.7 Room temperature dielectric constant and T_c of $Ba_{1-x}Pb_xTi_{0.90}Zr_{0.10}O_3$ ceramics samples

4.2.3 Ferroelectric and Piezoelectric Properties

Well saturated PE loops for all x are shown in figure 4.8. Increasing width of loop with x indicates that Pb^{2+} is acting as hardener for the selected BZT system and coercive field is increasing. The increase in coercive field indicates the formation of 90^o domains in the material with Pb substitution. The variation in coercive field (E_c), remanent polarization (P_r) and ratio of remanent to spontaneous polarization (P_r/P_s) with x are shown in table 4.3. The increase-decrease in P_r and P_r/P_s may be due to transition in phase of the material from

rhombohedral to tetragonal and other intrinsic factors like dipole moment and grain size etc [19,20].

Figure 4.9 shows the variation of E_c, P_r and P_r/P_s with temperature for all x. However, a decreasing trend in E_c could be noticed for x = 0, which indicates that the dipoles are becoming less stable with increase in temperature. While, for higher values of x this decrease is prominent only at higher temperatures (as T approaches T_c). This may be due to presence of 90^o domains, which can be perturbed only at higher temperatures. Thus, all the prepared materials soften after heating. The increase in P_r/P_s is mainly due to increase in internal energy caused by thermal excitation leading to greater dipole alignment [21]. Thus the value of E_c and P_r/P_s falls with increase in temperature and indicates that the phase is changing from ferroelectric to paraelectric.

Typical plot for the calculation of electromechanical coupling factor 'k_p' is given in figure 4.10 (for x = 0.05). Piezoelectric charge coefficient 'd_{33}' and planar electromechanical coupling factor 'k_p' is found to vary with x. The variation with x is given in figure 4.11. Improvement in d_{33} is observed with increase in x. However, k_p values remain smaller and changes in an irregular way. The charge coefficient 'd_{33}' increases sharply as x increases to 0.05, but for x greater than 0.05, there is a very small increase. Since the piezoelectric properties are strongly dependent on microstructure, hence sharp increase in 'd_{33}' can be related to density variation. Relative density increases sharply up to x = 0.05 and for x greater than 0.05, this increase is not sharp. Two factors, intrinsic (related to lattice cell deformations) and extrinsic (domain wall motion, grain boundary, etc) affect the piezoelectric properties [22-24]. However with increase in tetragonality, the internal stresses increases and favors the dipole formation. As the ceramic samples are

sintered at 1300^{o}C for 4 hrs. Thus, the small increase in relative density and d_{33} above x = 0.05 can be related to increasing amount of Pb, which causes increase in density of Pb vacancies at the grain boundaries in comparison to grain body. The increase in density of vacant sites at grain boundaries may also be responsible for increase-decrease in k_p. Extrinsic factors may be the cause for higher values of x.

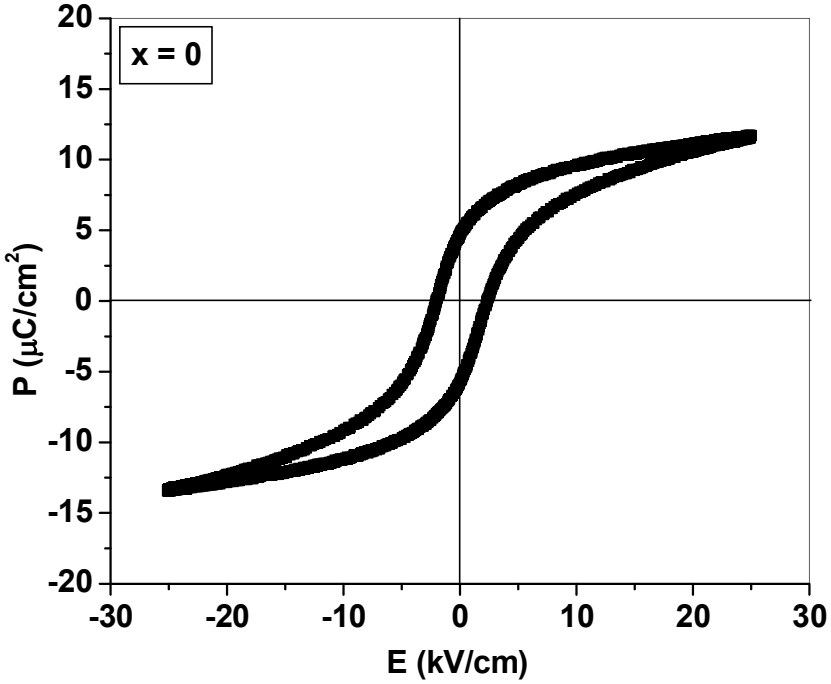
x = 0
P (μC/cm²)
E (kV/cm)
20
15
10
5
0
-5
-10
-15
-20
-30
-20
-10
0
10
20
30

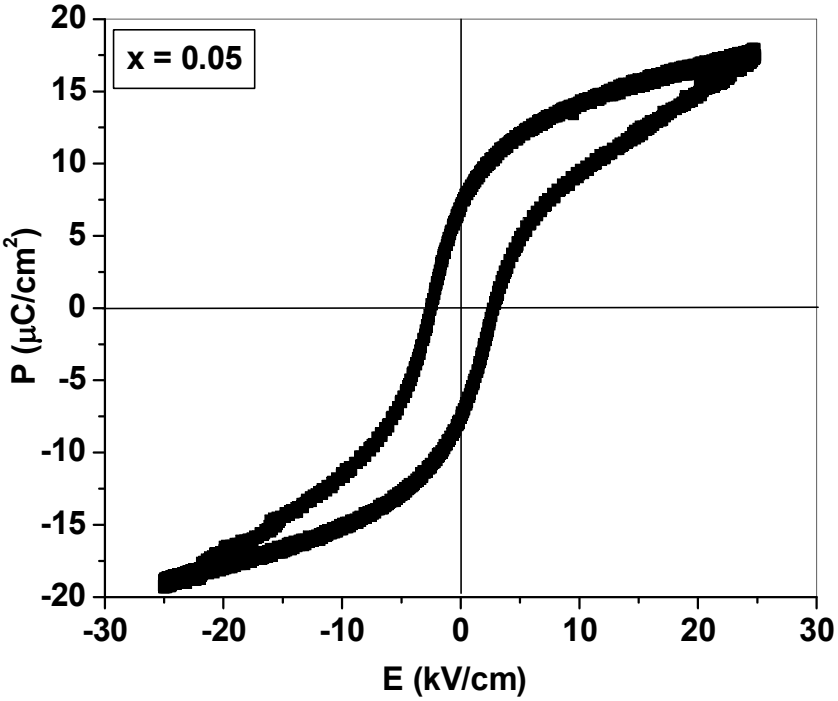
x = 0.05
P (μC/cm²)
E (kV/cm)
20
15
10
5
0
-5
-10
-15
-20
-30
-20
-10
0
10
20
30

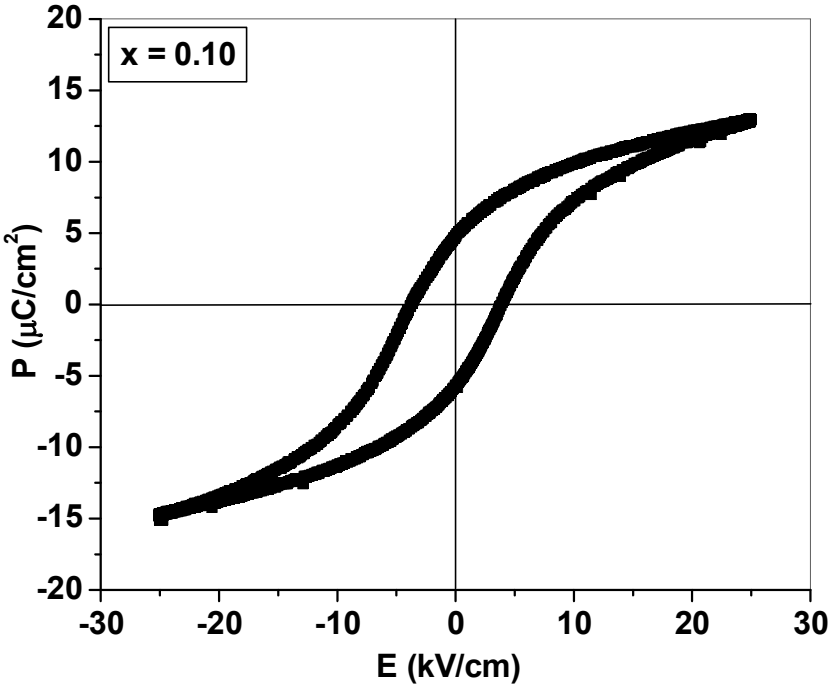
x = 0.10
P (μC/cm²)
E (kV/cm)
20
15
10
5
0
-5
-10
-15
-20
-30
-20
-10
0
10
20
30

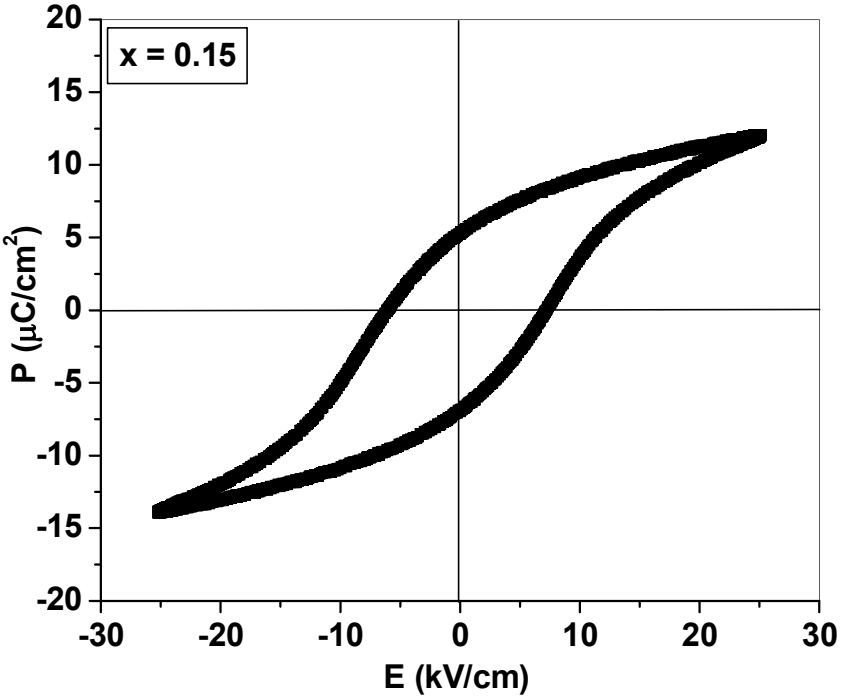
x = 0.15
P (μC/cm²)
E (kV/cm)
20
15
10
5
0
-5
-10
-15
-20
-30
-20
-10
0
10
20
30

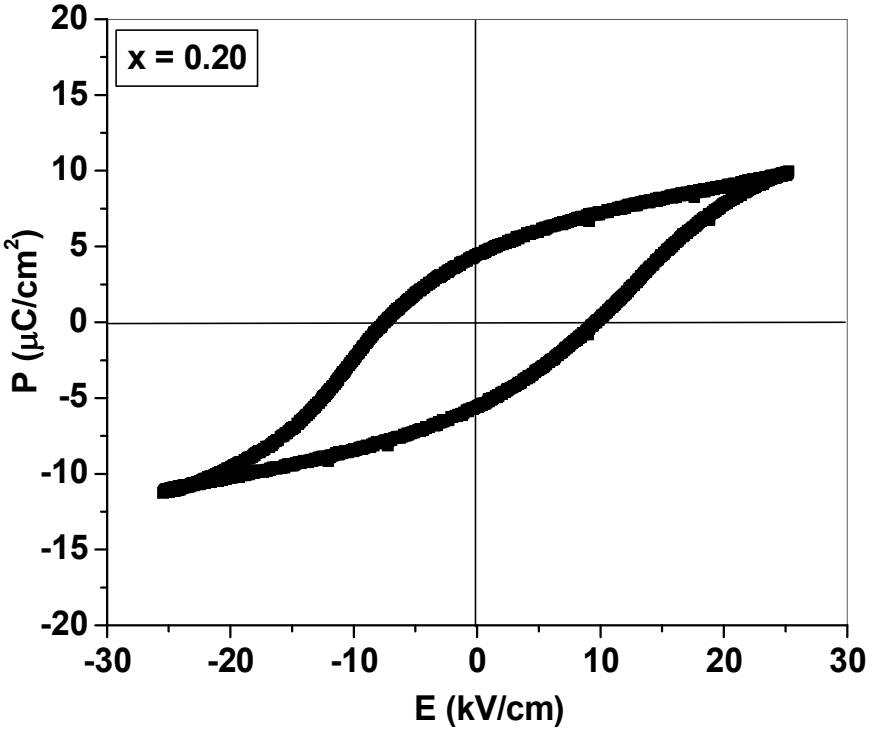

Figure 4.8 PE loops for all x at 30°C

Table 4.3 Coercive field (E_c), remnant polarization (P_r) and P_r/P_s ratio for all values of x

x	E_c (kV/cm)	P_r ($\mu C/cm^2$)	P_r/P_s
0	2.17	5.25	0.42
0.05	2.67	7.47	0.41
0.10	3.80	5.23	0.38
0.15	6.63	6.16	0.47
0.20	9.06	4.69	0.49

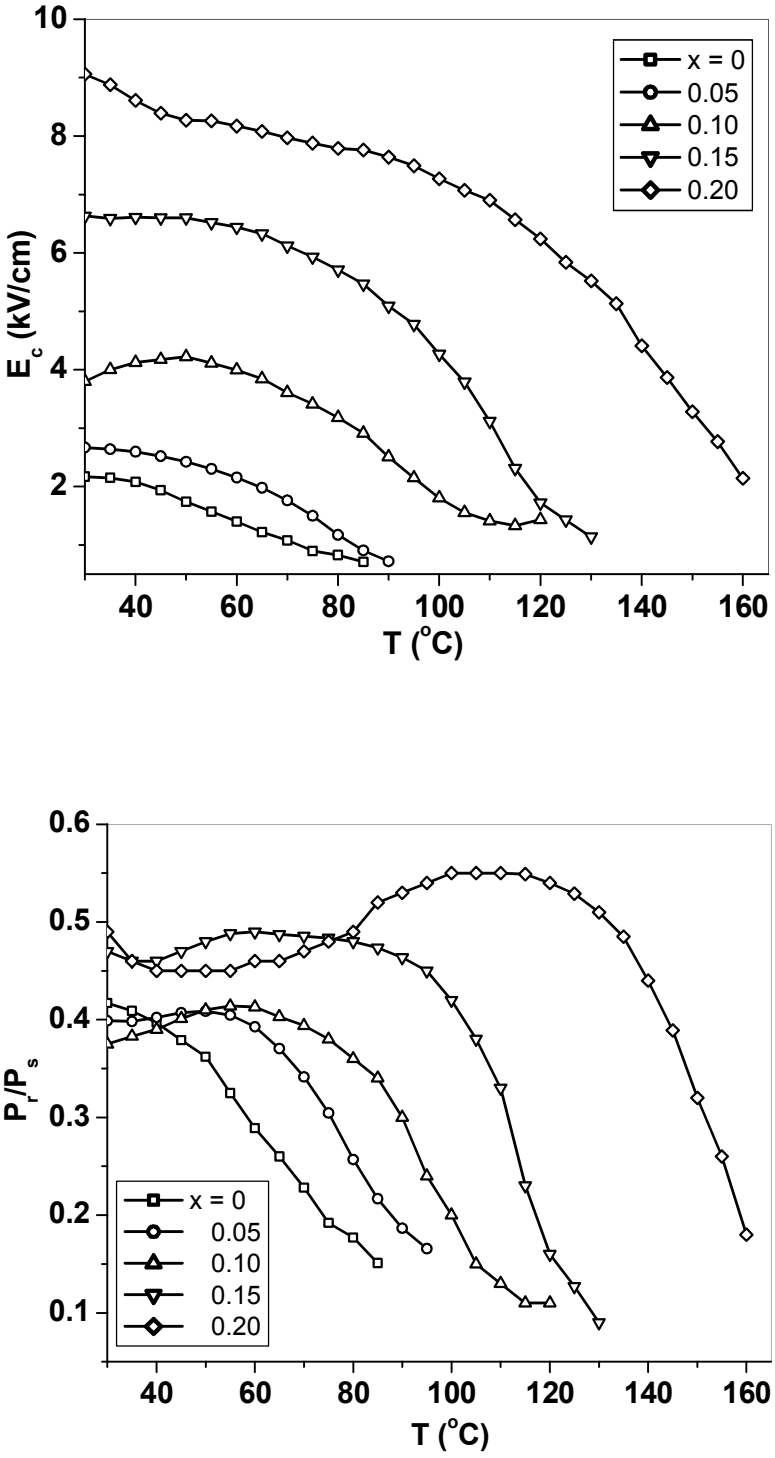

Figure 4.9 Variation of E_c and P_r/P_s with temperature for all x

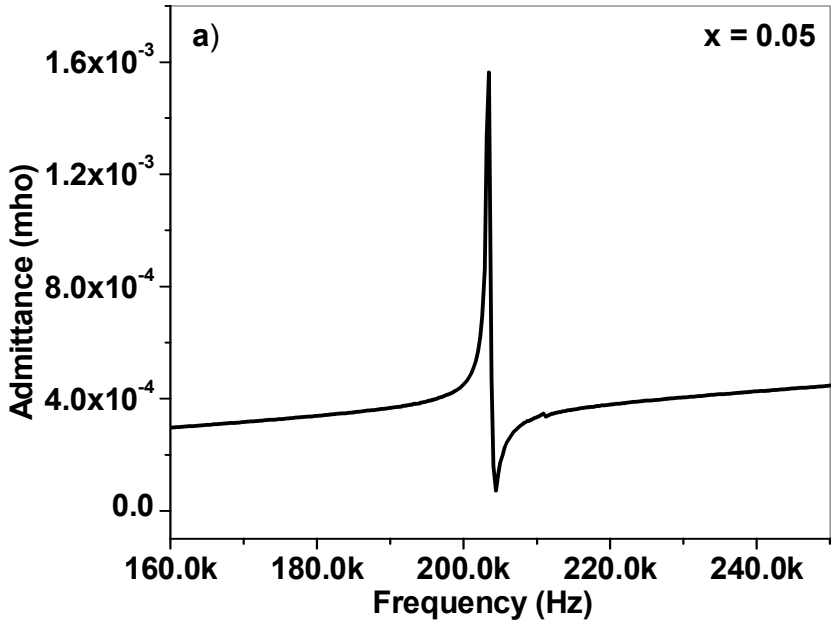

Figure 4.10 Typical resonance and antiresonance graph for k_p calculations

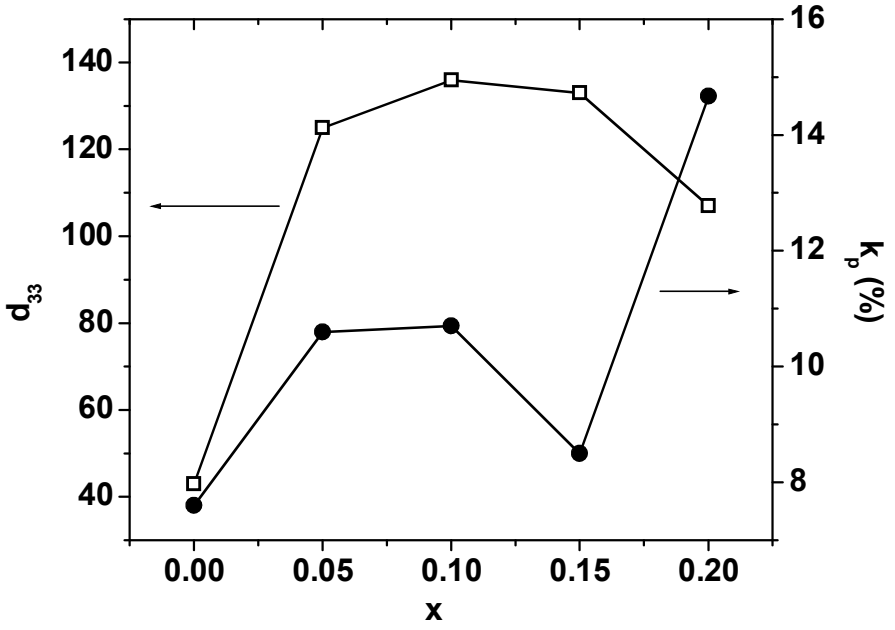

Figure 4.11 Variation of d_{33} and k_p with x

4.3 Zr^{4+} Substituted $Ba_{0.80}Pb_{0.10}TiO_3$ (*B-site Substitution)*

$Ba_{0.80}Pb_{0.20}Ti_{1-x}Zr_xO_3$ (BPZT) ceramics were prepared by solid-state reaction technique using the following chemical reaction:

$$0.80BaCO_3 + 0.20PbO + (1\text{-}x)\ TiO_2 + xZrO_2 \longrightarrow Ba_{0.80}Pb_{0.20}Ti_{1-x}Zr_xO_3 + CO_2\uparrow \quad (1)$$

with x ranging from 0 to 0.10 in the steps of 0.02.

The compacted discs were sintered at 1300^{o}C for 4 hrs with constant heating/cooling rates of 5^{o}C/min. To minimize lead loss, sintering was carried out in closed alumina crucibles. To provide lead rich atmosphere, PZT powder was also placed in a alumina boat inside the crucible.

4.3.1 Physical and Structural Properties

Figure 4.12 shows X-ray diffraction (XRD) patterns of the $Ba_{0.80}Pb_{0.20}Ti_{1-x}Zr_xO_3$ ceramics with different Zr concentration at room temperature. In figure, all the peaks in the pattern correspond to perovskite phase with tetragonal structure. From the observed d-values lattice parameters 'a' and 'c' were computed. Tetragonality (c/a) is found to decrease with increase in x. Tetragonality as a function of x is shown in figure 4.13.

Table 4.4 shows the variation of lattice parameters and structure of the BPZT ceramics as a function of Zr content. Theoretical (d_{th}) and experimental (d_{exp}) densities of all the samples of $Ba_{0.80}Pb_{0.20}Ti_{1-x}Zr_xO_3$ ceramics sintered at 1300^{o}C are given in table 4.5. The calculated theoretical (X-ray) density was found to decrease with increase in x. As,

expected the experimental density also decreases with the increase in x. This is due to the reason that $Ba_{0.80}Pb_{0.20}Ti_{1-x}Zr_xO_3$ ceramics with x = 0.00 composition is easy to sinter than sample with x = 0.10 at 1300°C for 4 hrs. SEM micrographs of $Ba_{0.80}Pb_{0.20}Ti1_{-x}Zr_xO_3$ were taken for all values of x and are given in figure 4.14. The variation of average grain size of $Ba_{0.80}Pb_{0.20}Ti1_{-x}Zr_xO_3$ ceramics as a function of x is shown in figure 4.15. Average grain size is found to decrease when x increases from 0 (17.7 μm) to 0.02 (2.4 μm) whereas it is found to increase with further increase in the values of x. This shows that it is easy to sinter $Ba_{0.80}Pb_{0.20}Ti1_{-x}Zr_xO_3$ ceramics with x = 0.00 in comparison to ceramics with other values of x. To achieve ceramics with high density and larger grain size, ceramics can be synthesized by increasing sintering temperature or time of sintering. The substitution of lead (Pb) limits the sintering temperature of all the compositions [25,26].

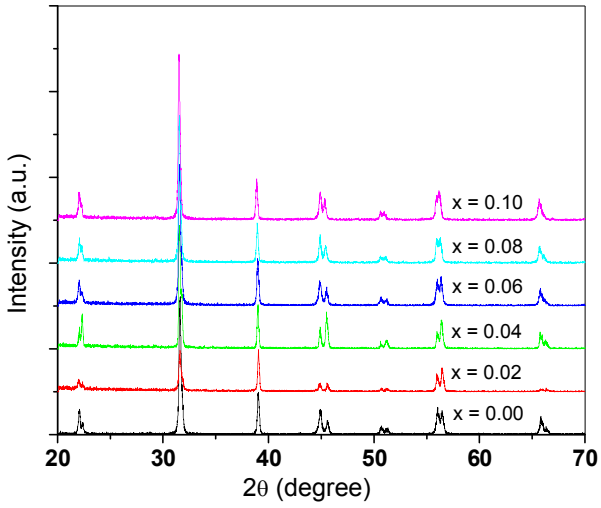

Figure 4.12 XRD patterns of $Ba_{0.80}Pb_{0.20}Ti_{1-x}Zr_xO_3$ for x = 0.00, 0.02, 0.04, 0.06, 0.08 and 0.10 recorded at 25°C

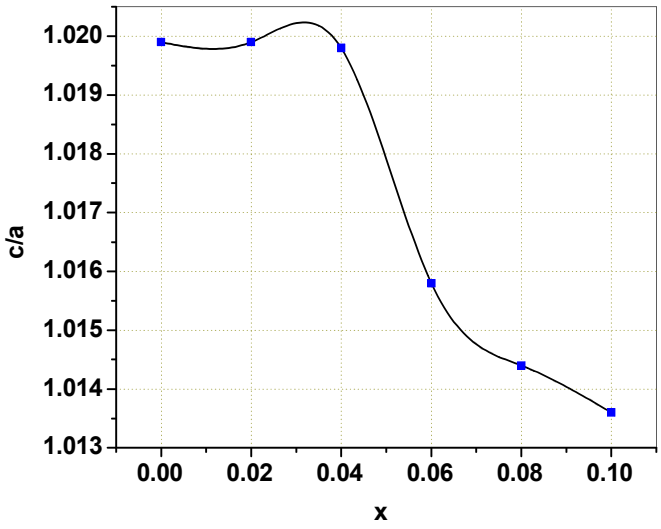

Figure 4.13 Variation in tetragonality (c/a) of $Ba_{0.80}Pb_{0.20}Ti_{1-x}Zr_xO_3$ with increase in x

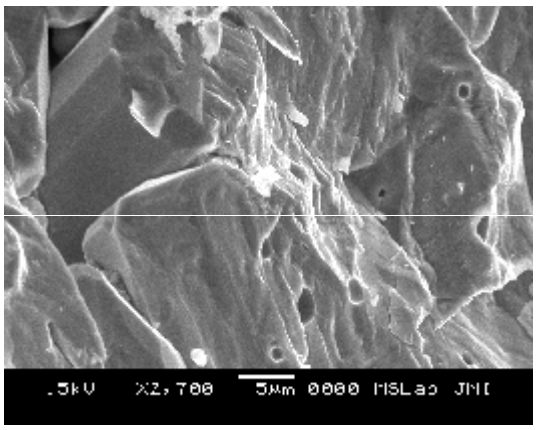

x = 0

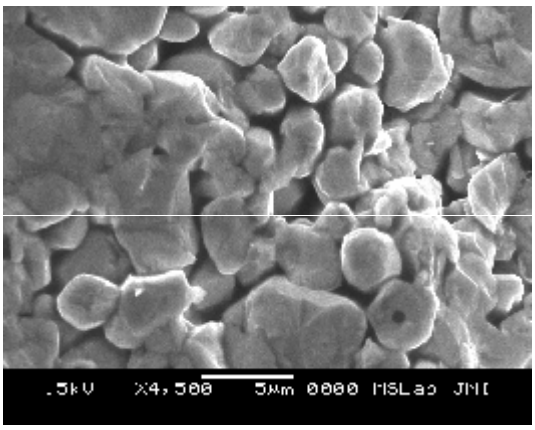

x = 0.02

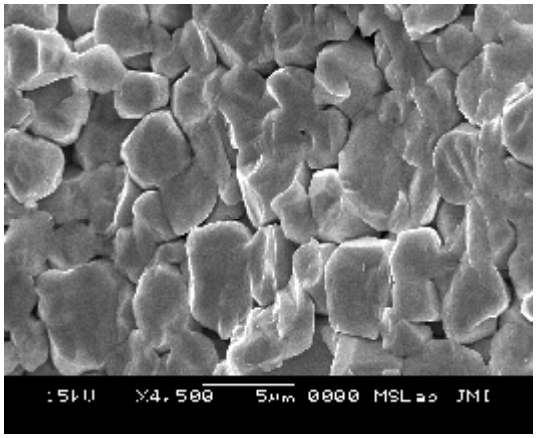

x = 0.04

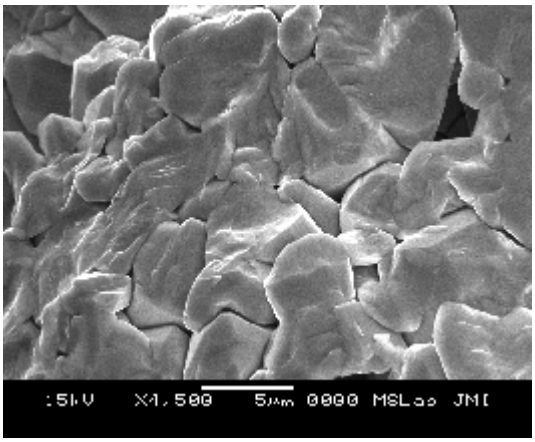

x = 0.06

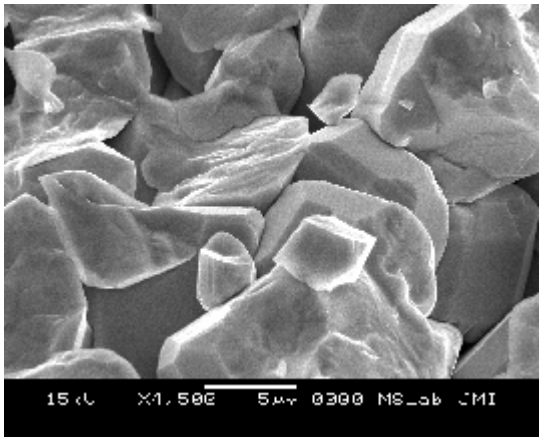

x = 0.08

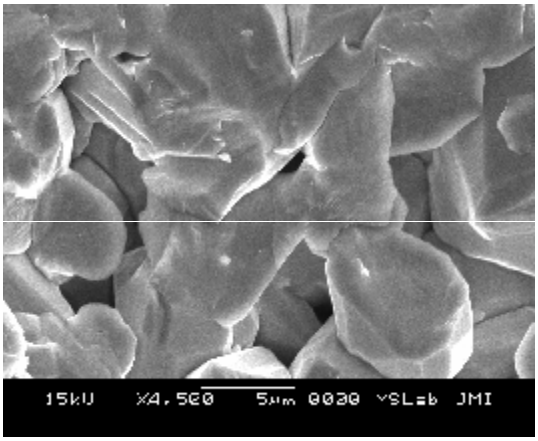

x = 0.10

Figure 4.14 SEM images of all BPZT samples

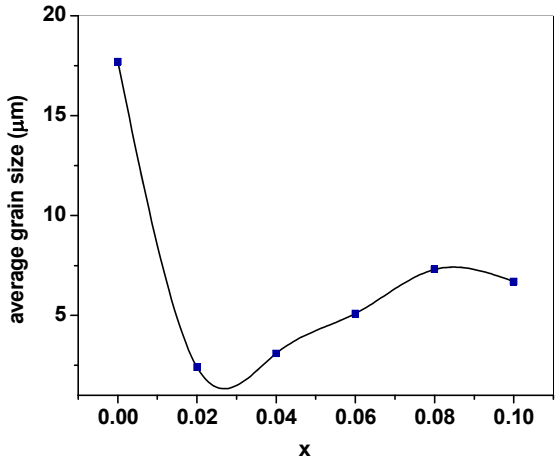

Figure 4.15 Variation in average grain size as a function of x

Table 4.4 lattice parameters 'a' and 'c', d_{exp}, d_{th}, relative density (d_{rel}) and apparent porosity (*P*) of $Ba_{1-x}Pb_xTi_{0.90}Zr_{0.10}O_3$ for all values of x

x	a (Å)	c (Å)	d_{exp} (g/cc)	d_{th} (g/cc)	d_{rel} (%)	Porosity (%)
0	3.9760	4.0552	6.33	6.76	93.64	6.36
0.02	3.9750	4.0542	5.93	6.43	92.22	7.78
0.04	3.9755	4.0541	5.87	6.45	91.01	8.99
0.06	3.9755	4.0382	5.85	6.50	90.0	10.00
0.08	3.9861	4.0435	5.81	6.48	89.66	10.34
0.10	4.0000	4.0542	5.78	6.44	89.75	10.25

4.3.2 Dielectric properties

Figure 4.16 shows the variation of dielectric constant (ε) of $Ba_{0.80}Pb_{0.20}Ti_{1-x}Zr_xO_3$ (BPZT) with frequency for all values of x at room temperature. The BPZT composition with x = 0.00, shows the lowest dielectric constant. The dielectric constant increases with Zr substitution. Maximum value of dielectric constant is for x = 0.10 composition. The increase in dielectric constant with increase in value of x may be due to the decrease in tetragonality. The decrease in tetragonality results in increased polarization and thereby dielectric constant.

A small decrease in ε is observed with respect to frequency for all the samples, whereas pronounced dispersion is observed at higher frequencies for tanδ. The higher value of dielectric constant at lower frequencies is due to the presence of various types of polarization mechanism. Dielectric loss (tanδ) increases with frequency in the higher frequency range. This increase in tanδ in the higher frequency range is due to some extrinsic loss phenomena [27,28]. This is to be noted that the frequency dependence of permittivity shows a small decrease in dielectric losses are very low for all the compositions in the bulk ceramics at small frequencies. The investigated materials are suitable for low loss application in the above given frequency range.

The dielectric properties for all samples were measured as a function of temperature, well above the transition temperature, T_c, at four different frequencies. Dielectric constant increases with increasing temperature and shows a peak which is characteristic of ferroelectric materials. The variation is shown in figure 4.17. From the dielectric constant vs temperature plot transition temperature is determined. It has been found that transition temperature decreases with increase in zirconium contents. The Curie point,

room temperature dielectric constant and maximum dielectric constant (at T_c) for the sample with composition $Ba_{0.80}Pb_{0.20}TiO_3$ are 217^oC, 265 and 3390, respectively, measured at 10 kHz. Variation of dielectric constant with temperature for different zirconium contents at a single frequency (10 kHz) is shown in figure 4.18, whereas, variation of T_c with x is shown in figure 4.19.

From figure 4.18, it is clear that in general maximum value of dielectric constant decreases with increasing zirconium contents and may be attributed to the decrease in tetragonality. However, the broadening of the peaks increases with increase in zirconium substitution, which is a characteristic of diffused phase transition. This may be due to disorder in the arrangement of various atoms, leading to a microscopic heterogeneity in the composition, and thus a distribution of different local Curie points [29]. The structural disorder arises due to the presence of a number of voids and impurities of different sizes. Values of tanδ at room temperature and T_c are given in table 4.5. Variation of T_c with x is given in figure 4.19. At room temperature (RT), the value of tanδ decreases with increasing x and it is between 0.6% and 1.6% which is good value for any application point of view. The temperature dependence of Dielectric loss for all the samples at 10 kHz is shown in figure 4.18.

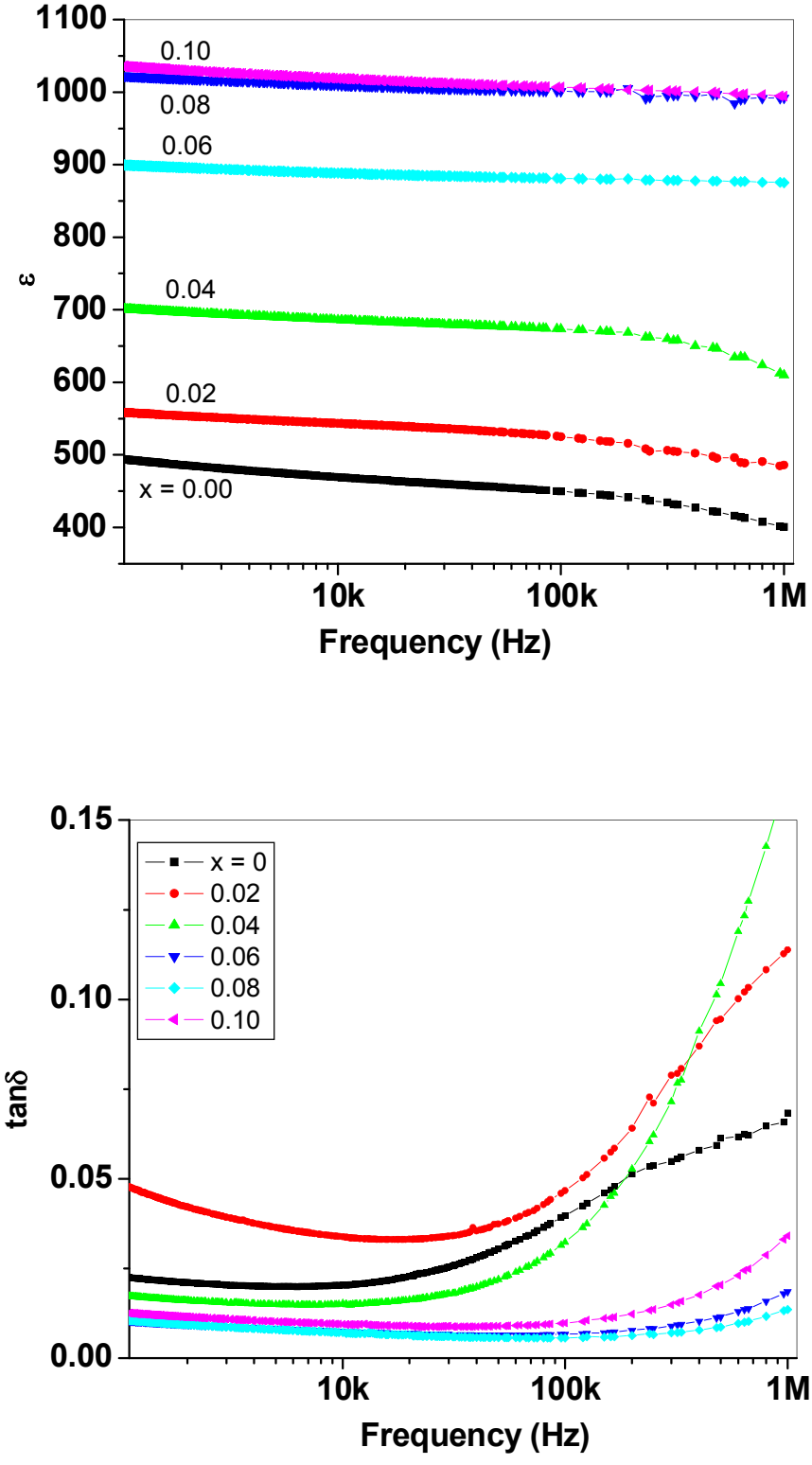

Figure 4.16 Variation of ε and tanδ with frequency for all values of x

Table 4.5 Variation of dielectric constant and tanδ with different values of x

x	T_c (^oC)	ε(at RT)	tanδ (at RT)	ε (at T_c)	tanδ (at T_c)
0.00	217	265	0.016	3390	0.026
0.02	208	375	0.011	3525	0.026
0.04	197	390	0.011	3590	0.017
0.06	173	495	0.010	3390	0.033
0.08	159	580	0.009	3480	0.035
0.10	140	675	0.006	3220	0.021

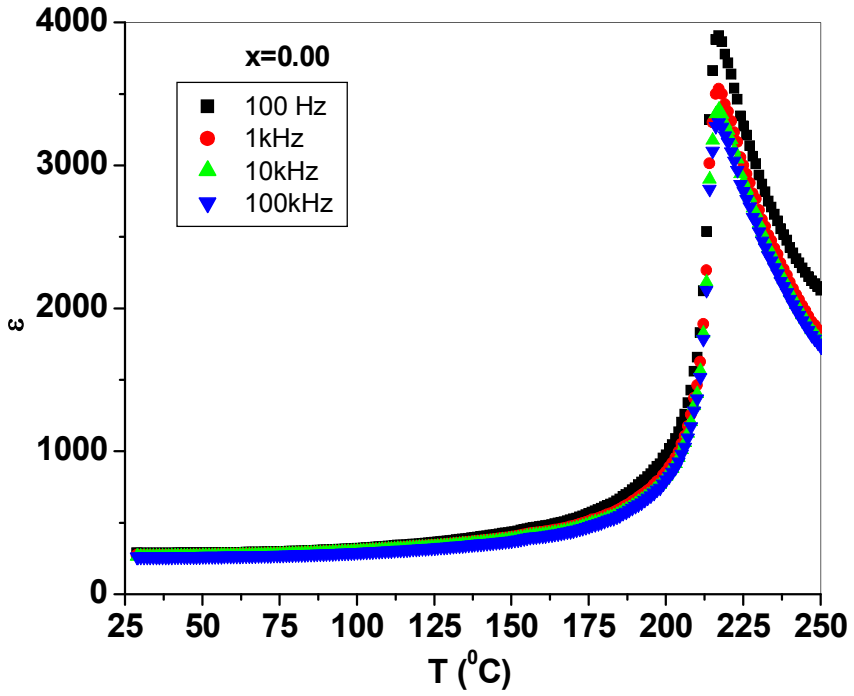
x=0.00
100 Hz
1kHz
10kHz
100kHz
ε
T (°C)
0
1000
2000
3000
4000
25
50
75
100
125
150
175
200
225
250

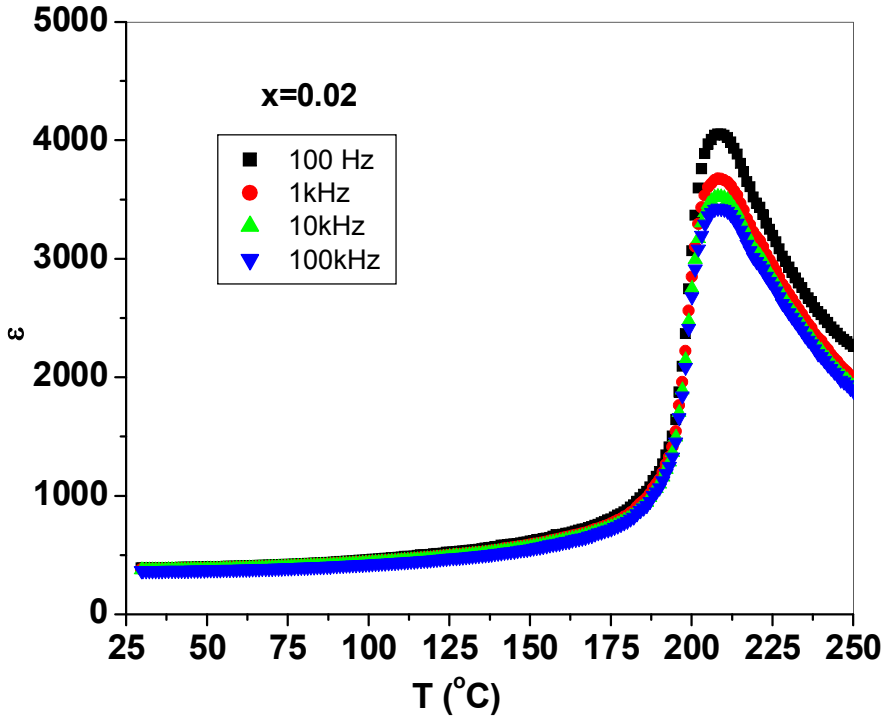
x=0.02
100 Hz
1kHz
10kHz
100kHz
ε
T (°C)
0
1000
2000
3000
4000
5000
25
50
75
100
125
150
175
200
225
250

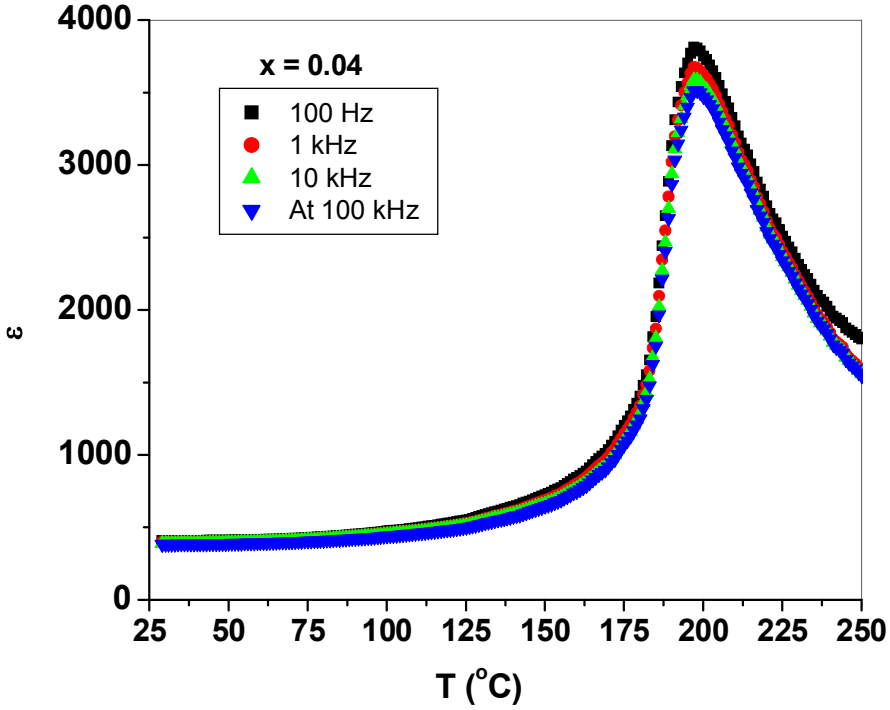
x = 0.04
100 Hz
1 kHz
10 kHz
At 100 kHz
ε
T (°C)

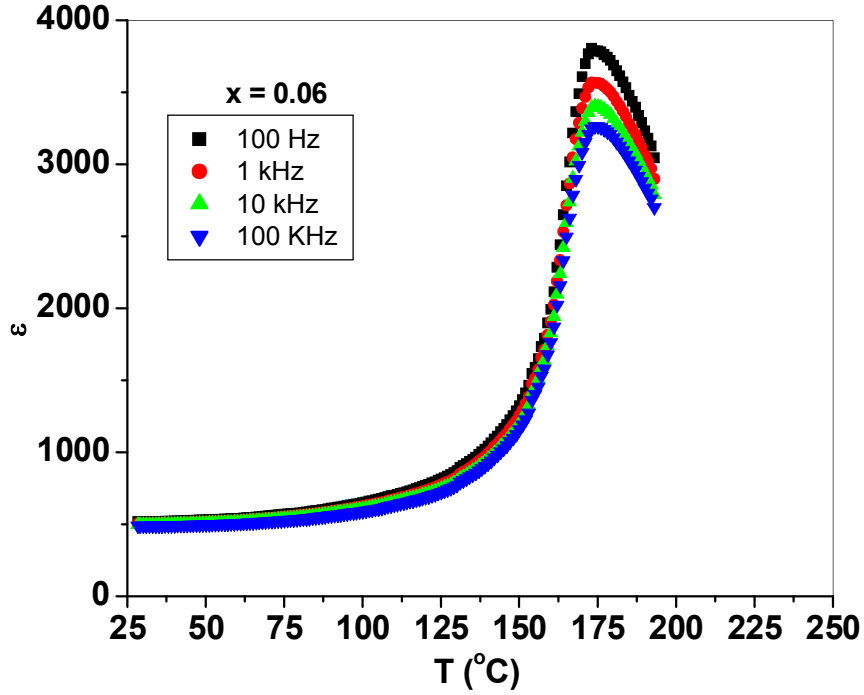
x = 0.06
100 Hz
1 kHz
10 kHz
100 KHz
ε
T (°C)

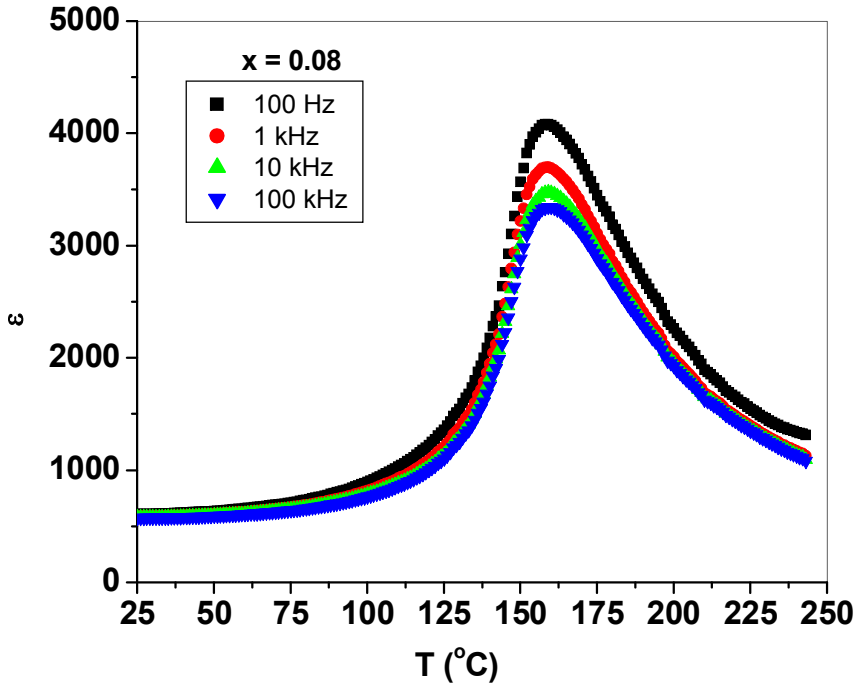

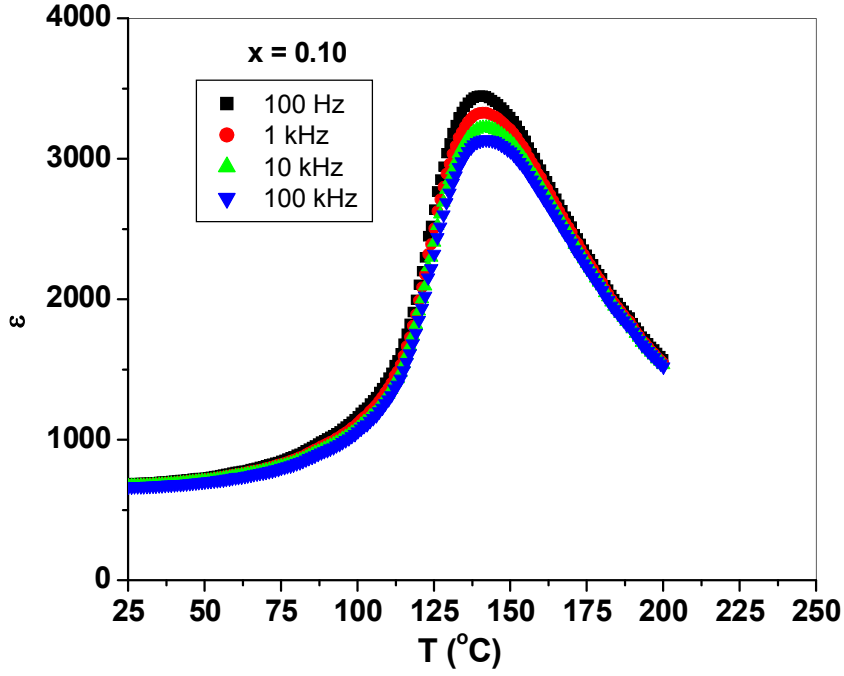

Figure 4.17 Temperature dependence of ε and tanδ

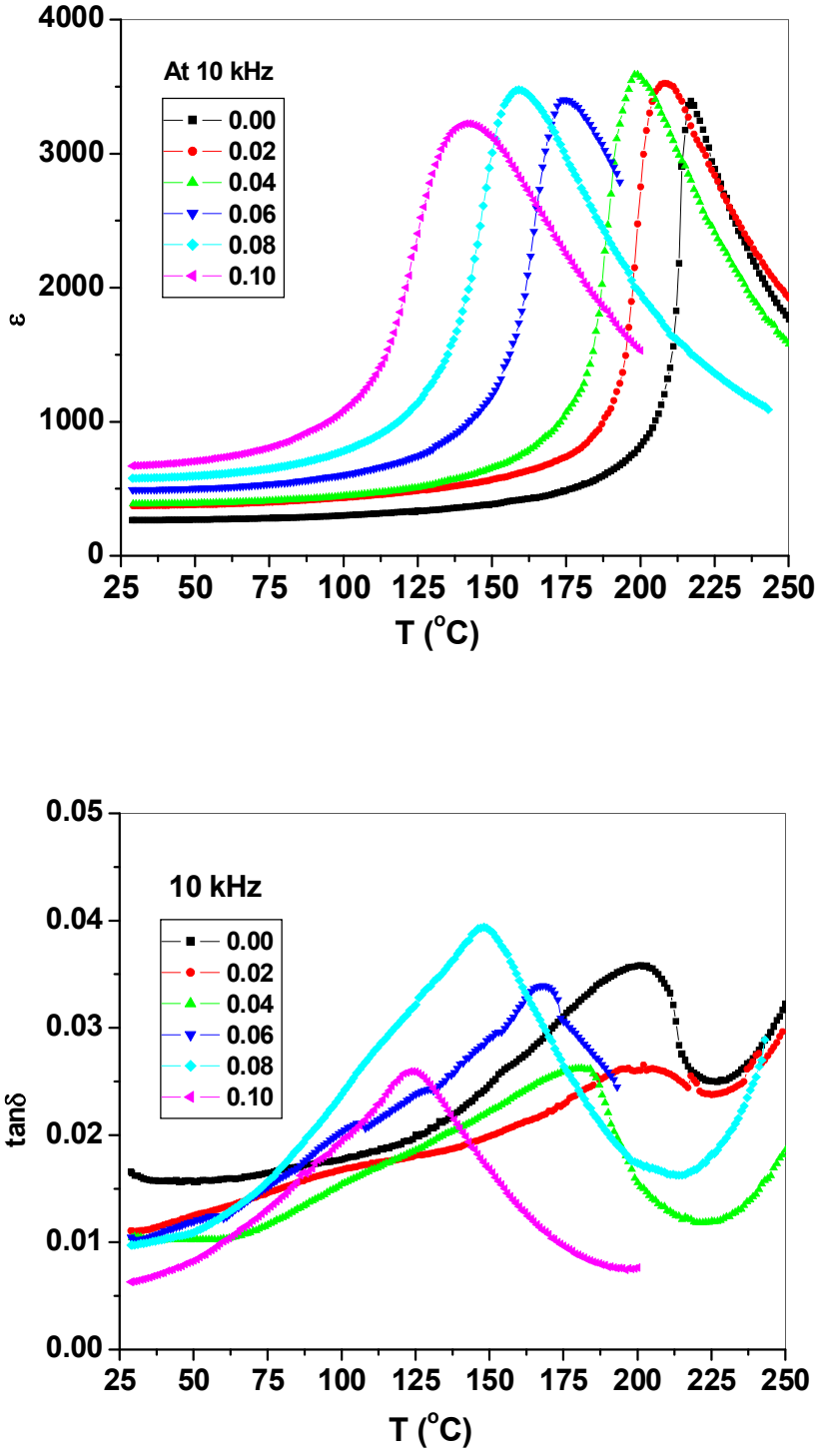

Figure 4.18 Variation of ε and tanδ with temperature for all samples at 10 kHz

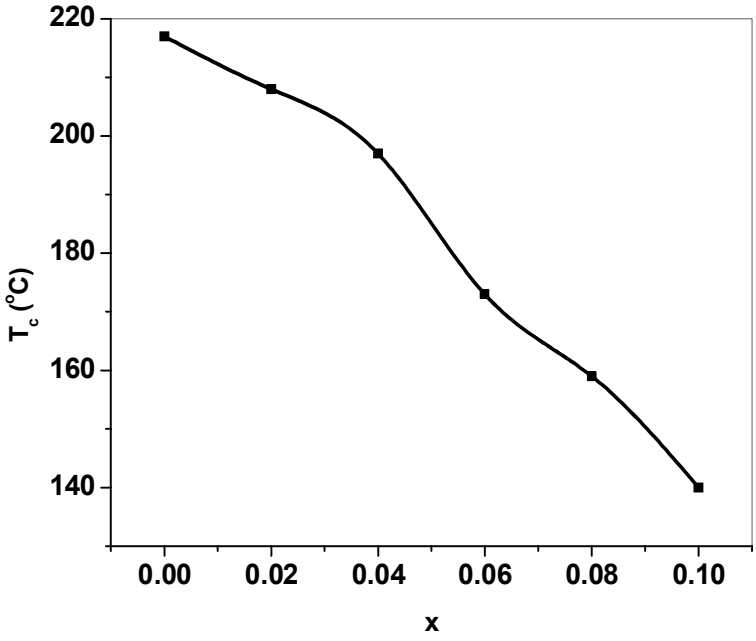

Figure 4.19 Variation of Curie temperature (T_c) as function of x

4.3.3 Ferroelectric Properties

All samples showed well defined ferroelectric behavior at 20 Hz and the P-E hysteresis loops of all the samples recorded at room temperatures are shown in figure 4.20. The ratio of remanent polarization (P_r) and spontaneous polarization (P_s) (P_r/P_s) indicates the squareness for the loop. The remanent polarization and P_r/P_s are found to increase with increase in temperature, whereas the coercive field (E_c) for all the samples decreases with increase in temperature. The increase in P_r is mainly due to increase in internal energy caused by thermal excitation leading to greater dipole alignment. The increase in P_r, P_{max} and P_r/P_s ratio with increase in temperature is shown in figure 4.21 (a-c), whereas figure 4.21 (d) shows the decrease in E_c with temperature for all samples. Decrease in coercive field with temperature shows that the material softens on heating.

The values of remnant polarization and coercive filed determined from the P-E loops are given in table 4.6. It can be seen that coercive field and P_r/P_s ratio decrease with increase in zirconium content. P_r decreases for 2 mol% Zr, followed by an increase from 4 mol% to 6 mol% Zr, and it then decreases again with further substitution of zirconium. This behavior can be correlated with the grain size variation and porosity, which also shows the same trend with the substitution of zirconium as shown in figure 4.14.

We know that E_c increases with the decrease in the grain size as each grain is mechanically clamped by its surroundings. This clamping effect, in addition to the mechanical stresses accompanying 90^o domain rotations, tends to impede the polarization reversal process, and hence, apparently results in an increase in E_c [21,27]. The decrease in P_r from x=0.06 to x=0.10 is due to presence of pores in addition to the increase in grain size.

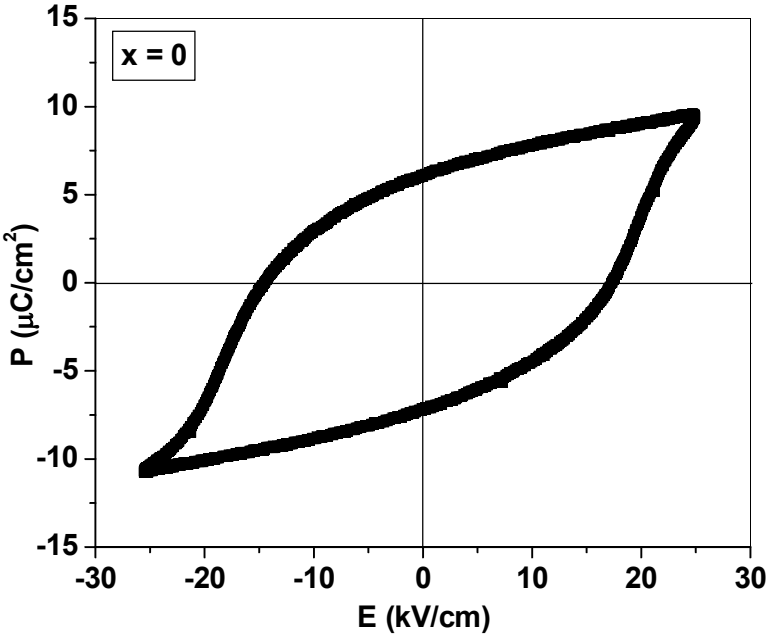
x = 0
P (μC/cm²)
E (kV/cm)
15
10
5
0
-5
-10
-15
-30
-20
-10
0
10
20
30

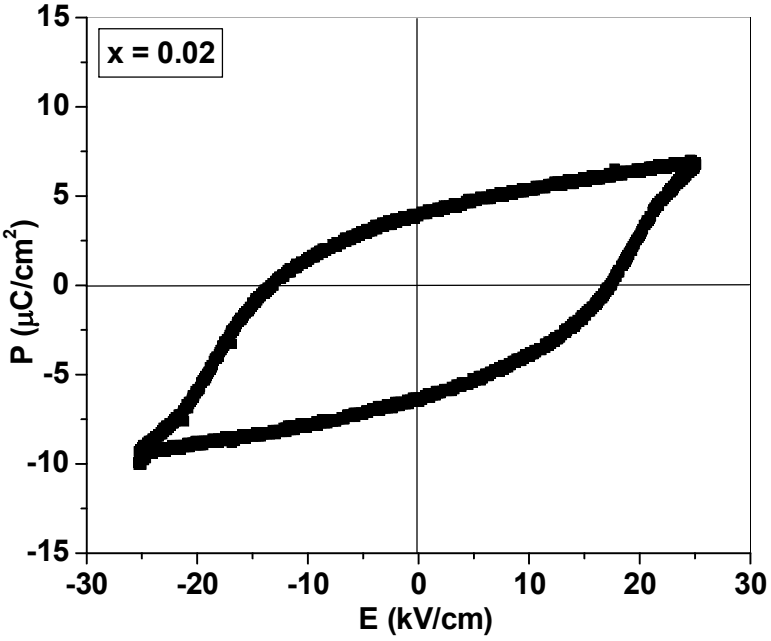
x = 0.02
P (μC/cm²)
E (kV/cm)
15
10
5
0
-5
-10
-15
-30
-20
-10
0
10
20
30

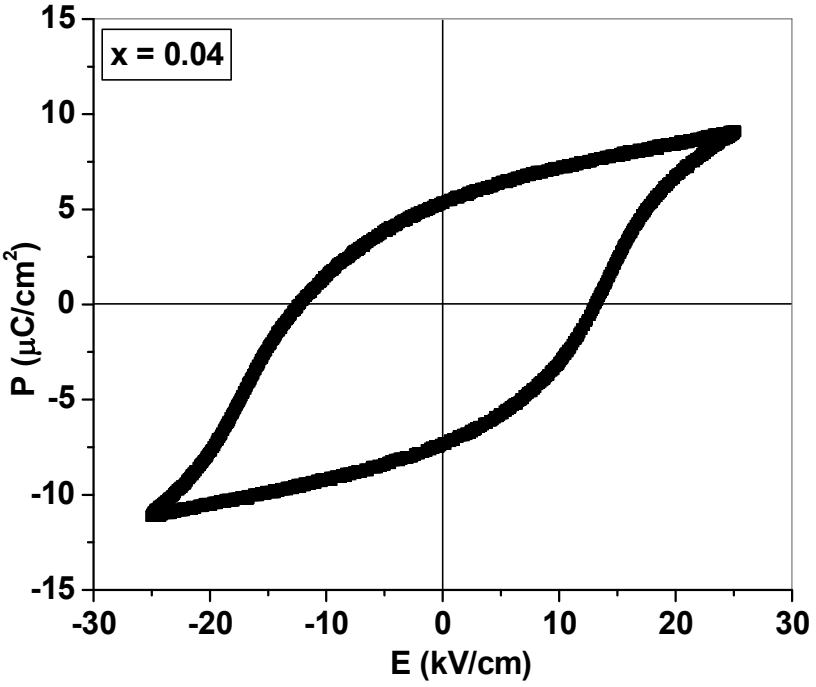
x = 0.04
P (μC/cm²)
E (kV/cm)
15
10
5
0
-5
-10
-15
-30
-20
-10
0
10
20
30

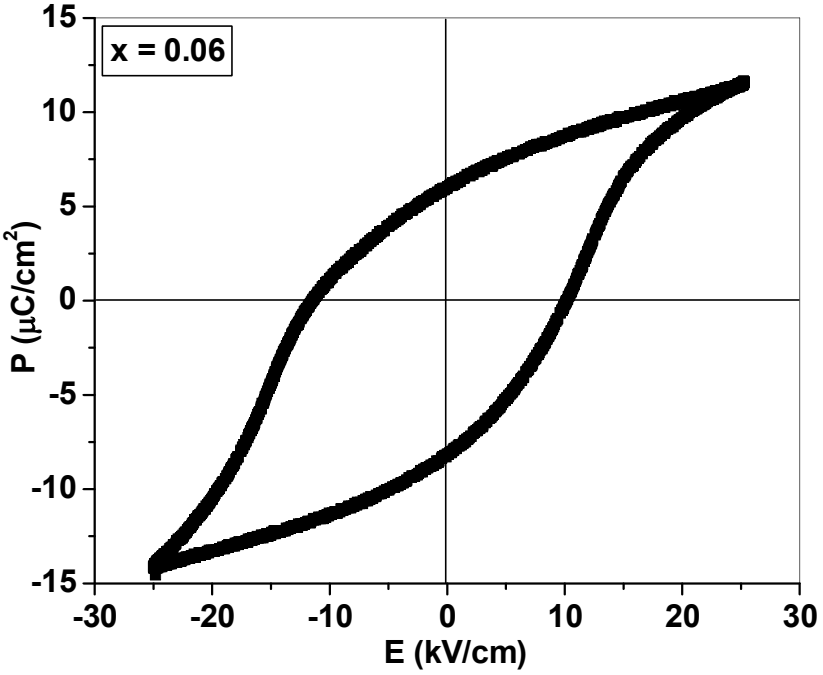
x = 0.06
P (μC/cm²)
E (kV/cm)
15
10
5
0
-5
-10
-15
-30
-20
-10
0
10
20
30

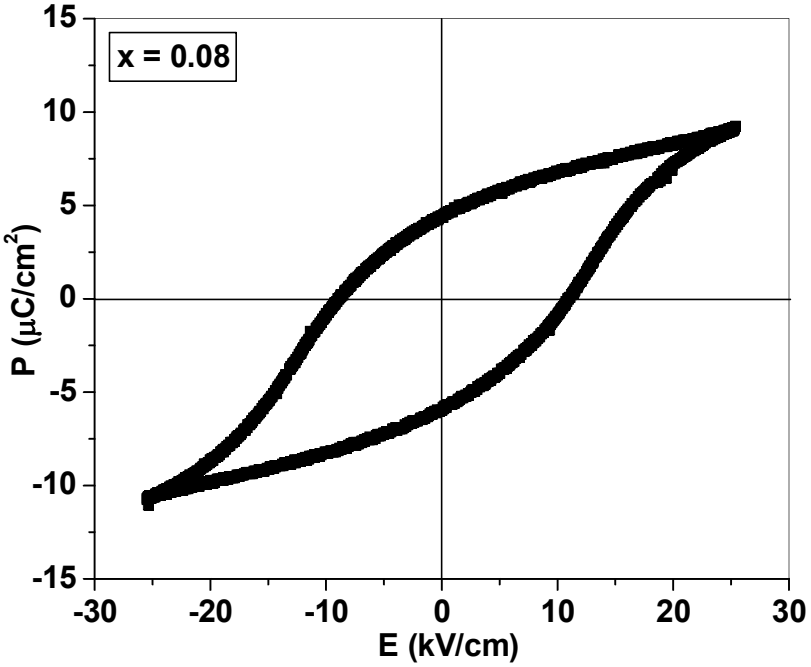

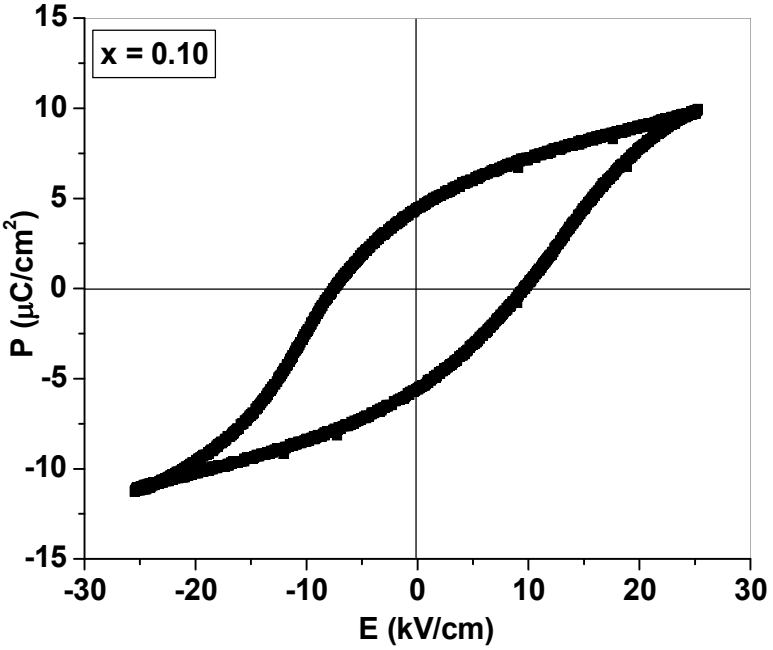

Figure 4.20 PE loops at 30°C for all x

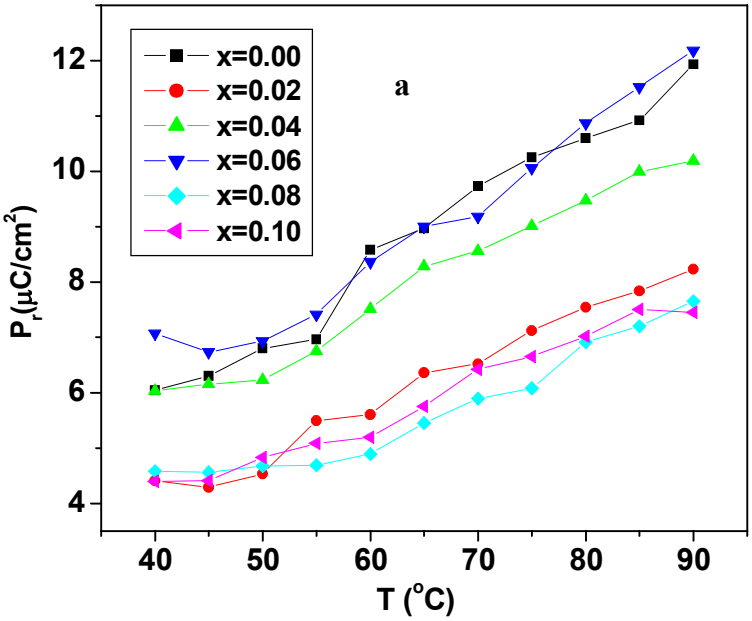
x=0.00
x=0.02
x=0.04
x=0.06
x=0.08
x=0.10
a
$P_r(\mu C/cm^2)$
T (°C)

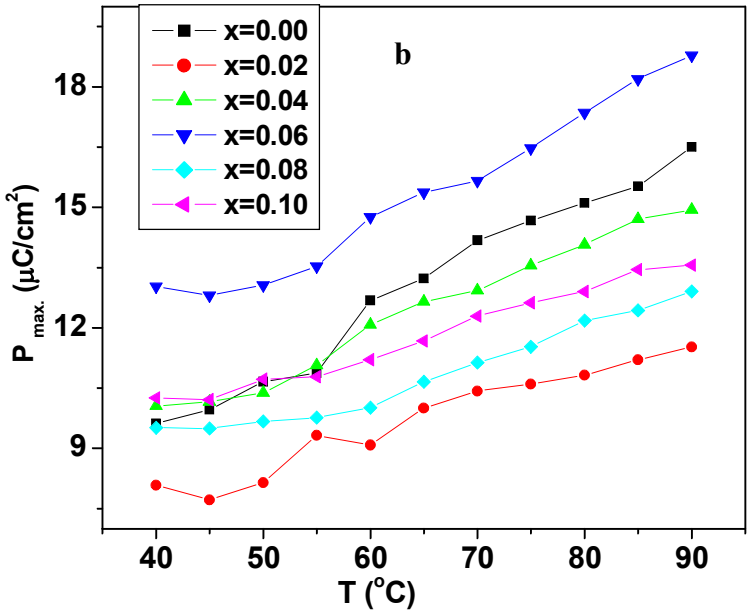
x=0.00
x=0.02
x=0.04
x=0.06
x=0.08
x=0.10
b
$P_{max.}$ ($\mu C/cm^2$)
T (°C)

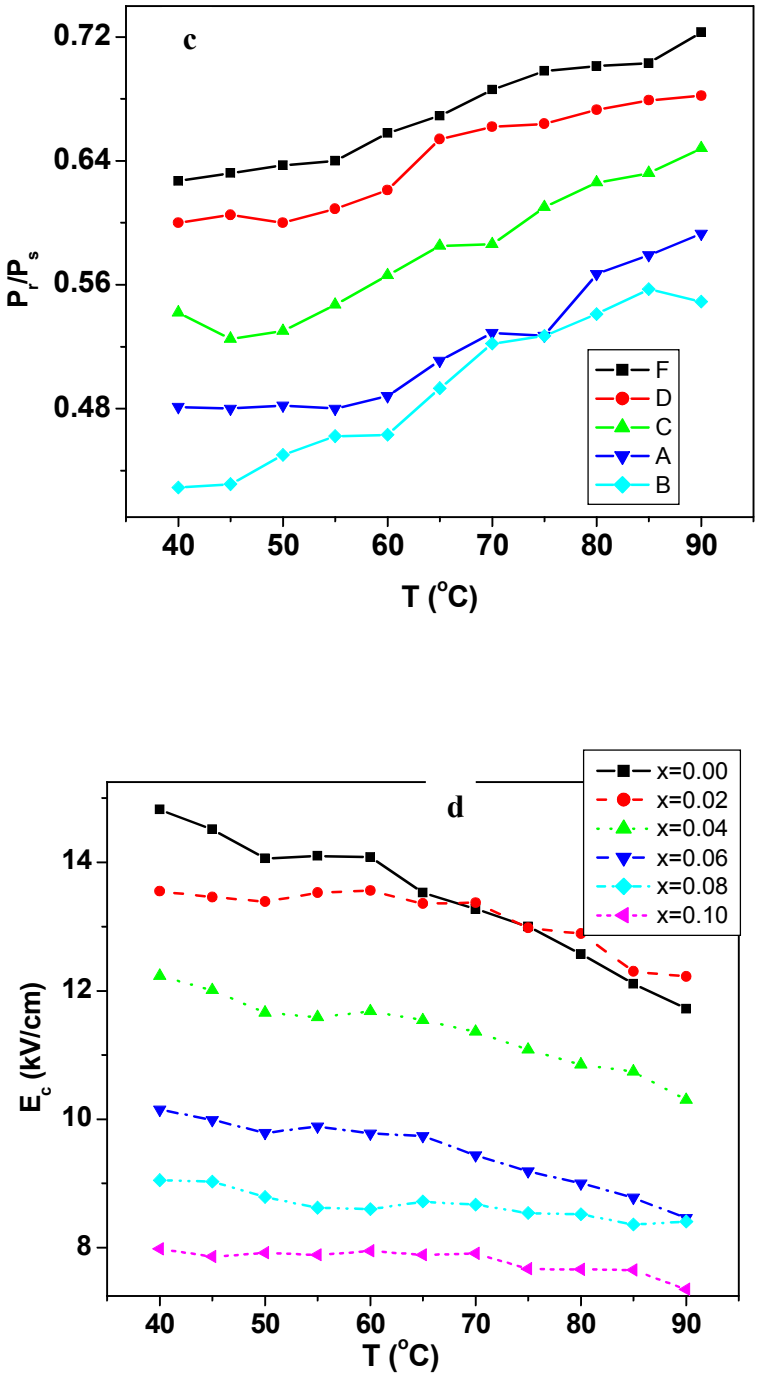

Figure 4.21 Variation in P_r, P_{max}, P_r/P_s ratio and Coercive field of all the samples with temperature

Table 4.6 Coercive field (E_c), remnant polarization (P_r) and P_r/P_s ratio for all values of x

x	E_c (kV/cm)	P_r ($\mu C/cm^2$)	P_r/P_s
0	14.82	6.04	0.658
0.02	13.55	4.41	0.643
0.04	12.23	6.03	0.621
0.06	10.15	7.07	0.566
0.08	9.05	4.58	0.488
0.10	7.98	4.40	0.463

4.4 Ca^{2+} Substituted $Ba_{0.80}Pb_{0.20}Ti_{0.90}Zr_{0.10}O_3$ Ceramics

Calcium modified BPZT ceramics with compositional formula $Ba_{0.80-x}Ca_xPb_{0.20}Ti_{0.90}Zr_{0.10}O_3$ (x = 0, 0.10 and 0.20) were synthesized by solid state reaction route. These samples were sintered at 1300^oC and characterized for structural, dielectric and ferroelectric properties. The results are discussed here.

4.4.1 Physical and Structural Properties

X-ray diffraction patterns for all the sintered samples are shown in figure 4.22. The analysis reveals that samples have single phase with perovskite tetragonal structure. Shifting of peaks towards higher angle side with Ca substitution indicates that the smaller Ca^{2+} (1.48Å) ions replace the larger Ba^{2+} (1.75Å) ions [30]. This indicates that lattice parameter

decreases with the increase in x. The value of lattice parameters (c and a) are given in Table 4.7. SEM micrographs of fractured cross-sectional region are shown in figure 4.23.

Table 4.7. Lattice parameters (a,c), relative density and dielectric properties (at 100 kHz)

x	c (Å)	a (Å)	relative density (%)	T_{max} (^oC)	ε_{RT}	$\tan\delta_{RT}$	ε_{max}	$\tan\delta_{Tmax}$
0	4.0542	4.0000	89.75	148	1375	0.04	5985	0.025
0.10	4.0206	3.9838	86.65	142	970	0.002	7930	0.010
0.20	4.0004	3.9607	85.83	142	950	0.012	4970	0.009

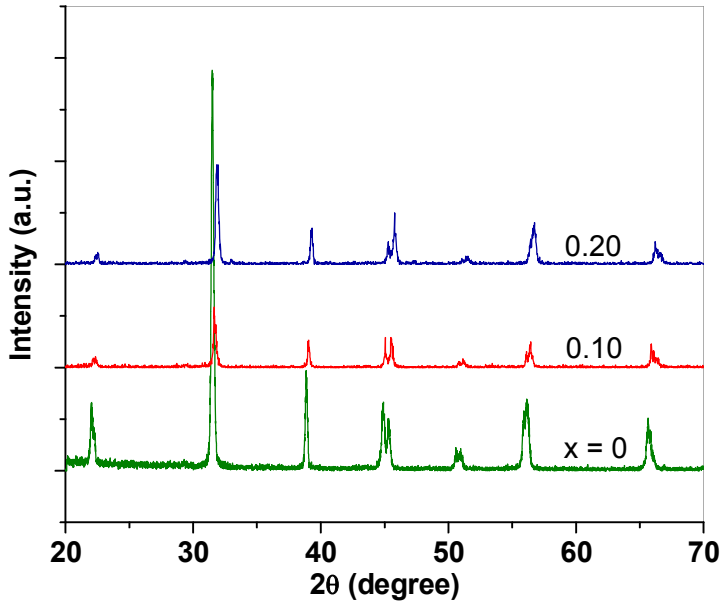

Figure 4.22 XRD patterns of $Ba_{0.80-x}Ca_xPb_{0.20}Ti_{0.90}Zr_{0.10}O_3$ ceramics

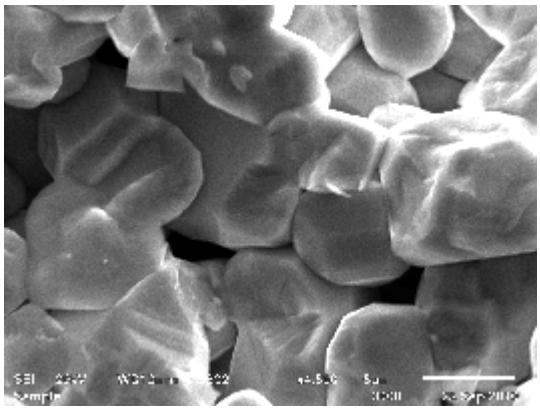

x = 0

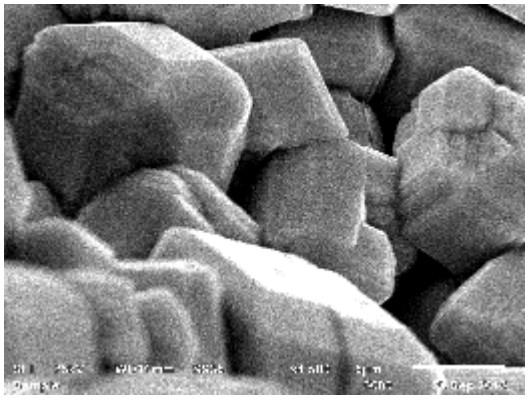

x = 0.10

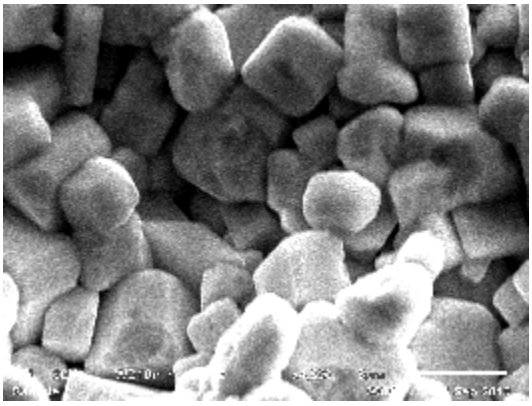

x = 0.20

Figure 4.23 SEM micrographs of sintered $Ba_{0.80-x}Ca_xPb_{0.20}Ti_{0.90}Zr_{0.10}O_3$ ceramics

4.4.2 Dielectric Properties

Variation of dielectric constant and tanδ with frequency at room temperature is shown in figure 4.24. Contribution from various polarizations (space charge, ionic, orientational and electronic polarizations) results in high dielectric constant at lower frequencies. Because mass of electrons is lower than ions thus they can oscillate at field with higher frequencies. This lower value of dielectric constant at higher frequencies is due to the contribution from only electronic polarizations. Also, tanδ decreases with increase in frequency upto 100 kHz [31]. However, a slight increase in tanδ can be observed at frequencies higher than 100 kHz, which may be due to some extrinsic factors. Variation of dielectric constant with temperature for all samples at four discrete frequencies (100 Hz, 1k, 10k and 100 kHz) is shown in figure 4.25. Observed dielectric peaks show their typical ferroelectric behavior and from these peaks, we can found ferroelectric to paraelectric phase transition temperature (T_{max}). T_{max} for all values of x are given in Table 4.8. A small decrease in T_{max} can be observed for both x = 0.10 and 0.20. Maximum height of dielectric peak is observed for x = 0.10 whereas for x = 0.20 dielectric peak gets broaden, as is expected. However this broadening of peak may be due to micro compositional fluctuations result in different local transition temperatures which also resulting in decrease in dielectric maxima [32,33]. Observed values of room temperature dielectric constant (ε_{RT}), $\tan\delta_{RT}$, dielectric maxima (ε_{max}) and tangent loss at T_{max} ($\tan\delta_{Tmax}$) are given in Table 4.8. Room temperature dielectric constant decreases when x increases from 0.0 to 0.20. This may be due to the fact that calcium substitution for barium strongly lowers the tetragonal-orthogonal transition temperature. Thus temperature stability of dielectric properties of BZT based ceramics gets improved for many engineering applications. A

marked improvement in tangent loss can be achieved by calcium substitution. Thus calcium modified BZT materials are potential candidates for dielectric applications like capacitors. Ceramic sample with x = 0.10 has minimum value of tanδ (0.2%) which is rarely reported in literature.

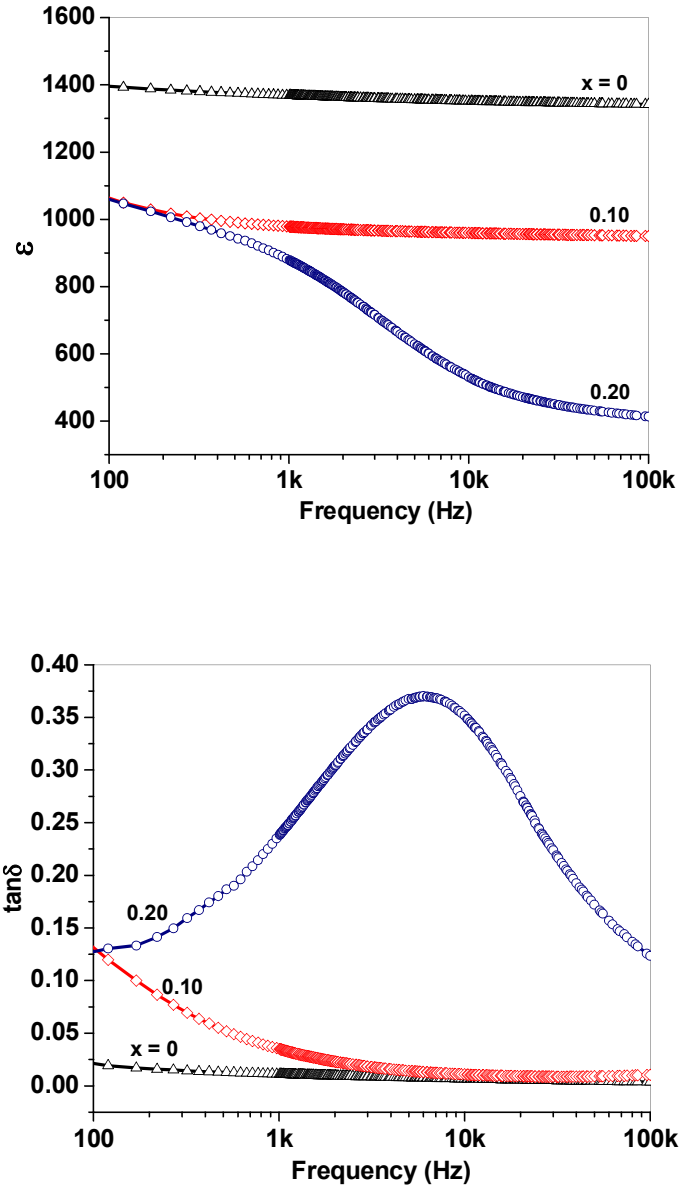

Figure 4.24 Variation of dielectric constant and tanδ with frequency

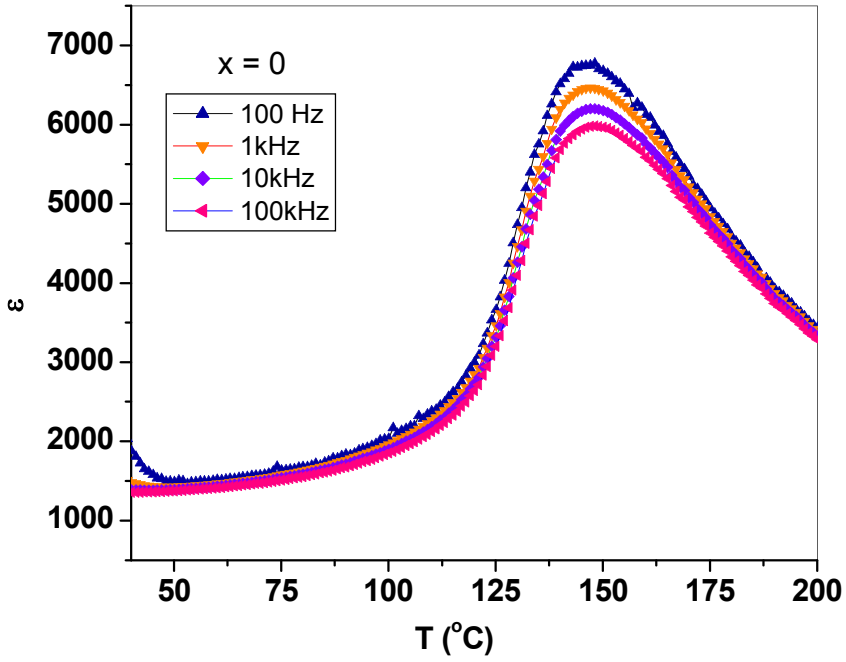
x = 0
100 Hz
1kHz
10kHz
100kHz
ε
T (°C)

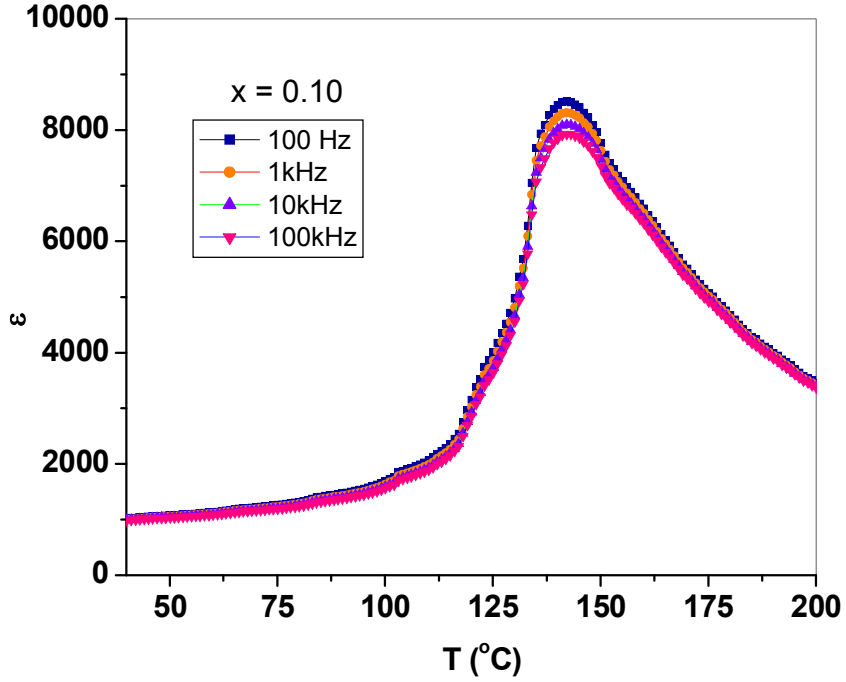
x = 0.10
100 Hz
1kHz
10kHz
100kHz
ε
T (°C)

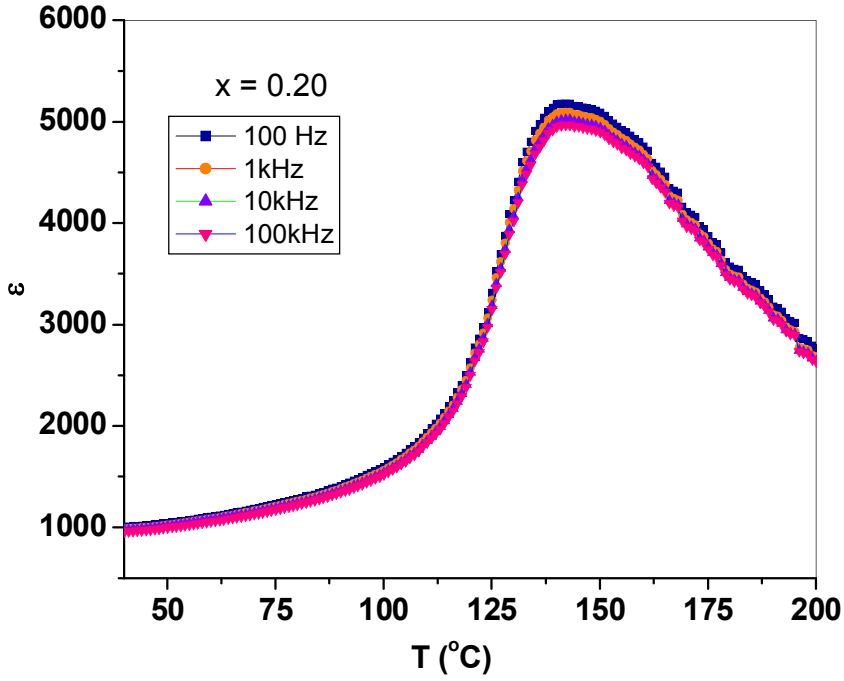

Figure 4.25 Variation of Dielectric constant with temperature

4.4.3 Ferroelectric and Piezoelectric Properties

P-E hysteresis loops recorded at 30°C are shown in figure 4.26. From the hysteresis loops various parameters like E_c, P_r and P_{max} were determined. Composition with no calcium content shows memory type P-E loop. But the squareness of P-E loop improves with calcium substitution. This squareness can be determined by ratio of remanent polarization to spontaneous polarization (P_r/P_s). Improvement in P_r/P_s indicates that material sample can be used as a better memory device. Variations in E_c, P_r and P_r/P_s for all values of x are given in table 4.8. It has been observed that sample with calcium content equal to 10 mol% have maximum value of E_c, P_r and P_r/P_s ratio. For calcium content greater than equal to 20 mol% value of these different parameters decreases. This may be

due to the formation of extra phases. Figure 4.27 shows P-E loops of samples with x = 0.10 and 0.20 at different temperatures. Shrinkage in the loops can be observed as temperature increases and finally ferroelectric nature diminishes at temperatures above tetragonal to cubic transition temperature (T_{max}). P-E loop for x = 0.10 at 120^{o}C shows a high P_r with smaller E_c. Also, fast switching can be observed at this temperature. Variations of E_c, P_r, P_{max} and P_r/P_s with temperature for all values of x are shown in figure 4.28. E_c decreases with increase in temperature whereas in P_r increases for a certain range of temperature and then it decreases for temperature. Decrease in E_c shows that the material softens on heating. Increase in P_r is mainly due to increase in internal energy caused by thermal excitation resulting in greater dipole alignment. Existence of polarization beyond T_c may be due to induced polarization. In sample with x = 0.10, P_r/P_s is found to be stable over a certain range of temperature and it decreases as temperature approaches T_c. Piezoelectric charge coefficient d_{33} and electromechanical coupling factors k_p and k_t are given in table 4.8. k_p and k_t were determined by using impedance spectroscopy (resonance-antiresonance method). It can be observed that d_{33} and k_p decreases when x increases. Although ceramic sample with x=0.10 has decreased dielectric constant at room temperature, the electromechanical coupling factor and d_{33} remains reasonably high. Such compositions can be substantially used for ultrasonics and for underwater sound applications.

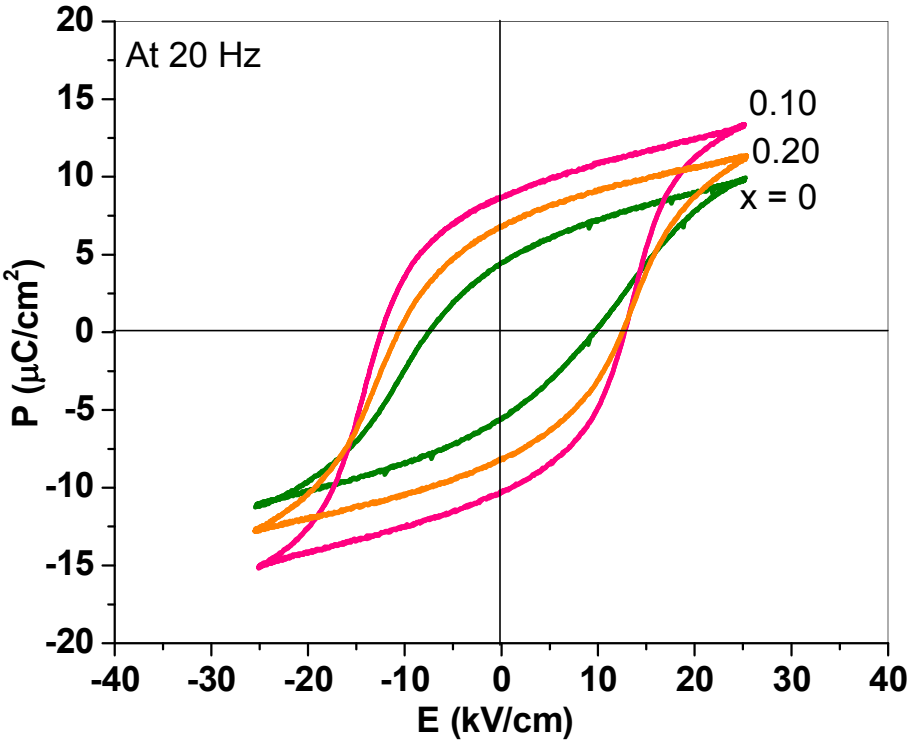

Figure 4.26 P-E hysteresis loops of BCPZT ceramics

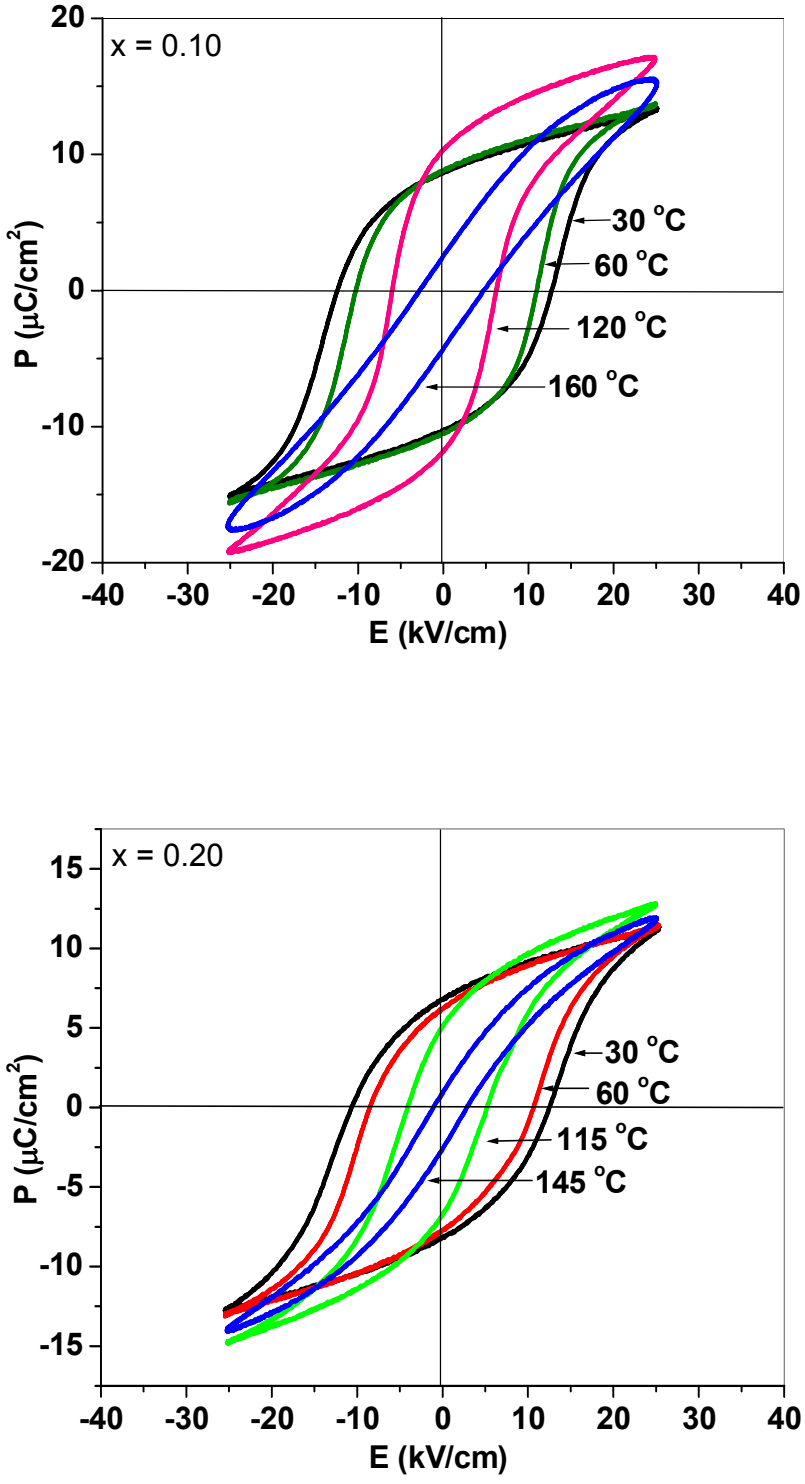

Figure 4.27 P-E hysteresis loops at different temperatures for x = 0.10 and 0.20

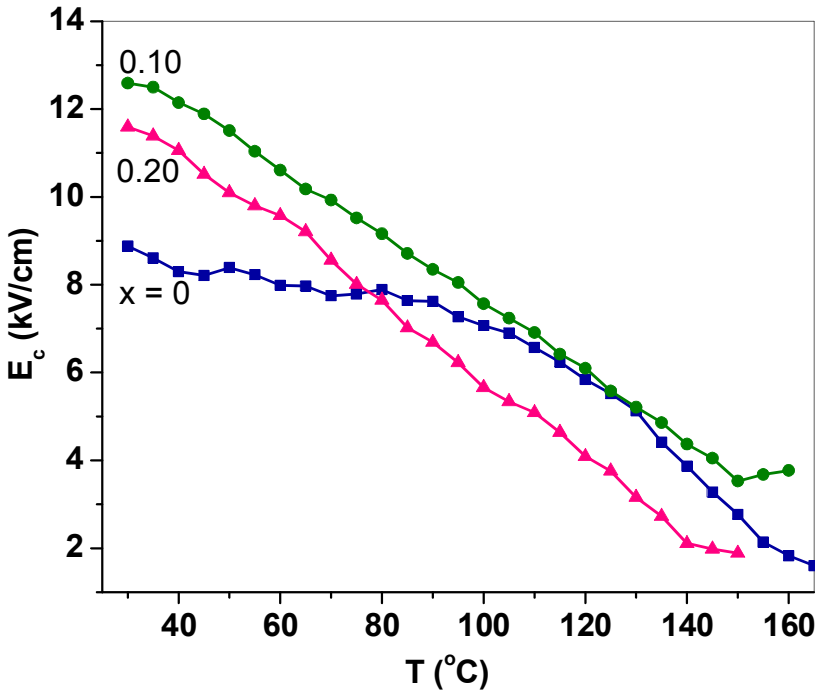
0.10
0.20
x = 0
E_c (kV/cm)
T (°C)

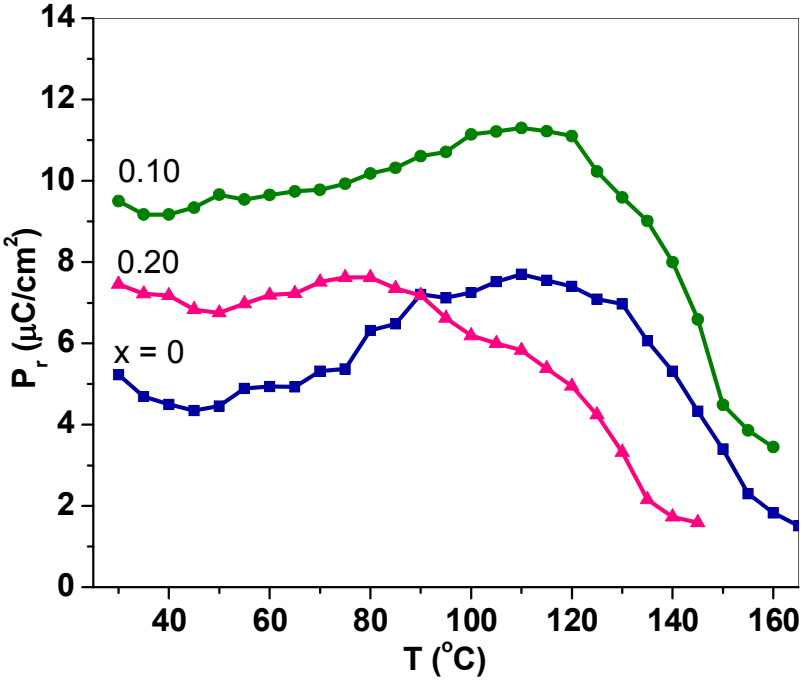
0.10
0.20
x = 0
P_r (μC/cm^2)
T (°C)

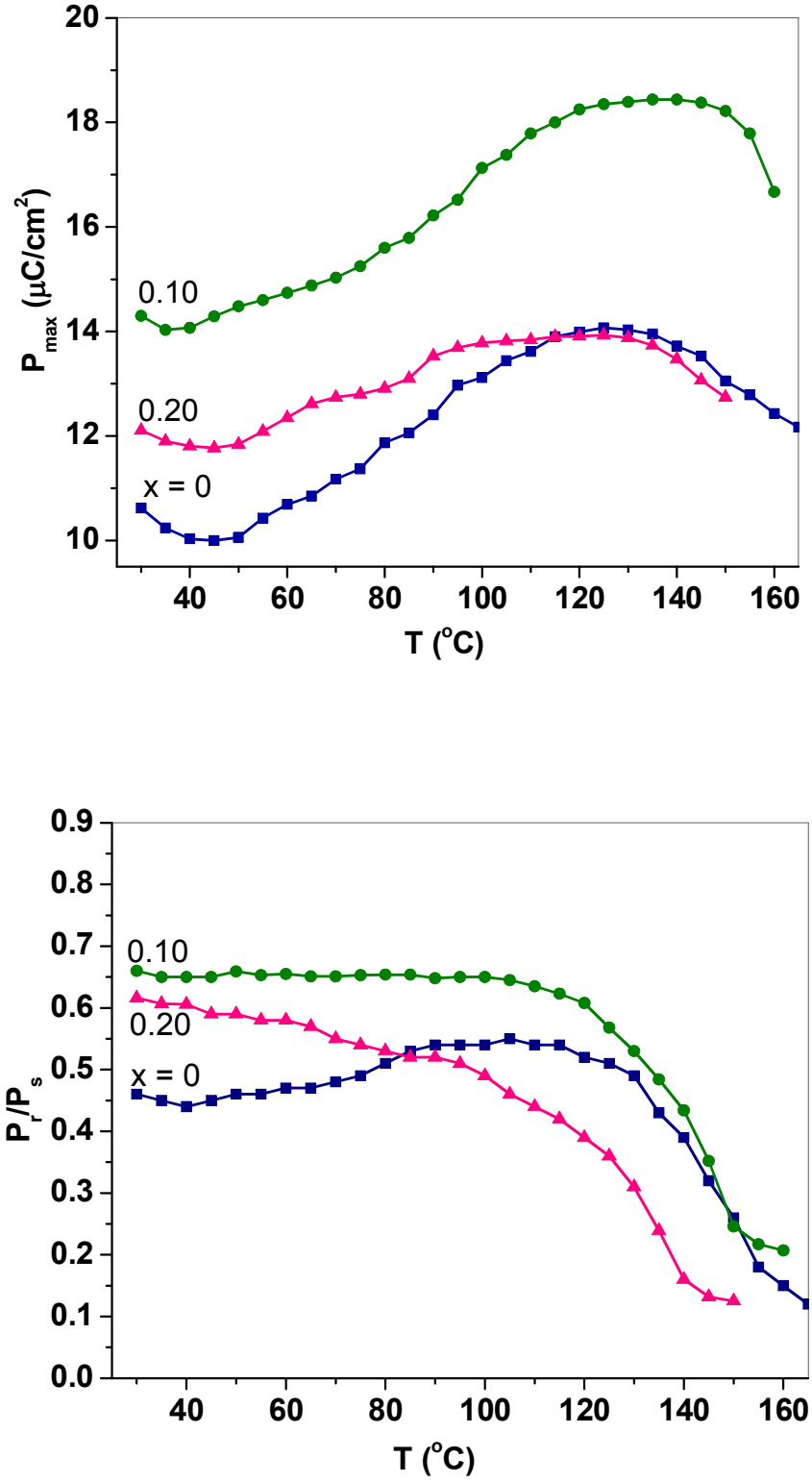

Figure 4.28 Variation of E_c, P_r, P_{max} and P_r/P_s with temperature

Table 4.8 Coercive field (E_c), Remanent polarization (P_r), P_r/P_s, d_{33}, k_p and k_t measured at 30°C

x	E_c (kV/cm)	P_r ($\mu C/cm^2$)	P_r/P_s	d_{33} (pC/N)	k_p (%)	k_t (%)
0	8.88	4.7	0.46	107	14.7	12.64
0.10	12.59	9.5	0.66	88	10.2	15.49
0.20	11.59	7.5	0.62	72	8.03	13.83

References

[1] P.W. Rehrig, S.E. Park, S.T. Mskinstry, G.L. Messing, B. Jones and T.R. Shrout, J. Appl. Phys., **86** (1999) 1657.

[2] Z. Yu, R. Guo and A.S. Bhalla, J. Appl. Phys., **88** (2000) 410.

[3] Y. Hirata and T. Kawazoe, J. Mater. Res., **11** (1996) 3071.

[4] S. Hoffmann and R. Waser, J. Eur. Ceram. Soc., **19** (1999) 1339.

[5] Y. Zhi, A. Chen, R. Guo and A.S. Bhalla, J. Appl. Phys., **92** (2002) 2655.

[6] X.G. Tang, K.H. Chew and H.L.W. Chan, Acta Mater., **52** (2004) 5177.

[7] U. Weber, G. Greuel, U. Boettger, S. Weber, D. Hennings and R. Waser, J. Am. Ceram. Soc., **84** (2001) 759.

[8] X.G. Tang and H.L.W. Chan, J. Appl. Phys., **97** (200) 5034109.

[9] P. Hansen, D. Henning and H. Schreinemacher, J. Am. Ceram. Soc., **81** (1998) 1369.

[10] Powder-X for Windows by Cheng Dong (Institute of Physics, Chinese Academy of Sciences, P.O. Box 603, Beijing 100080, P.R. China.

[11] K. Watanabe, H. Ohsato, H. Kishi, Y. Okino, N. Kohzu, Y. Iguchi and T. Okuda, Solid State Ion., **108** (1998) 129.

[12] M.T. Buscaglia, V. Buscaglia, M. Viviani, P. Nanni and M. Hanuskova, J. Eur. Ceram. Soc., **20** (2000) 15.

[13] M.W. Barsoum, Fundamentals of Ceramics, The McGraw Hill, New York, 1997.

[14] O.P. Thakur and C. Prakash, Phase Transitions, **76** (2003) 567.

[15] S.J. Kuang, X.G. Tang, L.Y. Li, Y.P. Jiang and Q.X. Liu, Scripta Materialia, **61** (2009) 68.

[16] G. Shirane and K. Suzuki, J. Phys. Soc. Japan**, 6** (1951) 274.

[17] S. Kuharuangrong, J. Mater. Sci., **36** (2001) 1727.

[18] W.C. Hsu, S.C. Chen, P.C. Kuo, C.T. Lie and W.S. Tsai, Mater. Sci. Eng. B, **111** (2004) 142.

[19] X.M. Chen, T. Wang and J. Li. Mater. Sci. Eng. B, **113 (**2004) 117.

[20] T.M. Kamel, J. Eur. Ceram. Soc., **28 (**2008) 851.

[21] K. Carl, Ferroelectrics, **9 (**1975) 23.

[22] W. Cao and C.A. Randall, J. Phys. Chem. Solids, **57 (**1996) 1499.

[23] Q.M. Zhang, H. Wang, N. Kim and L.E. Cross, J. Appl. Phys. **75** (1994) 454.

[24] X.L. Zhang, Z.X. Chen, L.E. Cross, W.A. Schulze, J. Mater. Sci., **18 (**1983) 968.

[25] J. Bera, and S.K. Rout, Mater. Res. Bull., **40** (2005) 1187.

[26] J. Bera. and S.K. Rout, J. Electroceram., **18 (**2007**)** 33.

[27] Sarabjit Singh, O.P. Thakur, Chandra Prakash and K.K. Raina, Phase Transitions, **78 (**2005) 655.

[28] L.I. Maissel, R. Glang, Handbook of Thin Film Technology, New York, McGraw-Hill, 1970.

[29] S.M. Pilgrim, A.E. Sutherland and S.R. Winzer, J. Am. Ceram. Soc., **73** (1990) 3122.

[30] A. Shukla, R.N.P. Choudhary, A.K. Thakur and D.K. Pradhan, Phys. B, **405 (**2010) 99.

[31] S.K. Sinha, S.N. Choudhary and R.N.P. Choudhary, J. Electroceramics, **7** (2001) 231.

[32] L.E. Cross, Ferroelectrics, **151 (**1994) 305.

[33] D. Viehland, M. Wutting and L.E. Cross, Ferroelectrics **120** (1991) 71.

Chapter 5

Influence of Sm and La on Structural and Electrical Properties of $Ba_{0.80}Pb_{0.20}Ti_{0.90}Zr_{0.10}O_3$

This chapter includes the effect of substitution of La and Sm on the structural, dielectric and ferroelectric properties of BPZT ceramics. The ceramics were synthesized by conventional solid state method and characterized for XRD, SEM, dielectric properties as function of temperature at different frequencies and ferroelectric properties. The results are discussed here.

5.1 Introduction

Compounds based on barium titanate are frequently used as capacitor materials due to their excellent dielectric and other electrical properties. Other main applications are piezoelectric sensors, transducers, actuators and ferroelectric random access memories and devices using the positive temperature coefficient of resistance (PTCR), [1-4]. The dielectric maximum of these materials is influenced by type and amount of substitutions and their dielectric properties are sensitive to temperature, field strength and frequency, especially near the Curie temperature. Small amounts of trivalent ions (such as Sm^{3+}, La^{3+}, Y^{3+}, Bi^{3+}, etc.) in the Ba site or pentavalent ions (such as Nb^{5+}, Ta^{5+} etc.) in the Ti site results in the decrease in room temperature resistivity [5-7]. Trivalent rare earth cations have been widely used in the modification of barium titanate based ceramics owing to their special electronic structure and their moderate ionic radii which allows them being incorporated in both A sites and B sites in ABO_3 lattice [8,9]. The influence of rare earth substituents on the dielectric properties of barium titanate and BZT ceramics has been widely studied as well. The substitution of samarium and lanthanum into BPZT ceramics, however, is rarely found in literature. In this chapter we are reporting the effect of samarium substitution on the dielectric properties of barium titanate based ceramics. Sm^{3+} and La^{3+} substituted $Ba_{0.80}Pb_{0.20}Ti_{0.90}Zr_{0.10}O_3$ (BPZT) material series with compositional formula:

$Ba_{0.80-x}Sm_xPb_{0.20}Ti_{0.90}Zr_{0.10}O_3$ (BSPZT)

$Ba_{0.80-x}La_xPb_{0.20}Ti_{0.90}Zr_{0.10}O_3$ (BLZPT)

Where, $0 \leq x \leq 0.01$, in steps of 0.0025

were synthesized for investigations. The material was synthesized by solid state reaction method; details are given in chapter 2. Reacted powders compacted in the form of circular discs were sintered in the range of 1300^{o}C to 1325^{o}C.

5.2 Physical and Structural Properties

All the samples of the series were subjected to XRD analysis. XRD patterns for samarium and lanthanum substituted $Ba_{0.80}$ $Pb_{0.20}Ti_{0.90}Zr_{0.10}O_3$ ceramics sintered at 1325^{o}C are illustrated in figure 5.1. All the samples were found to have pure perovskite phase with tetragonal structure. It has been already reported that aliovalent cations incorporated in perovskite lattice served as donor or acceptors, which can affect the electrical properties of the parent material greatly. It has been also reported that there are mainly three stages of substitution of rare earth elements in barium titanate based materials. In the first two stages, rare earth ions replace the original ions located in the lattice on the A or B site. In the third stage a secondary phase appears which indicates the insolubility of doped ions due to over limit of substitution [10,11]. The ionic radii of Ba^{2+} or Pb^{2+} in 12 coordinates and Ti^{4+} or Zr^{4+} in 6 coordinates are 1.75 Å, 1.63 Å, 0.75 Å and 0.86 Å respectively. The ionic radii of Sm^{3+} in 12 and in 6 coordinates are 1.38 Å and 1.09 Å, whereas ionic radii of La^{3+} in 12 and in 6 co-ordinates are 1.50 Å and 1.17 Å [12]. Therefore, Sm^{3+} and La^{3+} can occupy either A or B site in BPZT solution. From figure 5.1 it can also be observed that the splitting of the peak (at $2\theta \approx 45$ degree) revealing the existence of material with tetragonal structure in both Sm^{3+} and La^{3+} substitution. From the figure it is observed that the two peaks with peak indices (002) and (200) are merging into each other and finally for x = 0.010 only a single peak can be observed. This indicates that the structure of the material is

changing and the tetragonality is decreasing with increase in amount of Sm^{3+} and La^{3+}. FWHM also decreases with Sm^{3+} and La^{3+} substitution, supporting that tetragonality of the material is decreasing. All the sintered samples were subjected to scanning electron microscopy. Average grain size was found to decrease with increase in Sm^{3+} as well as La^{3+}. The average grain size in case of BSPZT series is greater than the average grain size calculated for the BLPZT series. This may be attributed to the larger ionic radius of La^{3+} ion than Sm^{3+} and hence comparatively lesser diffusivity into the crystal lattice [12]. The variation in lattice parameters, tetragonality and average grain size with varying amount of La^{3+} and Sm^{3+} is given in table 5.1. Experimental density 'd_{exp}', theoretical density 'd_{th}', relative density 'd_{rel}' and apparent porosity 'P' of BSPZT and BLPZT ceramic series are given in table 5.2. For BSPZT series, the maximum relative density was found for x = 0.0025, whereas for BLPZT series the maximum relative density is for x = 0.0050.

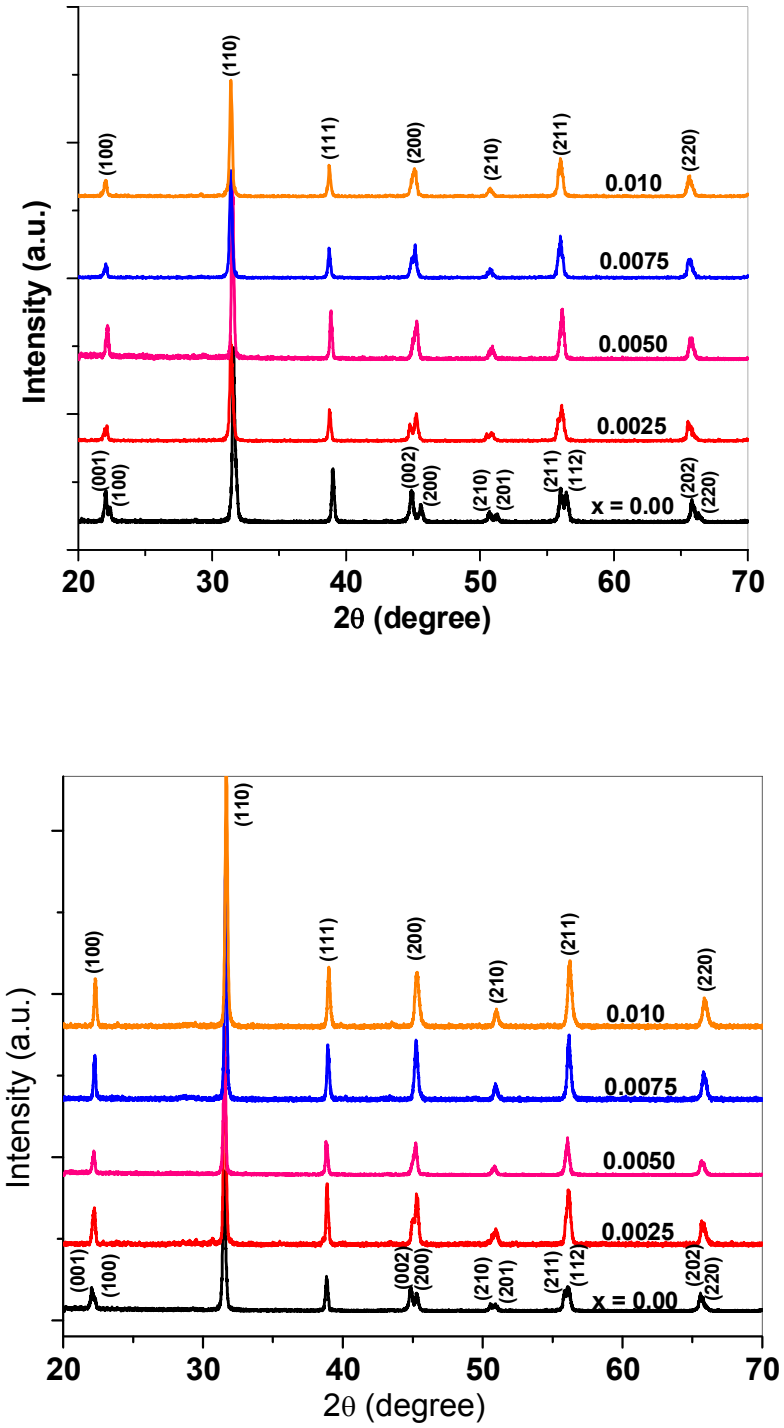

Figure 5.1 X-ray diffraction patterns for BSPZT (up) and BLPZT (down) ceramics

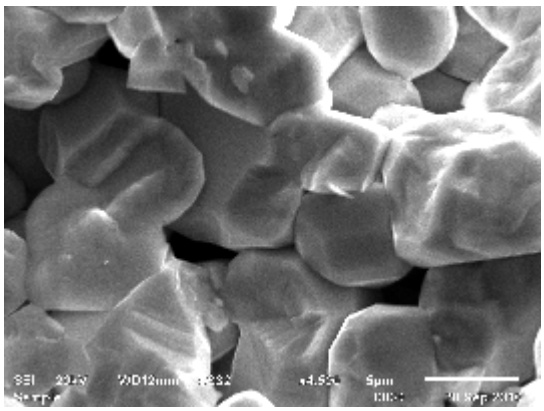

x = 0

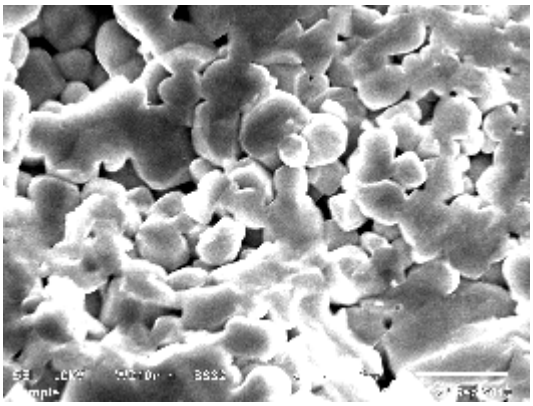

x = 0.0025

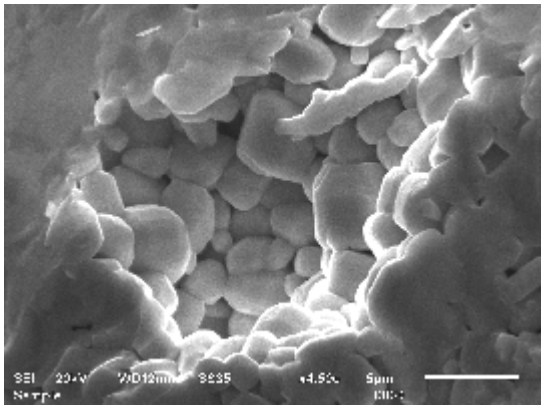

x = 0.0050

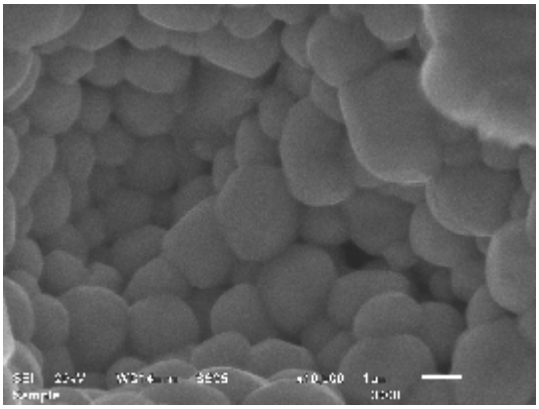

x = 0.0075

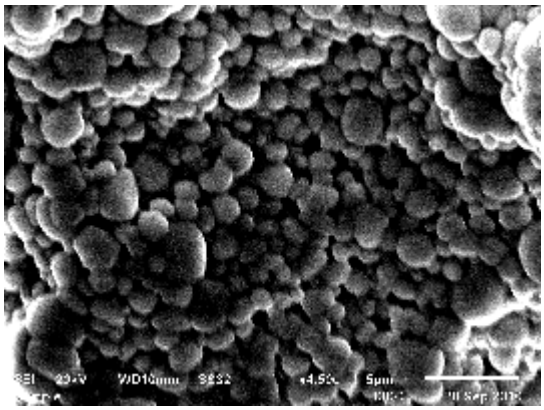

x = 0.01

Figure 5.2 SEM images of BSPZT ceramics

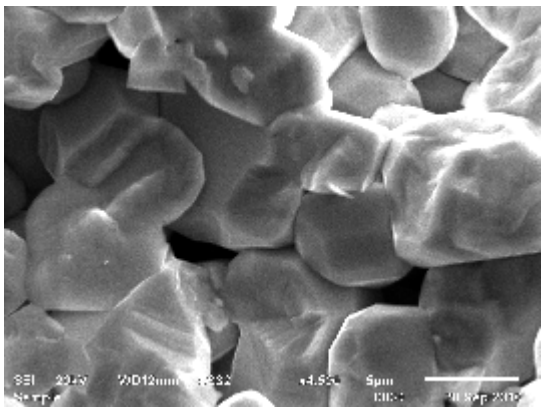

x = 0

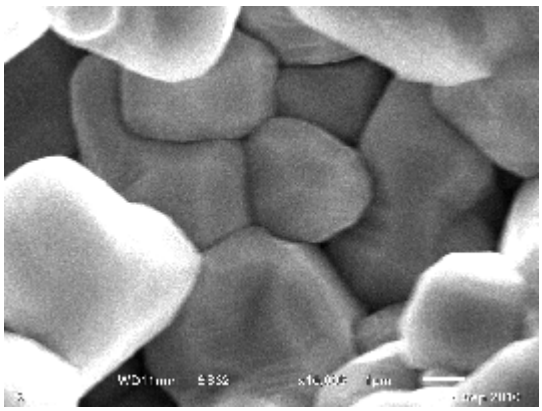

x = 0.0025

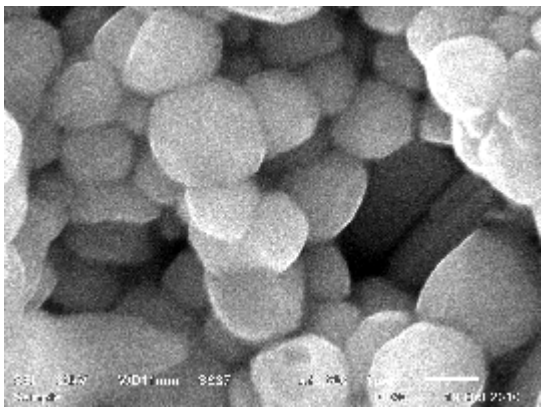

x = 0.0050

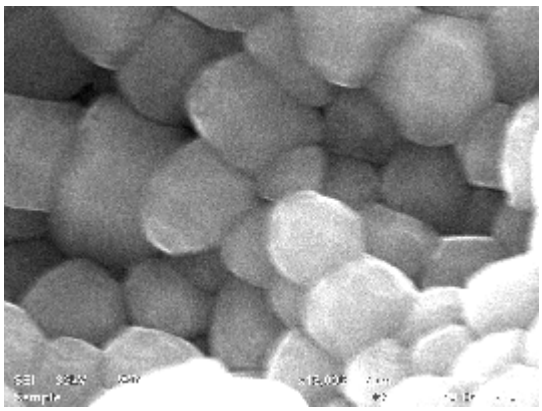

x = 0.0075

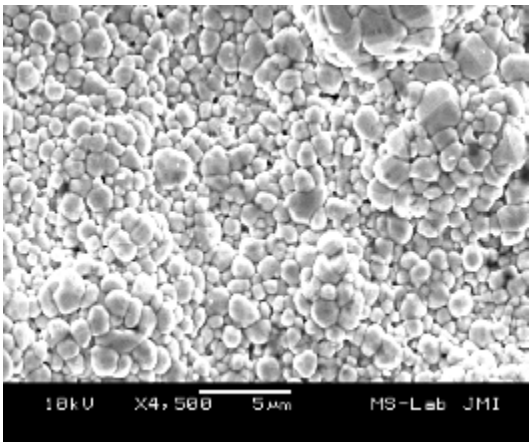

x = 0.01

Figure 5.3 SEM images of BLPZT ceramics

Table 5.1 Lattice parameters ‘a’ and ‘c’, tetragonality, ‘c/a’, and average grain size of BSPZT and BLPZT ceramics

BSPZT					BLPZT			
x	**a (Å)**	**c (Å)**	**c/a**	**grain size (µm)**	**a (Å)**	**c (Å)**	**c/a**	**grain size (µm)**
0	4.0000	4.0542	1.0136	6.7	4.0000	4.0542	1.0136	6.7
0.0025	4.0056	4.0466	1.0105	4.2	4.0020	4.0200	1.0040	2.55
0.0050	4.0097	4.0461	1.0091	2.5	4.0061	4.0168	1.0026	1.47
0.0075	4.0129	4.0385	1.0064	1.6	4.0035	4.0139	1.0025	1.34
0.010	4.0160	4.0309	1.0037	1.5	4.0025	4.0097	1.0010	1.02

Table 5.2 Experimental density 'd_{exp}', theoretical density 'd_{th}', relative density 'd_{rel}' and apparent porosity 'P' of BSPZT and BLPZT ceramics

	BSPZT				BLPZT			
x	**d_{exp} (g/cc)**	**$d_{x\text{-}ray}$ (g/cc)**	**d_{rel} (%)**	**P (%)**	**d_{exp} (g/cc)**	**$d_{x\text{-}ray}$ (g/cc)**	**d_{rel} (%)**	**P (%)**
0	5.78	6.44	89.75	10.25	5.78	6.44	89.75	10.25
0.0025	6.12	6.43	95.18	4.82	5.66	6.50	87.08	12.92
0.0050	5.99	6.52	91.87	8.13	6.06	6.49	93.38	6.62
0.0075	5.97	6.46	92.42	7.58	5.97	6.51	91.71	8.29
0.010	5.87	6.45	91.01	8.99	6.03	6.52	92.49	7.51

5.3 Dielectric Properties

The dielectric properties were measured as a function of temperature up to well above the transition temperature, T_c, of the corresponding samples at four different frequencies. Dielectric constant increases with increasing temperature and shows a peak which is characteristic of ferroelectric materials. Variation of dielectric constant with temperature for all x is shown in figure 5.4 and 5.5. For both Sm^{3+} & La^{3+} with x = 0.0025, dielectric constant does not show much dependence on frequency and temperature below transition temperature but the effect of both frequency and temperature becomes pronounced as the temperature approaches the transition temperature.

The temperature dependence of the dielectric constant of all the samples at 100 kHz and heated at the rate of 1^oC/min is shown in figure 5.6 and 5.7. One can observe that the maximum dielectric constant increases as x increases from 0 to 0.0025 and then decreases for further values of x [13,14]. As Sm^{3+} and La^{3+} ions substitute the A-site, they act as donor additives and vacancies for Ba-site will be produced. These Ba-site vacancies results in the reduction of Ti^{4+} ions into Ti^{3+} ions. The decrease in ε_{max} with x greater than 0.0025 also indicates that the dipole moment of the lattice reduced and lowers the peak dielectric constant for further substitution [15,16]. Dielectric peaks get broaden with substitution. The dielectric peaks in case of BLPZT series are comparatively broader than BSPZT series, which again indicating the larger ionic radius of La^{3+} ion increases the microstructural fluctuation.

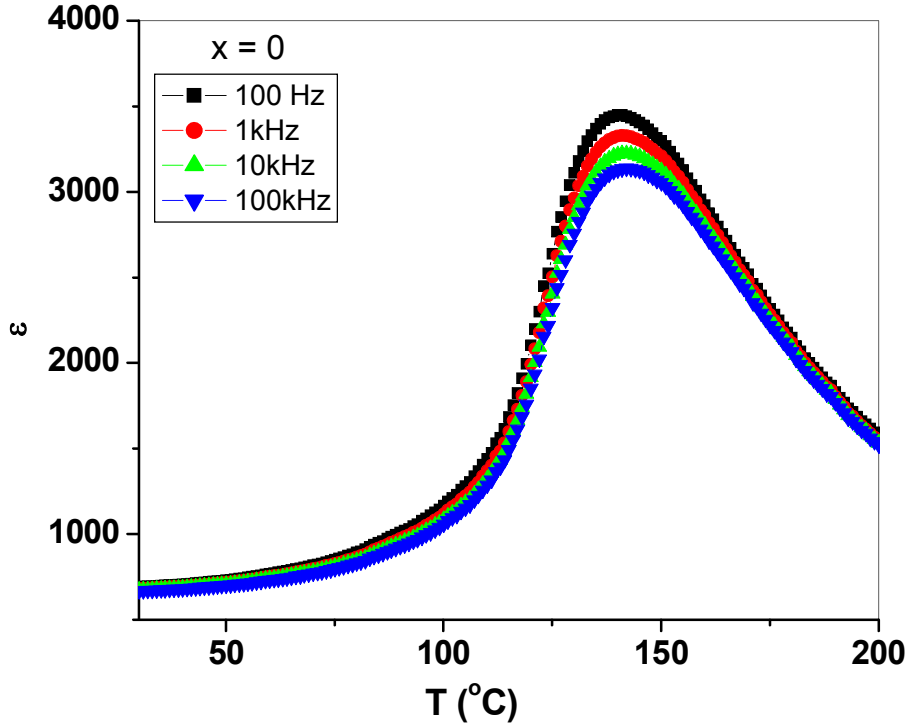
x = 0
100 Hz
1kHz
10kHz
100kHz
ε
T (°C)

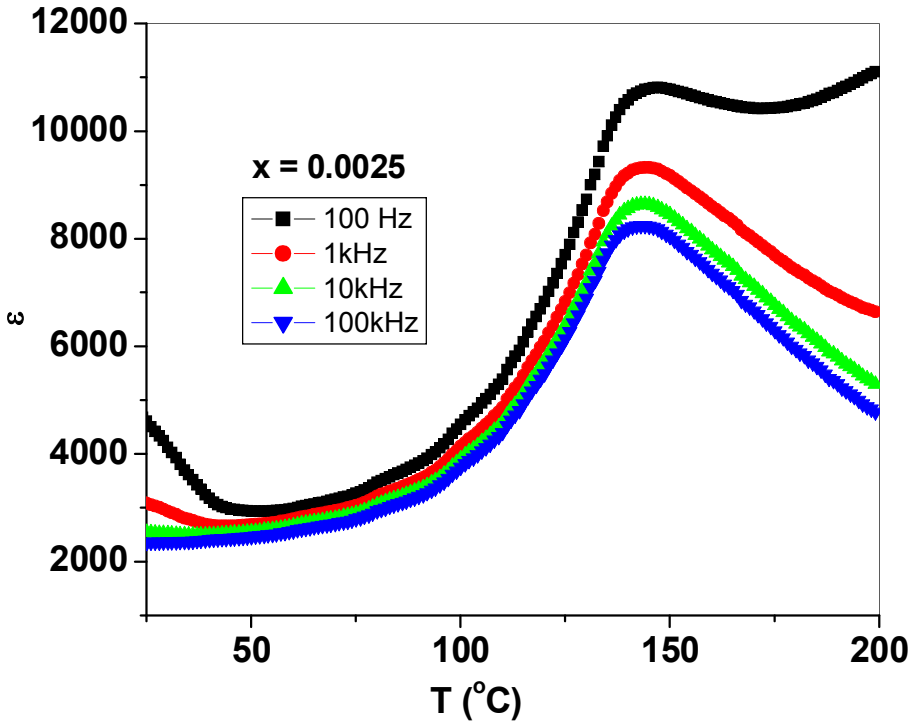
x = 0.0025
100 Hz
1kHz
10kHz
100kHz
ε
T (°C)

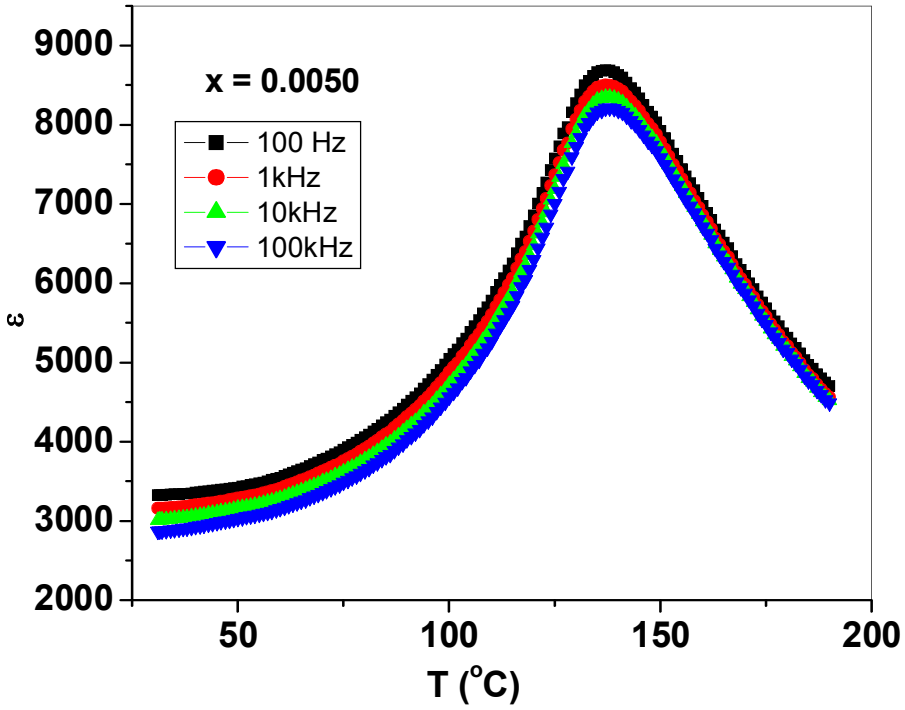
x = 0.0050
100 Hz
1kHz
10kHz
100kHz
ε
T (°C)
9000
8000
7000
6000
5000
4000
3000
2000
50
100
150
200

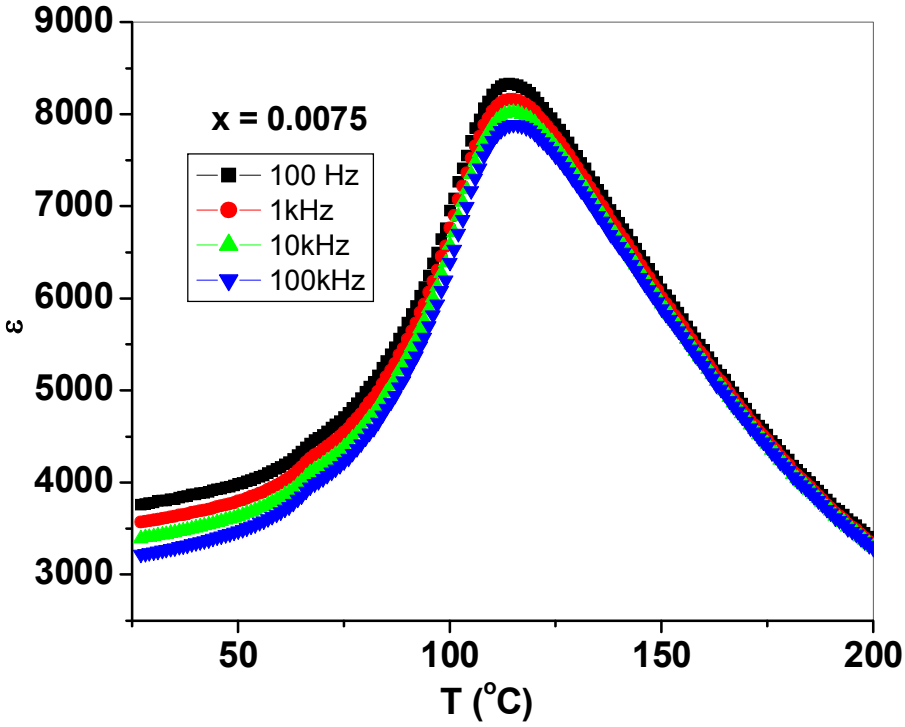
x = 0.0075
100 Hz
1kHz
10kHz
100kHz
ε
T (°C)
9000
8000
7000
6000
5000
4000
3000
50
100
150
200

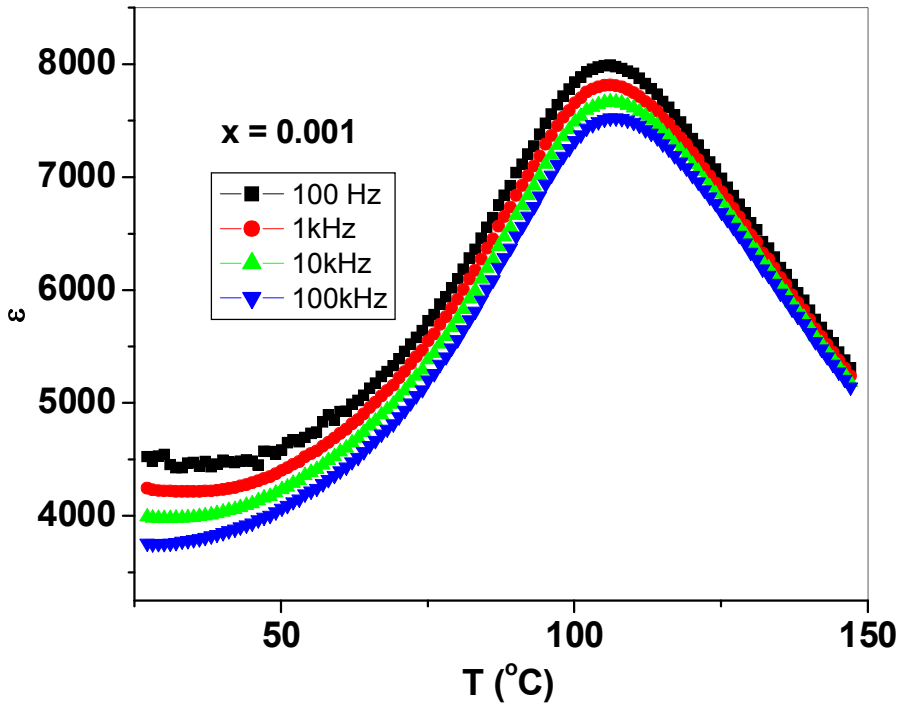

Figure 5.4 Variation of dielectric constant with temperature of BSPZT ceramics

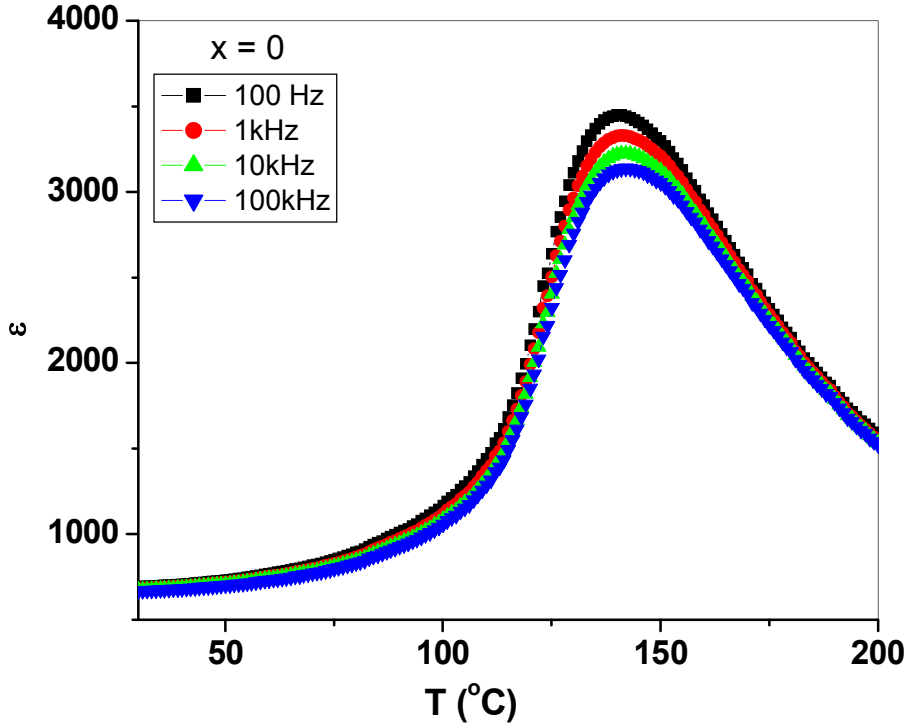
x = 0
100 Hz
1kHz
10kHz
100kHz
ε
T (°C)

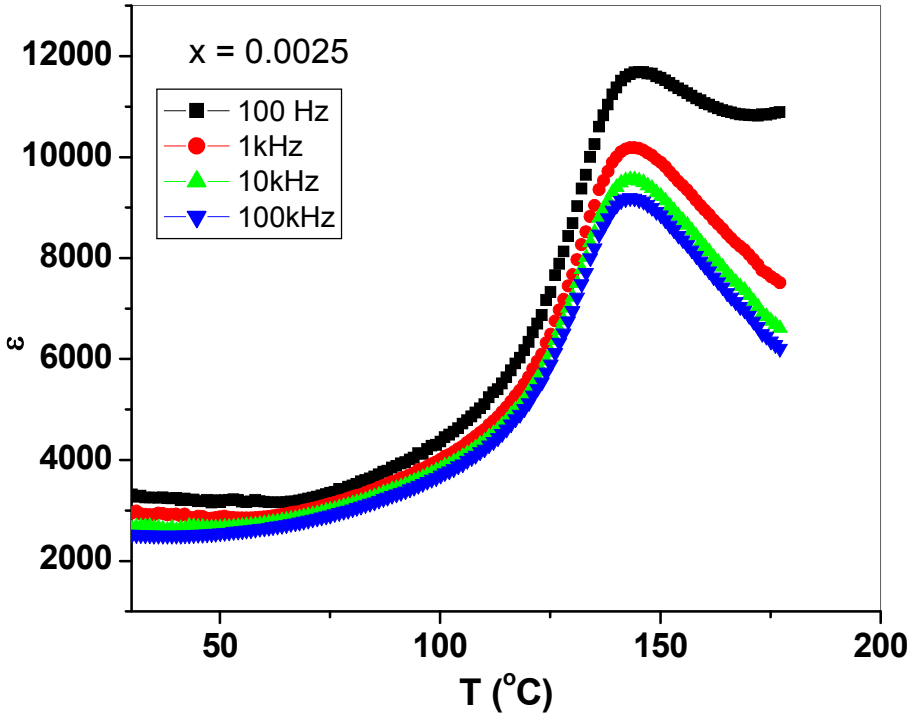
x = 0.0025
100 Hz
1kHz
10kHz
100kHz
ε
T (°C)

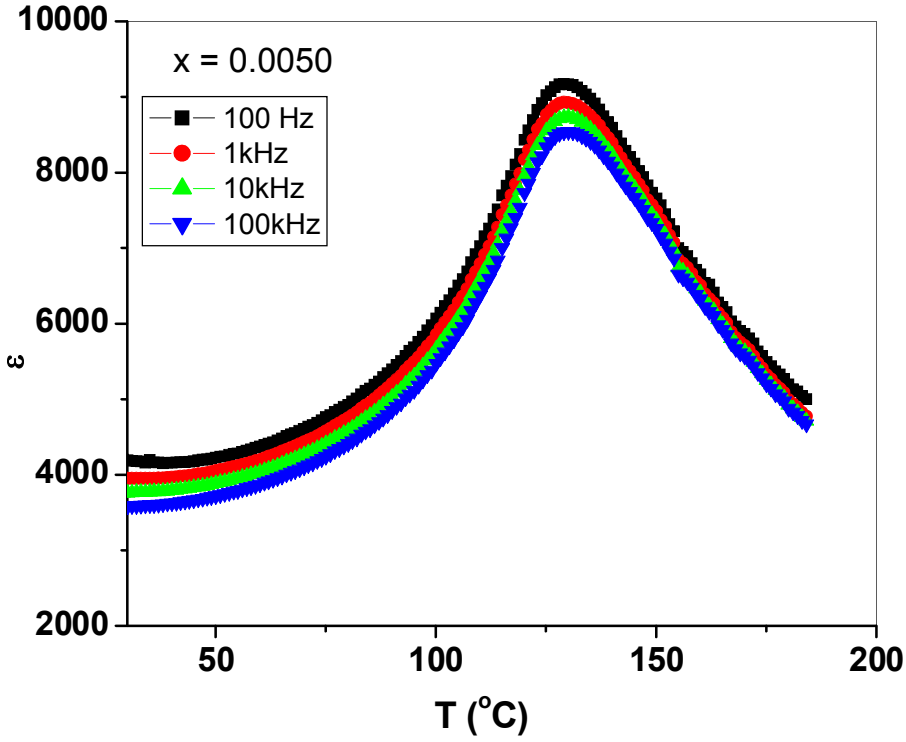
x = 0.0050
100 Hz
1kHz
10kHz
100kHz
10000
8000
6000
4000
2000
ε
50
100
150
200
T (°C)

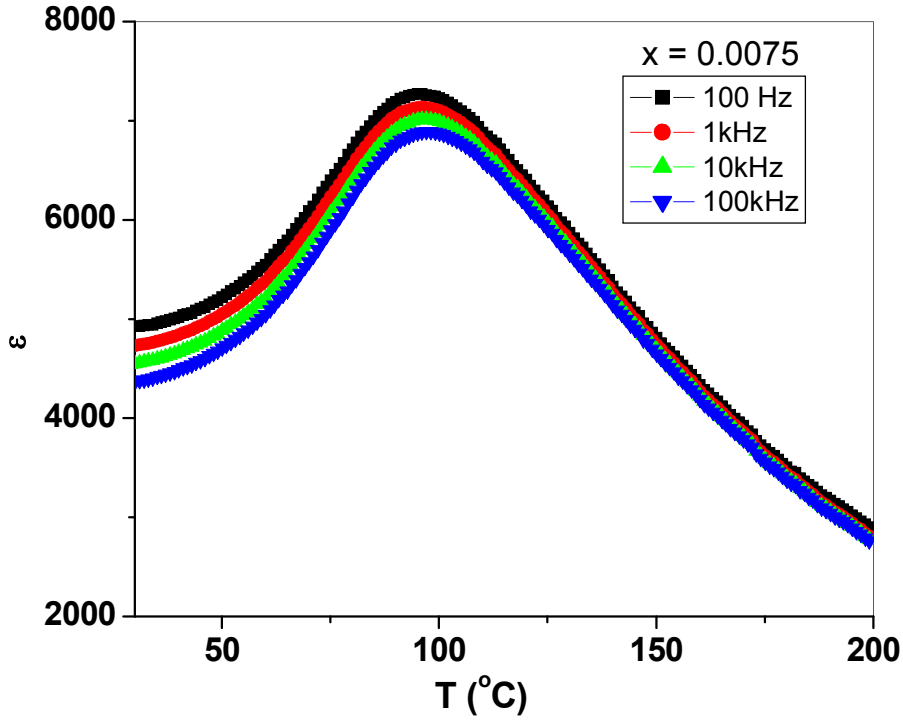
x = 0.0075
100 Hz
1kHz
10kHz
100kHz
8000
6000
4000
2000
ε
50
100
150
200
T (°C)

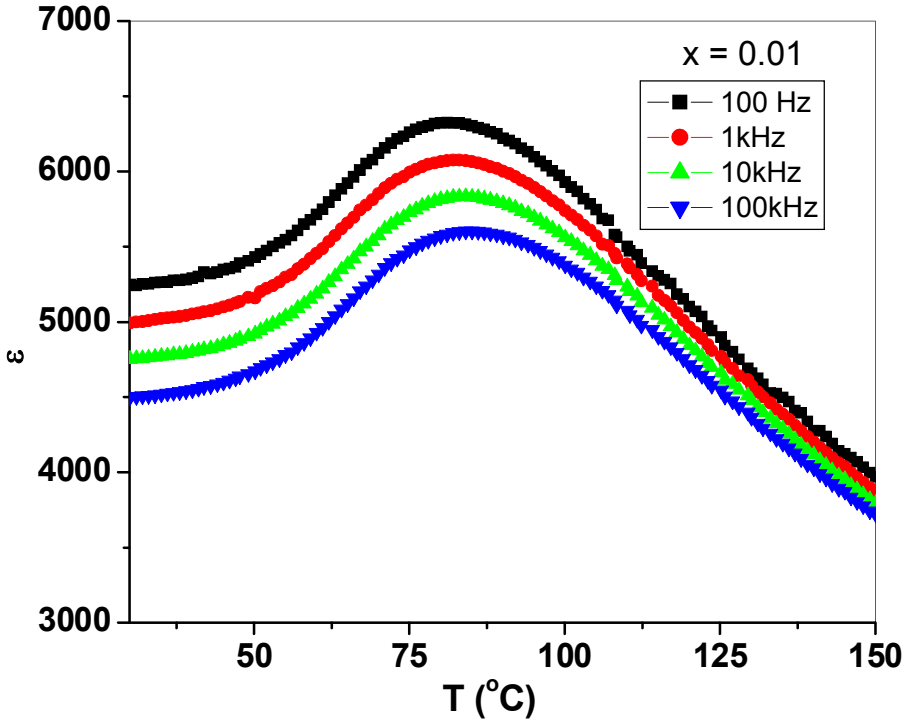

Figure 5.5 Variation of dielectric constant with temperature of BLPZT ceramics

Being a diffuse phase transition, the temperature with maximum dielectric constant T_m can be consider as the Curie temperature of the material. From the dielectric constant versus temperature plot Curie temperature (paraelectric to ferroelectric phase transition temperature) was determined. The origin of the transition from paraelectric to ferroelectric phase lies in the vibrations in the Ti-O bonds. Since substitution of Sm^{3+} causing the reduction of Ti^{4+} ion to Ti^{3+} ion which results in weakening of Ti-O bonds. Moreover the trivalent Sm^{3+} ions are strongly attracted by the oxygen ions in comparison to divalent Ba^{2+} and Pb^{2+} [17,18]. This results in overall reduction of stresses in the unit cell. Thus the dielectric peak shifts towards room temperature with increase in samarium contents and thereby room temperature dielectric constant increases [19].

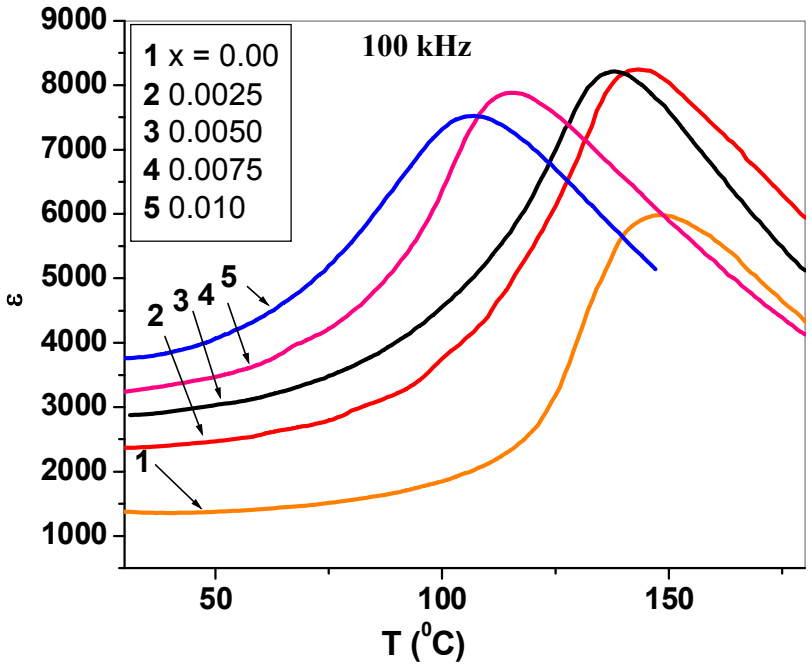

Figure 5.6 Variation of dielectric constant with temperature of BSPZT at 100 kHz

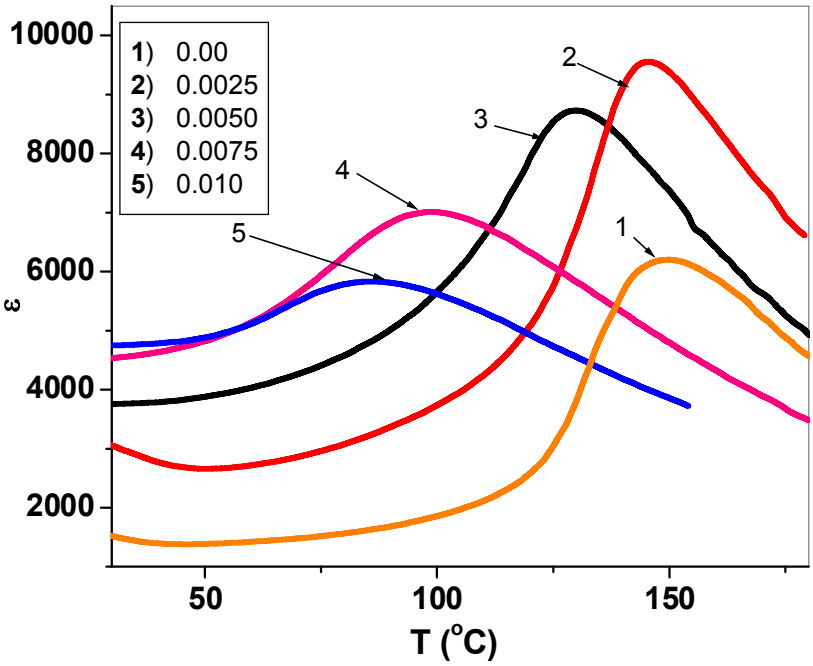

Figure 5.7 Variation of dielectric constant with temperature of BLPZT at 100 kHz

Table 5.3 Dielectric parameters of BSPZT and BLPZT ceramics for all x

BSPZT						BLPZT				
x	**ε_{RT}**	**tanδ**	**ε_{max}**	**$tan\delta_{max}$**	**T_c (^oC)**	**ε_{RT}**	**tanδ**	**ε_{max}**	**$tan\delta_{max}$**	**T_c (^oC)**
0	1375	0.042	5985	0.025	148	1375	0.042	5985	0.025	148
0.0025	2370	0.039	8245	0.032	143	3024	0.084	9555	0.027	145
0.0050	2875	0.038	8210	0.011	138	3760	0.033	8730	0.017	130
0.0075	3245	0.035	7885	0.014	115	4540	0.031	7010	0.015	98
0.010	3755	0.039	7525	0.015	107	4750	0.041	5835	0.029	86

5.4 Relaxor Behavior of $Ba_{0.80-x}La_xPb_{0.20}Ti_{0.90}Zr_{0.10}O_3$ (x = 0.01)

Strong frequency dispersion was observed around the dielectric peak for La substituted composition and the peak was found to shift to higher temperature with increase in frequency. This is characteristic of a typical relaxor behavior. There is a significant improvement in tanδ with La substitution. In most ferroelectrics, the temperature dependence of the dielectric constant above the Curie temperature (in paraelectric phase region) can be described by a simple relationship called the Curie-Weiss law [20]:

$$\varepsilon = \varepsilon_o + C/(T-T_o)$$

where, ε_o is free space permittivity, C is the Curie-Weiss constant and T_o is the Curie-Weiss temperature. Generally, in the case of a first-order phase transition, $T_o<T_c$, while for second-order phase transition $T_o = T_c$. Figure 5.8 shows the variation of inverse of dielectric constant with temperature in the vicinity of the transition temperature for both the material sample.

It can be seen that the dielectric constant of lanthanum substituted sample follows the Curie-Weiss law at temperature much higher than the $T_{\varepsilon m}$. Uchino and Nomura modified Curie-Weiss law for the diffusiveness of the phase transition and is given as;

$$\ln(1/\varepsilon - 1/\varepsilon_{max}) = \gamma \ln(T - T_c) + a$$

where ε_{max} is the maximum value of ε at T_c. The value of γ is the degree of diffusiveness, which lies in the range $1 \leq \gamma \leq 2$, where $\gamma = 1$ represents ideal Curie-Weiss behaviors i.e. for normal ferroelectrics and $\gamma = 2$ (quadratic) is valid for an ideal ferroelectric relaxor, while γ between 1 and 2 indicates diffused transition. Thus the value of γ can characterize the relaxor behavior. It was found to increase with the substitution of lanthanum which may be due to the compositional fluctuations and structural disordering in the arrangement

of cations in one or more crystallographic sites in the structure that finally results in a microscopic heterogeneity in the samples with local Curie points.

The diffusiveness of the phase transition can be explained by an empirical parameter

$$\Delta T_{diff} = T_{0.9\varepsilon m\,(100\ Hz)} - T_{\varepsilon m\,(100Hz)}$$

which is the difference between $T_{0.9\varepsilon m\,(100\ Hz)}$ (the temperature corresponding to 90% of the maximum of the dielectric constant at higher temperature side at 100 Hz) and $T_{\varepsilon m}$. The value of ΔT_{diff} was found to be 15°C and 25°C for x = 0 and 0.01 which indicates that sample with x = 0.01 shows more diffusive nature as compared to sample with x = 0.

The degree of relaxation behavior can be explained by a parameter ΔT_{relax}, which is defined as

$$\Delta T_{relax} = T_{\varepsilon m\,(100\ kHz)} - T_{\varepsilon m\,(100Hz)}$$

The value of ΔT_{relax} is shown in table 5.4 and indicates that degree of relaxation behavior is more pronounced in lanthanum substituted sintered sample. This above empirical characterization for parameters ΔT_{relax}, ΔT_{diff} and γ for both the material compositions shows that dielectric behavior of sample with x = 0.01 follows the Curie-Weiss law only at the temperature higher than $T_{\varepsilon m}$, significant diffusiveness of the phase transition and some frequency dispersion. The frequency dispersion near dielectric maxima in relaxor ferroelectrics has been attributed to the distribution of relaxation times [21,22]. The Gaussian diffuseness (δ_g) in lanthanum substituted BPZT ceramics was calculated using the relation $\ln(\varepsilon_{max}/\varepsilon) = (T-T_m)^2/2\ \delta_g^2$ as shown in figure 5.9 (a). This relation is valid within the limit $1 \leq \varepsilon_{max}/\varepsilon \leq 1.5$. As $\varepsilon_{max} > \varepsilon$, the only physically meaningful limit of δ_g is

$\varepsilon_{max}/\varepsilon \leq 1.5$. The value of δ_g, which is related to the broadening of the $\varepsilon(T)$ curve, can be used to determine the degree of compositional fluctuations in the material. This diffuseness parameter δ_g depends not only on the chemical composition of the material but also on the frequency of the electric field [23,13]. The values of δ_g for x = 0 and 0.01 are 35.01 and 36.79 at 10 kHz and 48.499 and 51.59 at 100 kHz respectively.

Table 5.4 Room temperature dielectric constant ε_{RT}, maximum dielectric constant ε, ΔT_{diff}, ΔT_{relax} and γ for compositions with x = 0 and 0.01 at 100 kHz

x	ε_{RT}	ε_{max}	T_c (^oC)	ΔT_{diff} (^oC)	ΔT_{relax} (^oC)	γ
0	1380	5970	146	15	1	1.4
0.01	4500	5600	85	25	5	1.83

The percentage temperature coefficient of capacitance defined as $T_{cc} = ((C_T - C_{T-1})/C_{T-1}) \times 100$ was calculated for both the compositions at frequency 100 kHz and plotted as a function of temperature as shown in figure 5.9 (b) [24]. The low value of T_{cc} for x = 0.01 also confirmed a diffuse phase transition in lanthanum substituted BPZT ceramics.

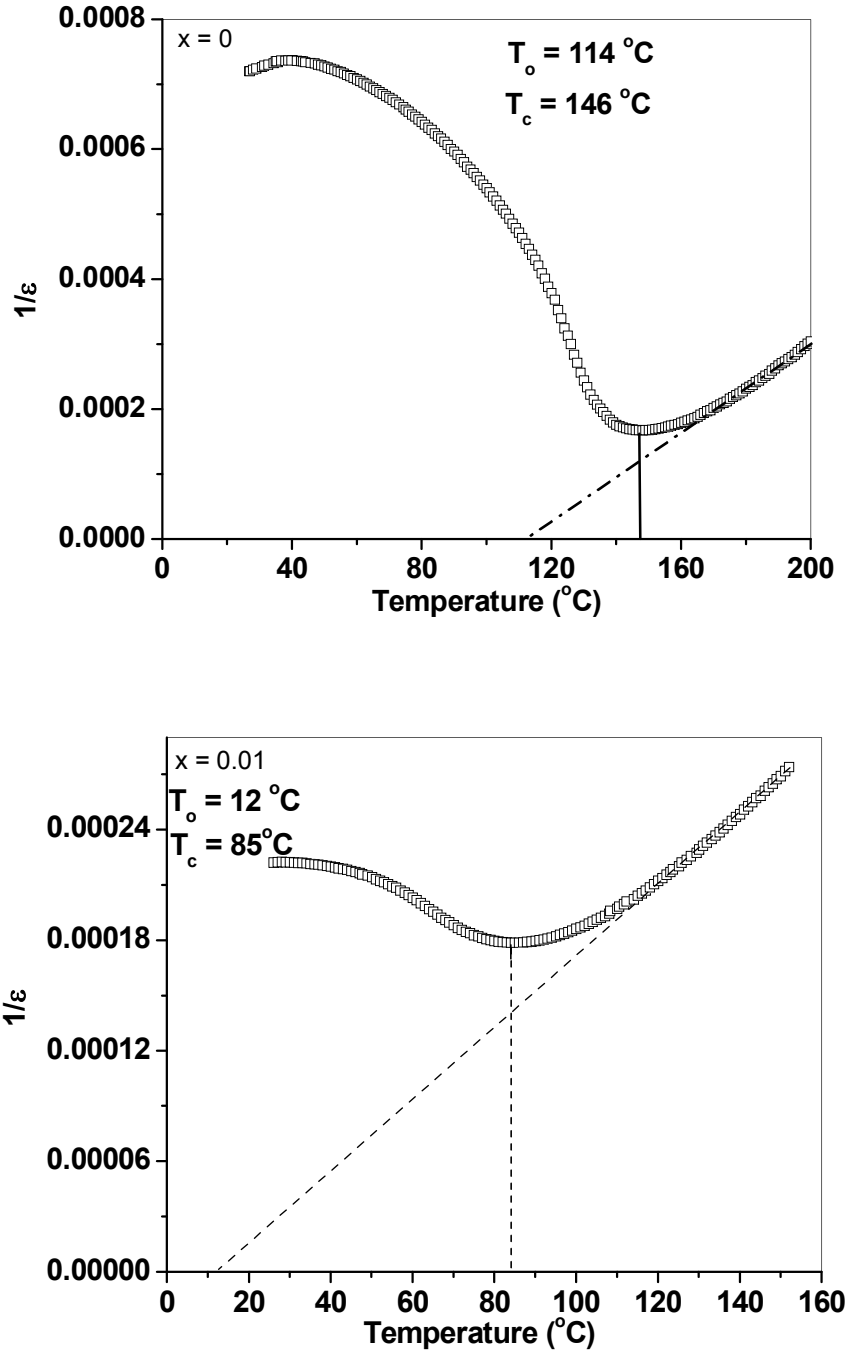

Figure 5.8 The inverse ε as a function of temperature at 100 kHz for x = 0 and 0.01

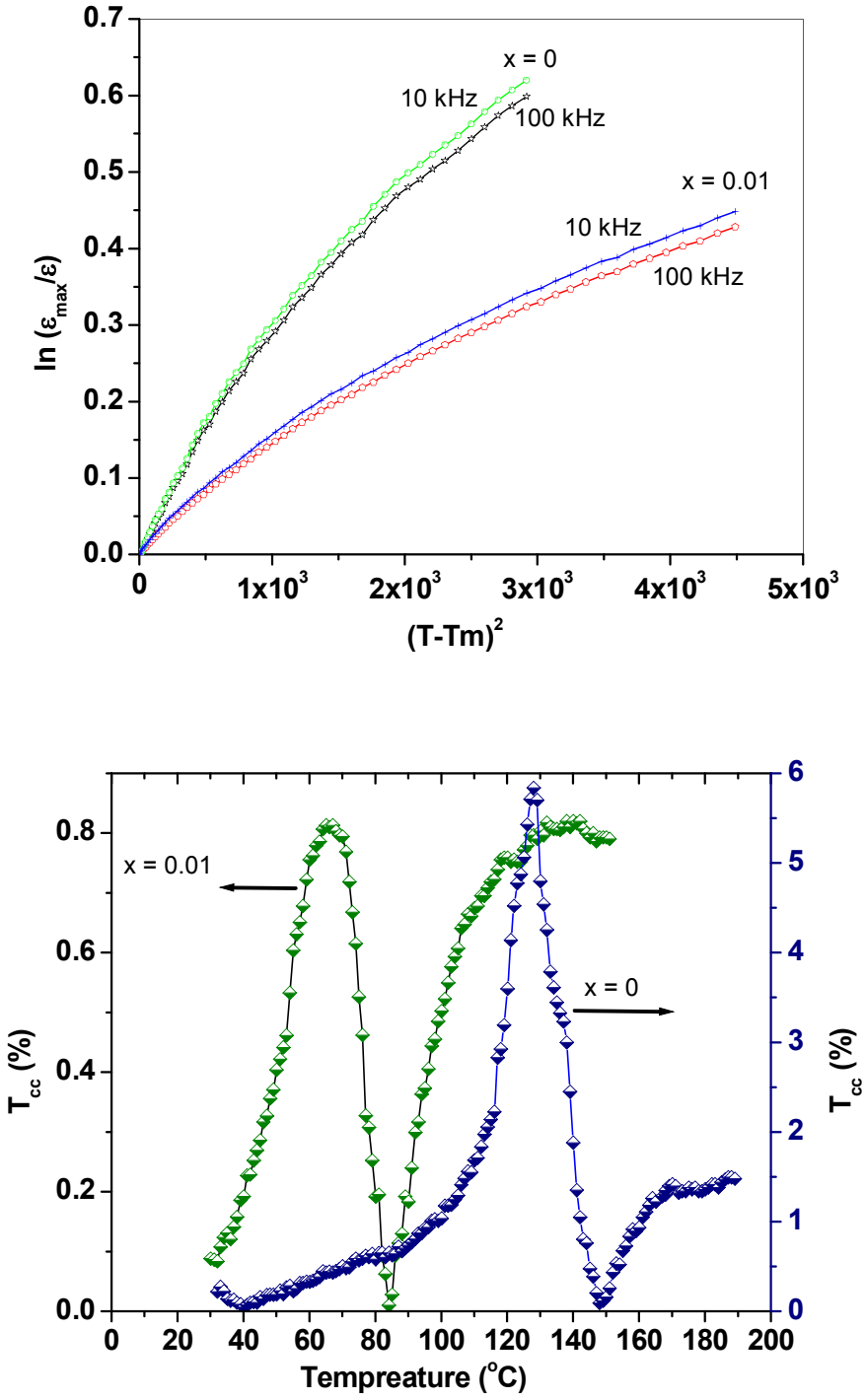

Figure 5.9 (a) Variation of $\ln(\varepsilon_{max}/\varepsilon)$ as a function of $(T-T_m)^2$ at frequencies 10 kHz and 100 kHz for x = 0 and 0.01, (b) T_{cc} vs. temperature at 100 kHz for x = 0 and 0.01

5.5 Ferroelectric and Piezoelectric Properties of BSPZT ceramics

To study the ferroelectric properties, well saturated PE hysteresis loops were recorded for all samples at different temperatures (30-105^{o}C). The PE loops at 30^{o}C for x = 0, 0.005 and 0.010 are shown in figure 5.10 and a comparatively slow domain switching with alternating field. The switching can be explained by remanent to spontaneous polarization ratio (P_r/P_s), which is a measure of squareness of the loop. P_r/P_s was found to have low values (Table 5.5). Coercive field (E_c) was found to decrease with increase in Sm content as well as with temperature as shown in figure 5.11. The decrease in E_c with increase in Sm content is an evidence of the donor nature of Sm^{3+} ions at Ba^{2+} site. As the ceramic samples were sintered at quite high temperature (1325^{o}C), therefore, some Pb vacancies can be formed at grain boundaries. Reduced tetragonality and A-site vacancies at grain boundaries is also responsible to the decrease in E_c [25]. A very small decrease in E_c with increase in Sm content from 0.0075 to 0.010 was observed, which can be attributed to the very small variation in average grain size, i.e., from 1.6 to 1.5 μm. Decrease in E_c with temperature can be related to the increase in internal energy and decrease in stability of the domains. The overall conclusion from this behavior of E_c is that for the present solid solution, Sm^{3+} ion is acting as donor/softener as in case of other perovskite ferroelectrics. Variation of P_r and P_r/P_s with temperature for different amount of Sm is shown in figure 5.12 and 5.13 respectively. P_r decreases with increase in temperature except for the sample having no Sm content. For this sample P_r increases with temperature in the entire temperature range and is mainly due to increase in internal energy caused by thermal excitation leading to greater dipole alignment. This kind of behavior gets reduced with increase in Sm content.

For x = 0.0025, negligible changes with temperature are observed, i.e., the P_r-T curve is approximately parallel to the temperature axis. While for further increase in Sm content, a decreasing trend can be observed which may be due to reduced tetragonality. This is due to the decrease in internal stresses with increase in Sm content [26,14]. As far as dependence of P_r on Sm content is concerned, it increases up to 0.0050 and then decreases for higher Sm content. This trend can be attributed to the fact that Sm substitution resulted in enhanced dipole moment up to 0.050 and beyond that grain size plays its role as smaller polarization exist in finer grains. Piezoelectric charge coefficient 'd_{33}' was also measured and it was found to decrease with increase in Sm content. For the ceramic samples with Sm content 0.0075 and 0.010, approximately equal value for d_{33} can be observed and the effect is once again mainly due to the grain size. Not only the reduced grain size but the reduced internal stresses and increased Pb vacancies at grain boundaries are also responsible for decreased values of d_{33} [27]. The values of d_{33} and k_p for all BSPZT ceramics are given in table 5.6.

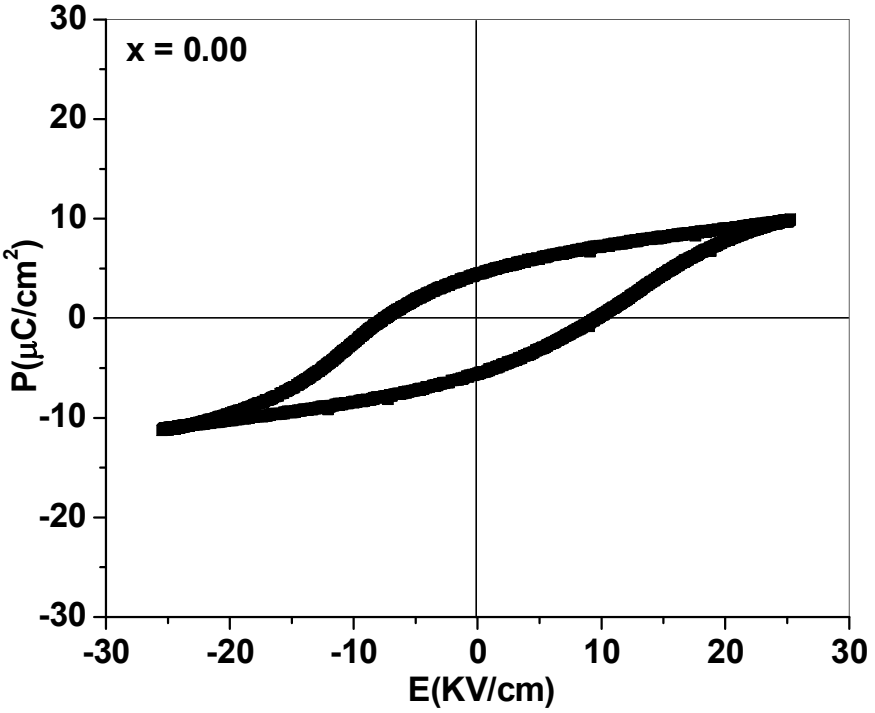
x = 0.00
P(μC/cm²)
E(KV/cm)
30
20
10
0
-10
-20
-30
-30
-20
-10
0
10
20
30

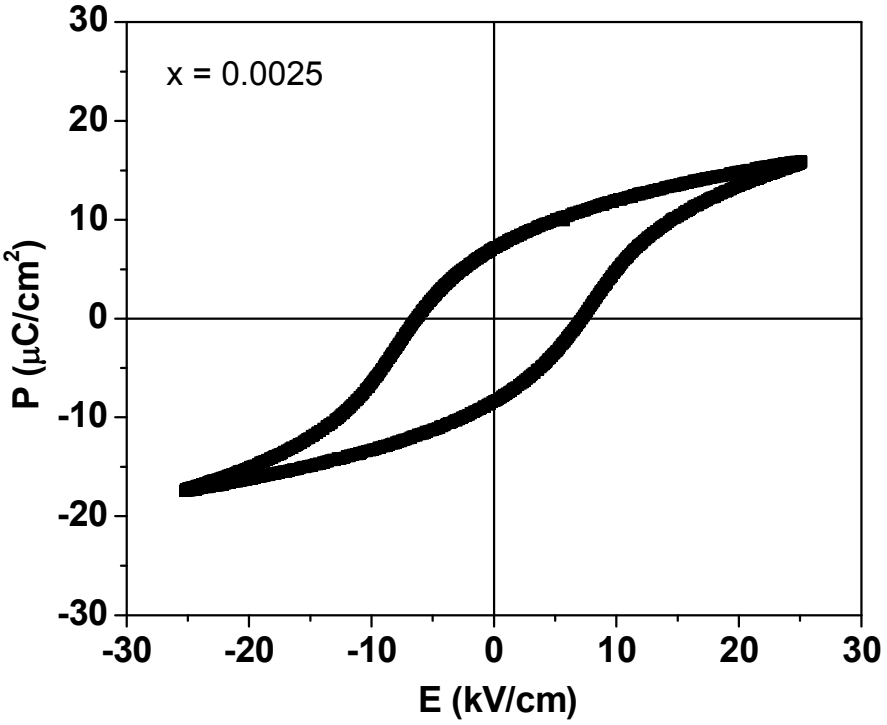
x = 0.0025
P (μC/cm²)
E (kV/cm)
30
20
10
0
-10
-20
-30
-30
-20
-10
0
10
20
30

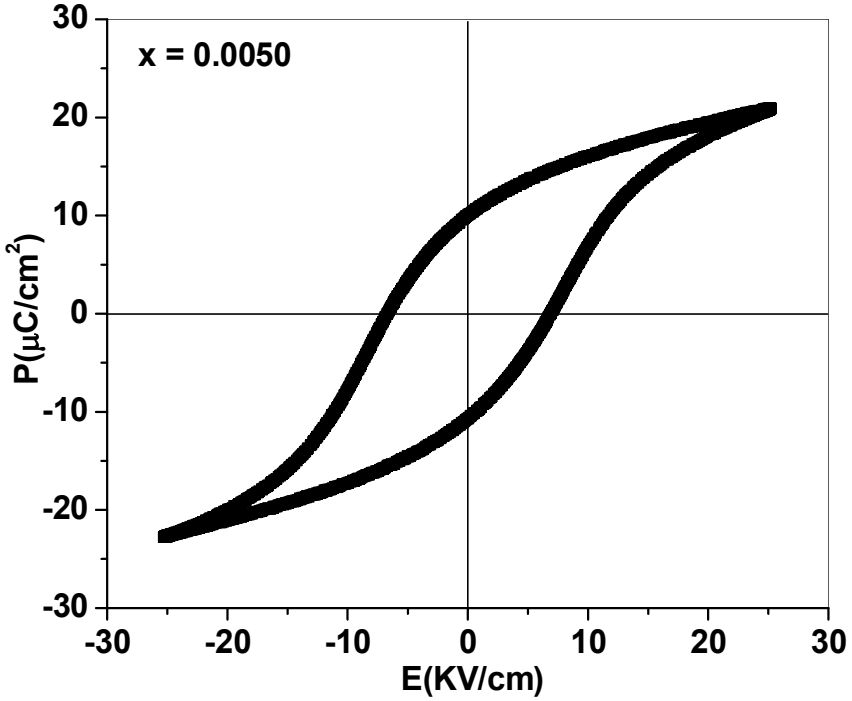
x = 0.0050
P(μC/cm²)
E(KV/cm)
30
20
10
0
-10
-20
-30
-30
-20
-10
0
10
20
30

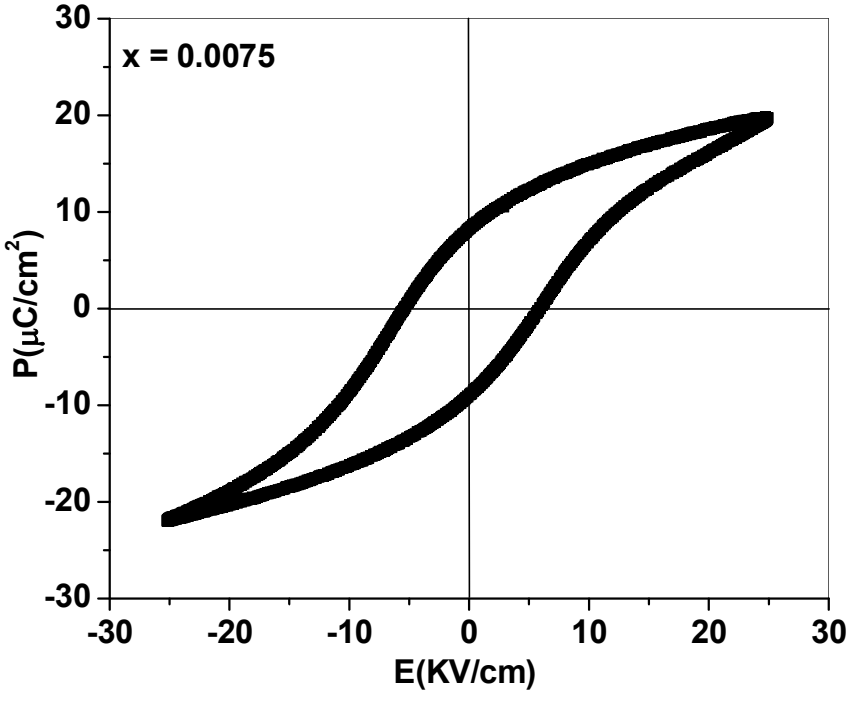
x = 0.0075
P(μC/cm²)
E(KV/cm)
30
20
10
0
-10
-20
-30
-30
-20
-10
0
10
20
30

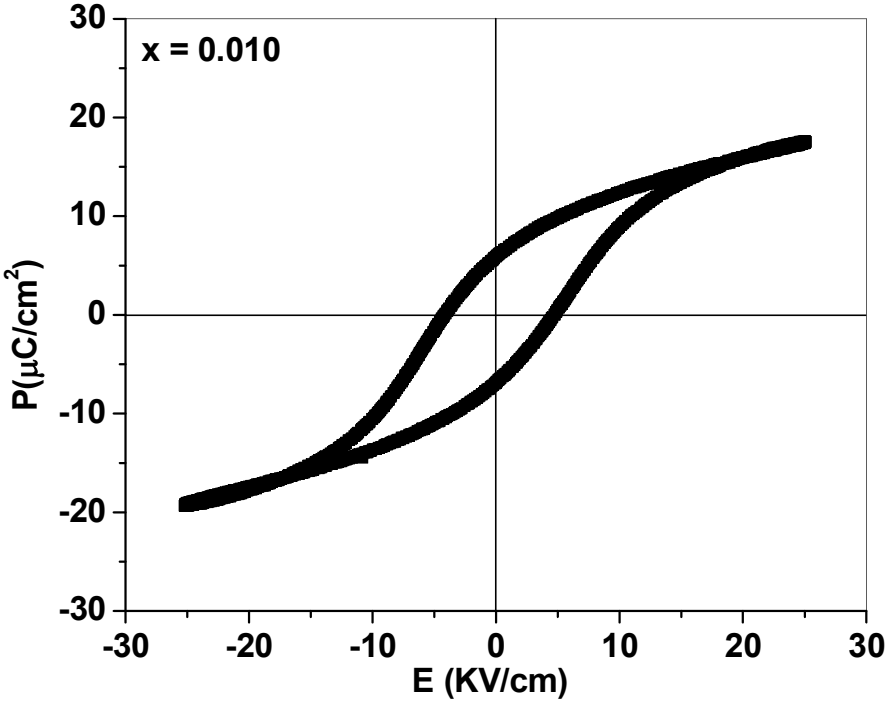

Figure 5.10 PE loops of BSPZT ceramics

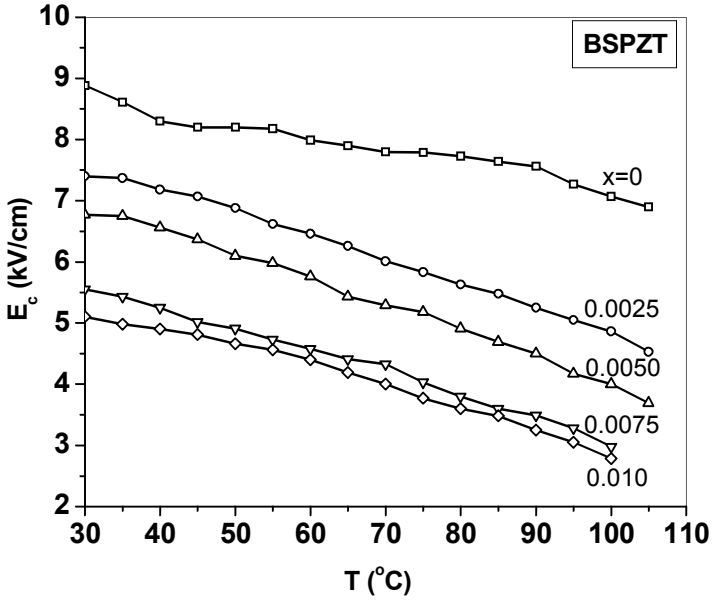

Figure 5.11 Variation of E_c with temperature for all BSPZT ceramics

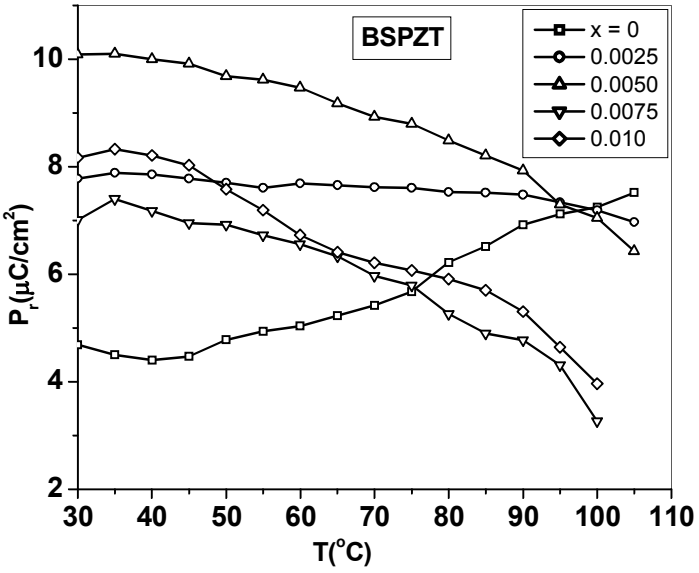

Figure 5.12 Variation of P_r with temperature for all BSPZT ceramics

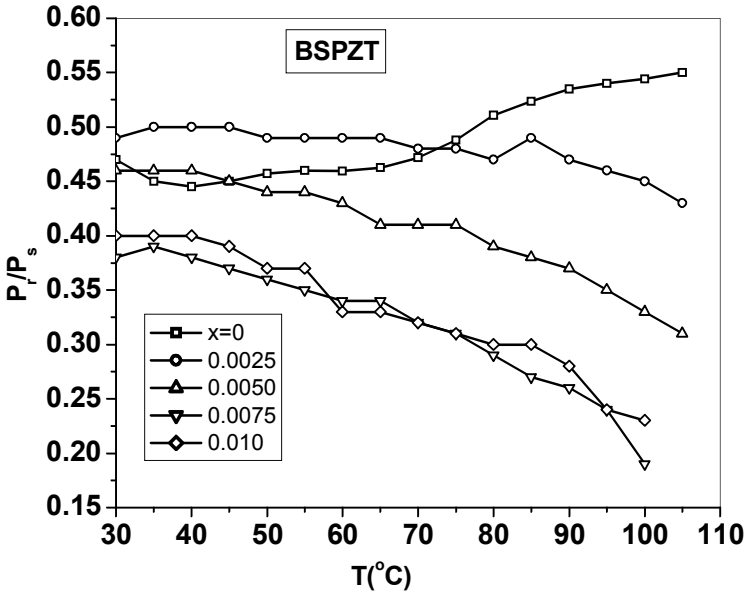

Figure 5.13 Variation of P_r/P_s with temperature for all BSPZT ceramics

5.6 Ferroelectric and Piezoelectric Properties of BLPZT ceramics

All sintered BLPZT specimens showed well defined ferroelectric behavior at 20 Hz and the P-E hysteresis loops of all the samples at two different temperatures 30°C are

shown in figure 5.14. The width of the P-E loop was found to decrease with increase in lanthanum substitution and temperature as shown in figure 5.14. The ratio of remanent polarization (P_r) and spontaneous polarization (P_s) i.e. P_r/P_s indicates the squareness for the loop ratio.

The decrease in E_c, P_r and P_r/P_s with increase in temperature is shown in figure 5.15, 5.16 and 5.17 respectively. The remanent polarization, P_r/P_s and Coercive field (E_c) were found to decrease with increase in temperature. P_r for x = 0.00 increases with increase in temperature. The decrease in P_r for x greater than 0.00 with temperature is mainly due to decrease in internal energy caused by thermal excitation leading to smaller dipole alignment [27]. The decrease in E_c indicates that materials soften on heating while the decrease in P_r/P_s shows that squareness of the P-E loop decreases with heating.

P_r/P_s ratio was found to increase up to x = 0.0025 while decrease for x greater than 0.0025. E_c was found to decrease with increase in lanthanum substitution from which one can predict that material get soften by lanthanum substitution. Increase in P_r/P_s ratio indicates that squareness of the P-E loop increases from x = 0.00 to 0.0025 whereas it decreases for further values of x. The values of d_{33} and k_p for all BLPZT ceramics are given in table 5.6.

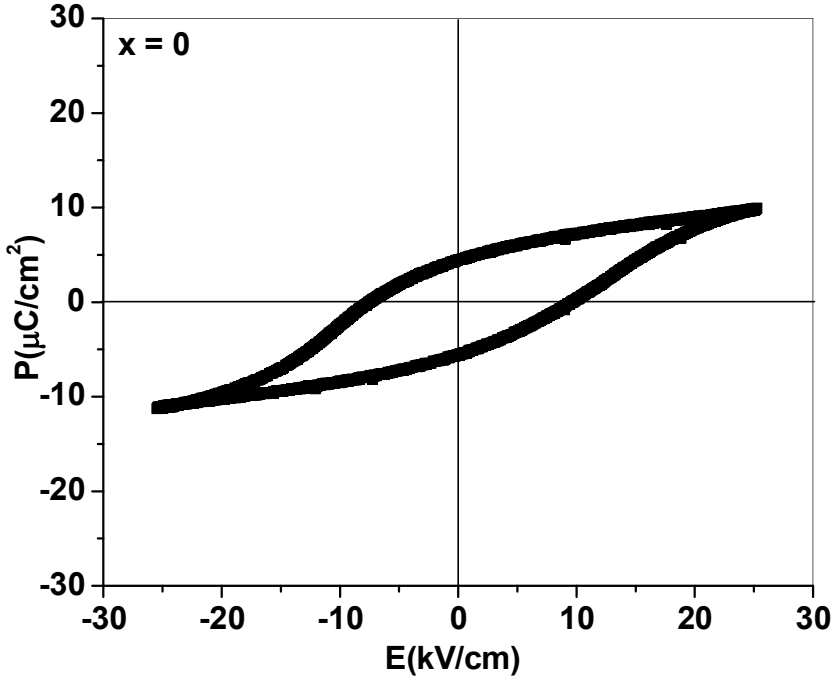
x = 0
P(μC/cm²)
E(kV/cm)
30
20
10
0
-10
-20
-30
-30
-20
-10
0
10
20
30

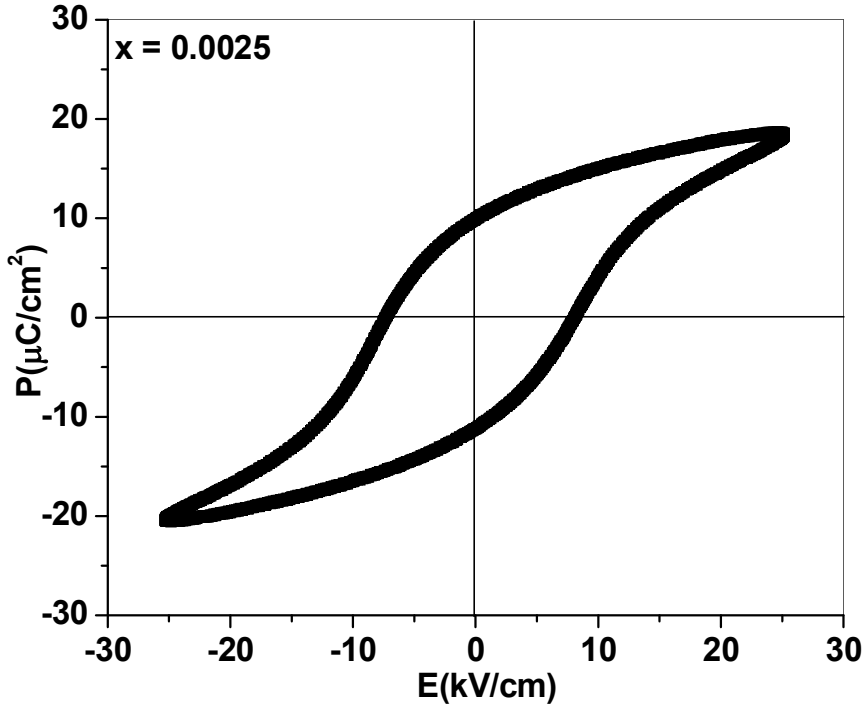
x = 0.0025
P(μC/cm²)
E(kV/cm)
30
20
10
0
-10
-20
-30
-30
-20
-10
0
10
20
30

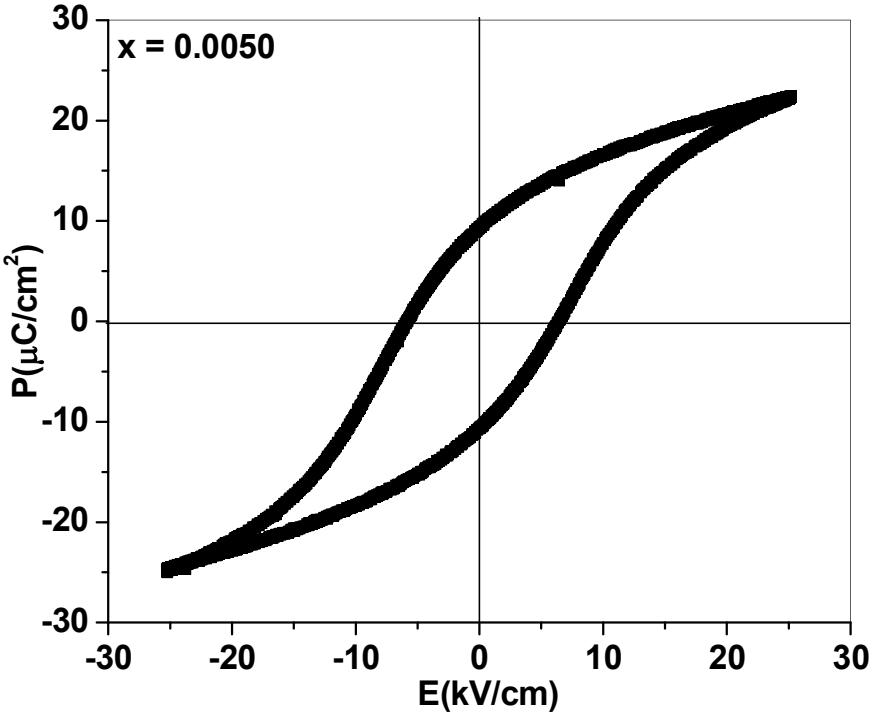
x = 0.0050
P(μC/cm²)
E(kV/cm)
30
20
10
0
-10
-20
-30
-30
-20
-10
0
10
20
30

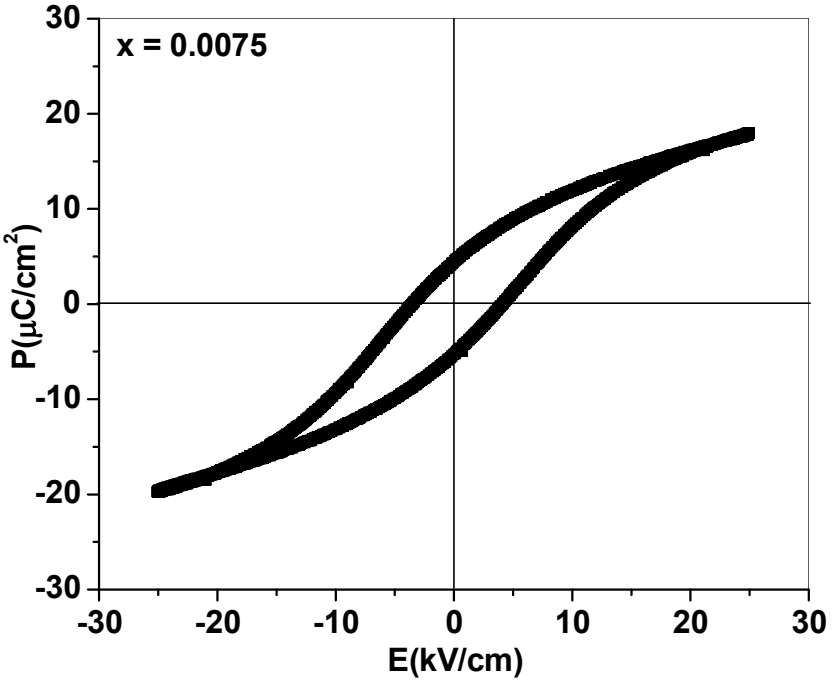
x = 0.0075
P(μC/cm²)
E(kV/cm)
30
20
10
0
-10
-20
-30
-30
-20
-10
0
10
20
30

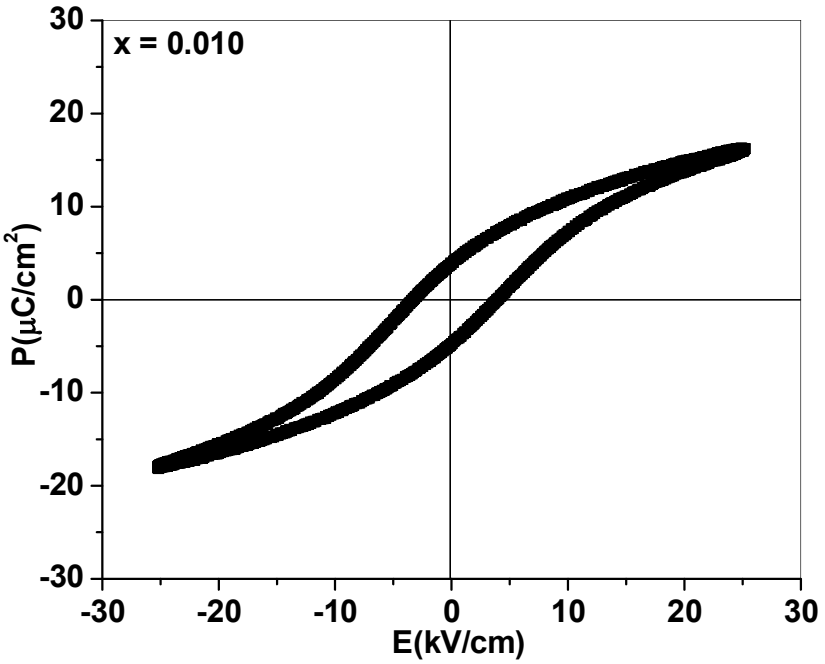

Figure 5.14 PE loops of all BLPZT ceramics

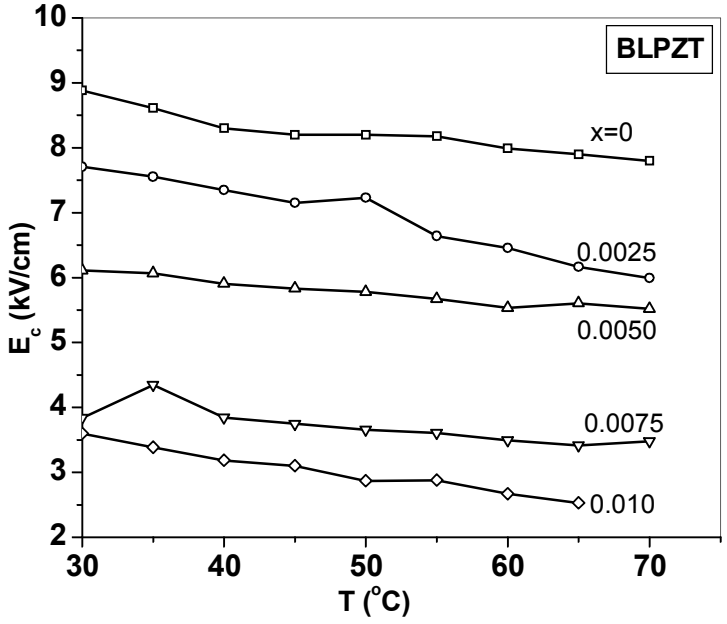

Figure 5.15 Variation of E_c with temperature for all BLPZT ceramics

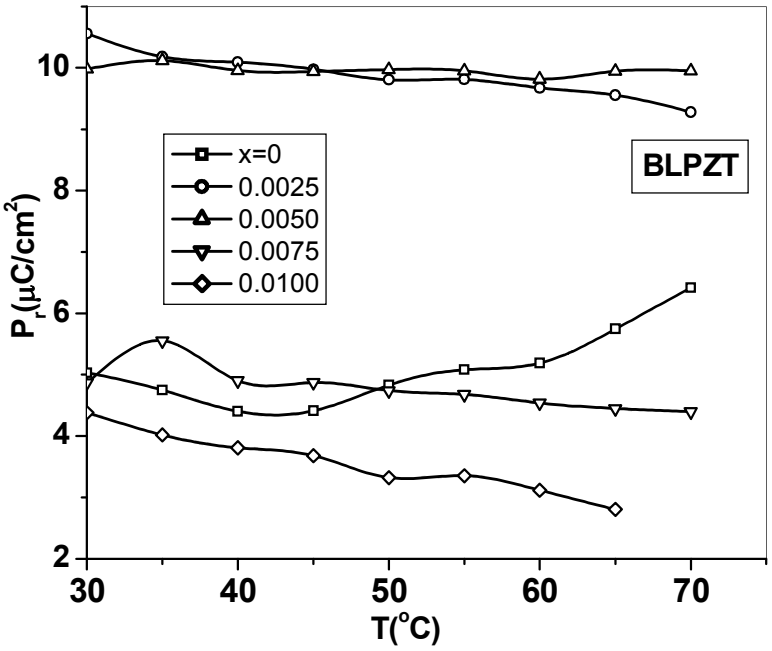

Figure 5.16 Variation of P_r with temperature for all BLPZT ceramics

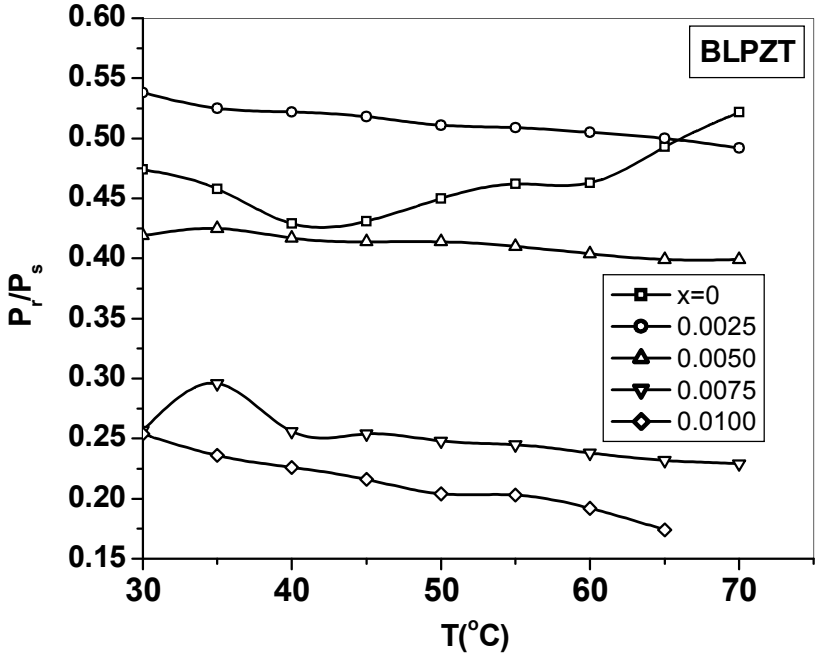

Figure 5.17 Variation of P_r/P_s with temperature for all BLPZT ceramics

Table 5.5 Coercive field 'E_c', remnant polarization 'P_r' and remnant to spontaneous polarization ratio 'P_r/P_s' of BSPZT and BLPZT ceramics

BSPZT				BLPZT		
x	**E_c (kV/cm)**	**P_r ($\mu C/cm^2$)**	**P_r/P_s**	**E_c (kV/cm)**	**P_r ($\mu C/cm^2$)**	**P_r/P_s**
0	8.9	4.69	0.46	8.9	4.69	0.46
0.0025	7.4	7.78	0.49	7.7	10.56	0.54
0.0050	6.8	10.09	0.46	6.1	9.98	0.42
0.0075	5.6	7.01	0.38	3.8	4.87	0.26
0.010	5.1	8.17	0.40	3.5	4.38	0.25

Table 5.6 Piezoelectric charge coefficient 'd_{33}' and electromechanical coupling factor 'k_p' of BSPZT and BLPZT ceramics

BSPZT			BLPZT	
x	**d_{33} (pC/N)**	**k_p (%)**	**d_{33} (pC/N)**	**k_p (%)**
0	107	14.67	107	14.67
0.0025	87	11.35	83	10.42
0.0050	65	12.04	66	13.53
0.0075	46	12.62	21	13.86
0.010	45	13.32	21	14.35

References

[1] Chin-Yi Chen and Wei-Hsing Tuan, J. Am. Ceram. Soc., **83** (2000) 2988.

[2] A.V. Turik, A.A. Yesis, and A. Reznitchenko, Ferroelectrics, **359** (2007) 111.

[3] V.A. Nepochatenko, Ferroelectrics, **341** (2006) 97.

[4] L. Mitoseriu, C.E. Ciomaga, V. Buscaglia, L. Stoleriu, D. Piazza et al., J. Eur. Ceram. Soc., **27** (2007) 3723.

[5] G.H. Haertling, J. Am. Ceram. Soc., **82** (1999) 797.

[6] R.C. Buchanan, Ceramic materials for Electronics Processing, Properties, and Applications Marcel Dekker Inc. (1991).

[7] N. Vittayakorn, J. Appl. Sci. Res., **2** (2006) 1319.

[8] H. Kishi, N. Kohzu, J. Sugino et al., J. Eur. Ceram. Soc., **19** (1999) 1043.

[9] N.V. Dergunova, E.G. Fesenko and V.P. Sakhnenko, Ferroelectrics, **83** (1988) 187.

[10] K. Watanabe, H. Ohsato, H. Kishi, Y. Okino, N. Kohzu, Y. Iguchi, T. Okuda, Solid State Ion., **108** (1998) 129.

[11] M.T. Buscaglia, V. Buscaglia, M. Viviani, P. Nanni, M. Hanuskova, J. Eur. Ceram. Soc., **20** (2000) 15.

[12] M.W. Barsoum, Fundamentals of Ceramics, The McGraw Hill, New York, 1997.

[13] S.M. Pilgrim, A.E. Sutherland and S.R. Winzer, J. Am. Ceram. Soc., **73** (1990) 3122.

[14] Sarabjit Singh, O.P. Thakur, Chandra Prakash and K.K. Raina, Phase Transitions, **78** (2005) 655.

[15] K. Okazaki, Ceram. Bull., **63** (1984) 1150.

[16] R. Tickoo, R.P. Tandon, K.K. Bamzai and P.N. Kotru, Mat. Sci. and Eng. B, **103** (2003) 149.

[17] Li Yuanliang and Qu Yuanfang, Mater. Chem. Phys., **110** (2008) 157.

[18] A.A. Sattar, H.M. El-Sayed, W.R. Agami and A.A. Ghani, Am. J. Appl. Sci., **4** (2007) 91.

[19] B. Jaffe, W.R. Cook and H. Jaffe, Piezoelectric Ceramics, Academic, New York, 1971.

[20] M.E. Lines and A.M. Glass, 1977. Principles and applications of ferroelectric and related materials Clarendon Press Oxford.

[21] C. Ang, Z. Jing and Z. Yu, J. Phys. Condens. Mater., **14** (2002) 8901.

[22] P. Victor, R. Ranjith and S.B. Krupanidhi, J. Appl. Phys., **94** (2003) 7702.

[23] S. Miga and K. Wojcik, Ferroelectrics, **100** (1989) 167.

[24] Jayati Ray, Peter Hing and R.N.P. Choudhary, Mater. Lett., **51** (2001) 440.

[25] K. Uchino, Ferroelectric Devices, Marcel Dekker, Inc., New York, 2000.

[26] K. Carl Ferroelectrics, **9 (**1975) 23.

[27] Kamel M Talal, With G de., J. Eur. Ceram. Soc., **28 (**2008) 851.

Chapter 6

Summary, Conclusions and Suggestions for Future Work

Barium zirconium titanate ($BaZr_{0.10}Ti_{0.90}O_3$) ceramics materials were synthesized by solid state reaction method. Modifications were carried by substitution of Pb^{2+}, Ca^{2+}, Zr^{4+}, $La^{3+}$and Sm^{3+} for the host ions. The substituted ceramics were characterized for their structural, dielectric and ferroelectric properties. This chapter includes the summary, conclusions and some suggestions for future work.

6.1 Summary and Conclusions

Being a potential candidate for dielectric applications, $BaTiO_3$ has been a centre of interest for the researchers in the field of material sciences. Apart from the dielectric applications it is also suitable for many other applications like PTCR applications, FRAM and DRAM, sensors etc. It's the very popular ferroelectric material showing good piezoelectric properties also. The piezoelectric materials are used in many devices. They are finding more and more application in sensors and actuators based on MEMS technology. There is a great scope for further improvements of its properties. The best ways of modifying its properties are: i) microstructural modifications via change in processing techniques and parameters and ii) chemical compositional modifications via substitution and doping. Dielectric and piezoelectric properties are of prime importance and are in general dependent on structural properties besides its chemical composition. Substitution and doping of different elements in the main chemical, of course with some constraints, have resulted in the present state of affair in the area of ferroelectrics.

Substitution can be done at both Ba as well as Ti site. Ions with higher charge valancy to be substituted (e.g. Sm^{3+}, La^{3+} for Ba^{2+} and Nb^{5+} for Ti^{4+}) act as softeners, while ions with lower charge valancy act as hardeners. However the solubility of these ions is different for different parent matrix system. In the work reported in this thesis, studies carried out on Pb^{2+}, Zr^{4+}, Ca^{2+}, Sm^{3+} and La^{3+} substitution in substituted barium titanate are described. These substituents affect the ferroelectric, piezoelectric and dielectric properties favorably which are reported in the present study. Conclusions of the work carried out for this thesis are described below:

Present thesis has been divided into six chapters. The first chapter is introductory in nature. Theoretical background related to various types of substitutions, dielectric and piezoelectric properties has been presented. Effect of A-site and B-site substitution, which is the aim of present study, has also been discussed.

In the Second Chapter, procedure adopted for the preparation of samples is described. Samples were prepared by conventional solid-state reaction method. Appropriate amount of starting material were weighed and wet ball milled followed by drying and calcinations. Reacted powders were pressed uniaxially in the form of discs and were finally sintered in the range 1300 to 1350^{o}C for 4 hrs in closed alumina crucibles. Electroded discs were poled at 25kV/cm at 170^{0}C for one hour in silicone oil bath. Following series of substituted barium titanate were synthesized by the conventional solid-state reaction method, and studied:

$BaTi_{0.90}Zr_{0.10}O_3$ (sintered at 1200, 1250, 1300 and 1350^{o}C)

Series A $Ba_{1-x}Pb_x\ Zr_{0.10}Ti_{0.90}O_3$ ($0 \leq x \leq 0.20$; in the steps of 0.05)

Series B $Ba_{0.80}Pb_{0.20}Ti_{1-x}Zr_xO_3$ ($0 \leq x \leq 0.10$; in steps of 0.02)

Series C $Ba_{0.80-x}Ca_xPb_{0.20}Ti_{0.90}Zr_{0.10}O_3$ (for x=0, 0.10 and 0.20)

Series D $Ba_{0.80-x}Sm_xPb_{0.20}Ti_{0.90}Zr_{0.10}O_3$ ($0 \leq x \leq 0.01$; in steps of 0.0025)

Series E $Ba_{0.80-x}La_xPb_{0.20}Ti_{0.90}Zr_{0.10}O_3$ ($0 \leq x \leq 0.01$; in steps of 0.0025)

Third chapter is devoted to the physical properties related to $BaTi_{0.90}Zr_{0.10}O_3$; BZT (10/90) sintered at 1200, 1250, 1300 and 1350^{o}C. X-ray diffraction patterns were recorded for the calcined and sintered samples. XRD analysis shows that single phase with tetragonal structure was obtained for the sample sintered at 1350^{o}C. With the increase in

sintering temperature all other phases representing the unreacted ZrO_2 and other intermediate components get eliminated. Finally at 1350^oC the material is having proper rhombohedral phase. The grain size also found to increase with increase in sintering temperature. The increase in grain size resulted in dielectric data less dependent on the frequency, which may be due to reduction in surface charge polarization. The interesting behavior in the variation of dielectric constant with temperature also noticed. BZT sample sintered at 1200^oC has dielectric variation similar to the pure barium titanate, whereas in case of sample sintered at 1350^oC, it is having Curie point at 92^oC with a quite broad dielectric peak. Coercive field was found to decrease whereas the remnant polarization was found to increase with increase in sintering temperature. It is concluded from the study that the best BZT sample with purely rhombohedral structure can be prepared by sintering the sample at 1350^oC.

The fourth chapter is devoted to the study of Pb^{2+}, Zr^{4+} and Ca^{2+} substitution in modified barium titanate ceramics. Substitution of Pb^{2+} **(Series A)** resulted in increase in tetragonality, average grain size, Curie temperature and improved ferroelectric properties. The room temperature dielectric constant was found to decrease with increase in Pb content. This may be due to shifting of Curie temperature towards the Curie temperature of $PbTiO_3$ (490^oC), whereas the other transition temperatures towards lower temperature. Piezoelectric charge coefficient 'd_{33}' increases upto 10 mol% and then it decreases. This unexpected variation may be due to volatile nature of Pb. Zr^{4+} substitution to $Ba_{0.80}Pb_{0.20}TiO_3$ **(Series B)** was studied and it was found that the Curie temperature shifted towards lower temperature, thereby increasing the room temperature dielectric constant. The dielectric peaks broadened with Zr substitution. The tetragonality and relative density

was found to decrease with increase in Zr content. The decrease in tetragonality and Curie temperature was due to larger ionic radius of Zr^{4+} as compared to the Ti^{4+}. Ca^{2+} substitution in $Ba_{0.80}Pb_{0.20}Ti_{0.90}Zr_{0.10}O_3$ **(Series C)** did not affect the Curie temperature, but it reduces tanδ to a very small value. It also improves the ferroelectric properties. For sample with Ca equal to 10 mol%, we observed lowest tanδ value along with thermally stable ferroelectric properties suggesting that the sample is suitable for dielectric as well as memory devices over a temperature range.

In the fifth chapter we report, the effect of rare earth ions (Sm^{3+} and La^{3+}) **(Series D and E)** on the structural, ferroelectric, piezoelectric and dielectric properties of $Ba_{0.80}Pb_{0.20}Ti_{0.90}Zr_{0.10}O_3$ ceramics. The relative density was found to improve by substitution of Sm and La. Room temperature dielectric constant increased with substitution of Sm and La, however the effect is pronounced in case of La^{3+} because of its larger ionic radius than Sm^{3+}. Broadening of dielectric peak was also pronounced in case of La^{3+} substitution. The grain size was also found to decrease with increase in Sm and La content. The piezoelectric properties were found to depend on the grain size of the prepared substituted ceramics sample in series D and E.

Sixth chapter includes the conclusions and suggestions for the future work.

6.2 Suggestions for the Future Work

These materials are widely used for dielectric applications. For better understanding of ferroelectric and piezoelectric phenomenon in these materials some more studies are suggested for these materials. These are:

i) Study of pyroelectric properties.

ii) Study of dielectric properties as a function of applied dc field.

iii) Study of S-E hysteresis loop.

iv) Synthesis and study of selected good samples by using novel techniques.